EXPERIMENTAL INVESTIGATION OF NANOFLUIDS USING
TERAHERTZ TIME DOMAIN SPECTROSCOPY (THz TDS)

A THESIS SUBMITTED TO
THE GRADUATE SCHOOL OF NATURAL AND APPLIED SCIENCES
OF
MIDDLE EAST TECHNICAL UNIVERSITY

BY

CAN KORAL

IN PARTIAL FULFILLMENT OF THE REQUIREMENTS
FOR
THE DEGREE OF MASTER OF SCIENCE
IN
MICRO AND NANOTECHNOLOGY

JUNE 2012

Approval of the Thesis:

**EXPERIMENTAL INVESTIGATION OF NANOFLUIDS USING
TERAHERTZ TIME DOMAIN SPECTROSCOPY (THz TDS)**

Submitted by **CAN KORAL** in partial fulfillment of the requirements for the degree of **Master of Science in Micro and Nanotechnology Department, Middle East Technical University** by,

Prof. Dr. Canan ÖZGEN
Dean, Graduate School of **Natural and Applied Sciences**   _____

Prof. Dr. Mürvet VOLKAN
Head of Department, **Micro and Nanotechnology**   _____

Assist. Prof. Dr. Tuba OKUTUCU
Supervisor, **Mechanical Engineering Dept., METU**   _____

Assoc. Prof. Dr. HAKAN ALTAN
Co-advisor, **Physics Dept., METU**   _____

Examining Committee Members:

Assoc. Prof. Dr. Almıla YAZICIOĞLU
Mechanical Engineering Dept., METU   _____

Assist. Prof. Dr. Tuba OKUTUCU
Mechanical Engineering Dept., METU   _____

Assoc. Prof. Dr. Hakan ALTAN
Physics Dept., METU   _____

Dr. Halil BERBEROĞLU
Physics Dept., METU   _____

Assist. Prof. Dr. Bülend ORTAÇ
Institute of Material Science and Nanotechnology (UNAM),
Bilkent University   _____

Date: _____**13/06/2012**_____

I hereby declare that all information in this document has been obtained and presented in accordance with academic rules and ethical conduct. I also declare that, as required by these rules and conduct, I have fully cited and referenced all material and results that are not original to this work.

Name, Last Name: CAN KORAL

Signature:

ABSTRACT

EXPERIMENTAL INVESTIGATION OF NANOFLUIDS USING TERAHERTZ TIME DOMAIN SPECTROSCOPY (THz TDS)

Koral, Can

M.Sc. Department of Micro and Nanotechnology

Supervisor: Assist. Prof. Dr. Tuba Okutucu

Co-Supervisor: Assoc. Prof. Dr. Hakan Altan

June 2012, 84 pages

In this study, suspensions of metallic nanoparticles in base fluids, nanofluids, are investigated by using terahertz time domain spectroscopy (THz-TDS). Nanofluids are used as the working fluid in a variety of applications especially for the purpose of heat transfer enhancement. Polar fluids are being used as the base in nanofluids for their tendency to stop aggregation and sedimentation. Polar fluids highly absorb THz signal. In order to select the best possible host, various polar liquids have been investigated, and isopropanol (99.5%) is selected to be the best candidate for its low THz absorptivity when compared to ethanol (99.5%), ethylene glycol (99%), methanol (95%) and distilled water.

Ag, Pd and Cu nanoparticles have been custom-made in isopropanol by laser ablation method, and the size distributions have been characterized by Zeta Potential Analyzer. The nanoparticle diameters are measured to be on average 10 nm, 12 nm and 75 nm for Ag, Cu and Pd, respectively. Nanofluids of 1X, 2X and 3X concentrations of Ag, Cu and Pd nanoparticles have been prepared by diluting with pure (99.5%) isopropanol. Measurements have been repeated after 7 days up to 12 days in order to check for aggregations and sedimentations.

THz-TDS is a strong tool to analyze the refractive index and absorption coefficient, but no distinct difference was observed in the frequency domain analysis for the nanofluid samples.

On the other hand, in the time domain data analysis, a shift on the time data with a change in transmission was observed. For Ag nanoparticles a positive time shift with a decrease in transmission with increasing concentration was observed. For Cu nanoparticles an interesting negative time shift and an increase in the intensity was observed with increasing concentration. The Pd nanoparticle solution scans showed almost no shift initially, but a negative time shift after a wait period on the order of days.

A model of the transmission of the THz pulse through the nanofluid was developed based on transmission/reflection coefficients due to both dielectric and conducting layered media. The model well explains the positive time shift seen with Ag nanoparticle suspensions but fails to explain the shift seen with the Cu nanoparticle suspensions due to the long path length inside the nanofluid. Negative time-shifts can only be explained by decreasing the path length which suggests additional layering inside the nanofluid medium, or assuming that the chemical composition of the isopropanol host has changed with the addition of Cu and/or Pd nanoparticles. The positive time shifts observed with the Ag nanoparticle suspensions allowed for estimating the change in refractive index of the base fluid. From this change, using effective medium theory based on Maxwell-Garnett model, the concentrations of the nanoparticles were estimated. The results agree within an order of magnitude to commercially available nanofluids which are also non-aggregate.

ÖZ

NANO AKIŞKANLARIN ZAMANA DAYALI TERAHERTZ SPEKTROMETRESİ İLE DENEYSEL OLARAK İNCELENMESİ

Koral, Can

Yüksek Lisans Mikro ve Nanoteknoloji Bölümü

Tez Danışmanı: Y. Doç. Dr. Tuba Okutucu

Tez Yardımcı Danışmanı: Doç. Dr. Hakan Altan

Haziran 2012, 84 sayfa

Bu çalışmada, nanoakışkanlar, bir baz akışkan içinde metal nanoparçacıkların süspansiyonları, zamana dayalı terahertz spektroskopisi (THz-TDS) yöntemiyle incelenmiştir. Nanoakışkanlar, özellikle ısı transfer artırımı amacıyla çeşitli uygulamalarda kullanılmaktadır. Polar yapıya sahip sıvılar topaklanma ve çökelme gibi etkilerini durdurma eğilimleri sebebiyle nanoakışkan üretiminde baz sıvı olarak kullanılmaktadır. Polar sıvılar THz sinyalini yüksek oranda soğurmaktadırlar, Yapılan ölçümler sonucunda saf isopropanolün (%99,5) soğurma katsayısının etanol (%99,5), etilen glikol (%99), metanol (%95) ve damıtılmış su örneklerine kıyasla düşük olması sebebiyle baz sıvı olarak kullanılması kararlaştırılmıştır.

Ag, Pd ve Cu nanoparçacıklar özel olarak isopropanol içinde lazer ablasyon yöntemiyle üretilmiştir. Sırasıyla 10 nm, 12 nm ve 75 nm ortalama parçacık çaplarında olan Ag, Cu ve Pd örnekleri Zeta potansiyeli analizörü kullanılarak ölçülmüştür. Elde edilen nanoakışkanlar saf isopropanol (%99,5) ile seyreltilerek 1X, 2X ve 3X derişimlerine sahip çeşitli nanoakışkan örnekleri hazırlanmıştır. Hazırlanan bu örneklerle alınan ölçümler, topaklanma ve çökelme etkenlerini kontrol etmek amacıyla 7 gün ile 12 gün sonrasında tekrarlanmıştır.

THz-TDS kırılma indisi ve soğurma katsayılarını analiz etmek için güçlü bir tekniktir. İncelenen nanoakışkan örneklerinde, frekansa bağlı analizler sonucunda kırılma indisi ve soğurma katsayılarında belirgin bir farklılık gözlemlenmemiştir.

Öte yandan zamana dayalı analizlerde zamanda bir kayma ve geçirgenlik değişimi gözlemlenmiştir. Ag nano parçacık içeren nano sıvıda artan derişimle birlikte zamanda artı yönde bir kayma ve geçirgenlikte bir azalma gözlemlenmiştir. Cu nanoparçacık ihtiva eden sıvılarda ise derişim arttıkca ilginç bir zamanda eksi yönde kayma ve geçirgenlikte artış gözlemlenmiştir. Pd nanoparçacık içeren sıvılarda ise ilk ölçümlerde bir değişiklik gözlemlenmezken günler sonra yapılan kontrol ölçümlerinde zamanda eksi yönde bir kayma gözlemlenmiştir.

Nanoakışkandan geçen THz sinyali dielektrik ve iletken katmanlara bağlı olarak geçirgenlik ve yansıma katsayıları baz alınarak modellenmiştir. Bu model, Ag nanoparçacıkların dinamiğini tam olarak izah etmektedir. Oluşturulan mdel, THz sinyalinin numune içinde kat ettiği mesafenin çok uzun olmasından dolayı Cu nanoparçacık içeren sıvılarda gözlemlenen zamanda eksi yöndeki kaymayı desteklememektedir Zamandaki negatif yönde kayma ancak nanoakışkan içerisinde THz sinyaline temel olarak etkiyen ince ek bir katman oluşması durumuyla ya da baz sıvının kimyasının eklenen Pd veya Cu nanoparçacıklarla değişmesiyle açıklanabilir. Ag nanoparçacık içeren sıvılarda gözlemlenen zamanda artı yöndeki kayma ölçülerek, parçacık eklenmesiyle oluşan kırılma indisi farkı tahmin edilebilmiştir. Bu fark kullanılarak ve Maxwell-Garnett modelini temel alarak nanoparçacık derişimleri tahmini olarak hesaplanmıştır. Derişim hesaplamaları, ticari amaçla satılan, topaklanmayan nanoparçacık derişimleriyle uyum sağlamaktadır.

To my Family

ACKNOWLEDGEMENTS

TABLE OF CONTENTS

LIST OF TABLES

LIST OF FIGURES

LIST OF ABBREVIATIONS

nm: Nanometer

NP: Nanoparticle

NF: Nanofluid

NOMENCLATURE

Nanometer: One nanometer (10^{-9}m) is one millionth of a millimeter

Nanoparticle; refers to the particles at nanometer scale(1nm to 100nm range)

Nanotechnology; refer to the ability to engineer materials at nanometer scales.

Nanofluid; are fluids which contain suspended nanometer sized metallic or nonmetallic particles or nanotubes.

Micrometer: One micrometer(10^{-6}m) is one millionth of a meter.

Microchannel; are chanels at micrometer scale.

Microchannel Heat Sink; refers to a micro sized component that cools a device by exterminating heat into the surrounding media

CHAPTER I

INTRODUCTION

Nanotechnology is playing an ever more important part in the daily lives of human beings. One nanometer (10^{-9}m) is one millionth of a millimeter such that a nano-structure or nano material would have to contain tens or hundreds of atoms, since atoms are at the order of 1Å in size which is equal to 0,1nm.

Nobel prize winner, Richard Feynman presented the concept of use of materials at atomic scale and how people can construct atomic scale machines and systems in his famous talk "there is a plenty of room at the bottom" in 1959. This talk introduced the concept of use of nanomaterials for the first time [1], and his vision and imagination was at the forefront of a new trend of miniaturization in modern science and technology.

The term nanotechnology was first used in 1974 by the late Norio Taniguchi [2] to refer to the ability to engineer materials at nanometer scales. This term comprised the design, characterization, production and application of materials, devices and systems at the nano scale.

Until the 1980's, Feynman's vision of future technology and the Taniguchi's terminology of engineering was a fiction till the invention of Scanning Tunneling Microscopy (STM) [3] which made possible to image, transport and use atoms precisely to form new systems and even materials which do not exist naturally [4]. This touchstone invention brought the Nobel Prize in physics to Benning and Rohrer in 1986 [5].

With the advent of nanotechnology, a world which was once fictional has become more real. Some notable examples include prosthesis parts imitating human neural system, processors that compute algorithms that can mimic human brains, nanorobots which automatically attack the diseased cells and repair internal damage in human bodies, nano coated surfaces that never get dirt, fabrics that automatically change colour and pattern, human integrated computers which maintains any organ disablement and many more examples which are only limited to our imagination. As can be figured out from the above examples, nanotechnology has a broad range of potential applications combining contributions from physics, chemistry, biology, materials science, engineering, pharmacology and many other disciplines.

Synthesising and using nanomaterials as building blocks for new structures and devices, construction of tools for characterization, detection and production of nanostructures and nanomaterials seem to be the main aspects of Nanotechnology but on the other hand it is also very important to understand the physical properties related to the nanometer scale. As size of the material reduces down to nano scale physical properties become significantly different from the bulk materials. Larger fraction of surface atoms, larger surface energy, spatial confinement and reduced imperfections can be listed as the main mechanizms for the change of properties[5]. For example; The enhancement in mechanical strength is a result from the reduced probability of defects [6]. For magnetic materails, ferromagnetism disappears and transfers to superparamagnetism as a result of the huge surface energy [6] . The color of metallic nanoparticles change with their sizes due to surface plasmon resonance and also the optical absorption peak of a semiconductor nanoparticle shifts to a short wavelength, due to an increased band gap [6] . Electrical conductivity decreases due to increased surface scattering in certain nanomaterials [6] . Thermal conductivity, heat transfer coefficients increase and the melting point decrease due to reduced defects and surface energy due to the changes in the ratio of surface energy to volume energy [6] .

Mechanical, magnetic, chemical, electronic and optical properties are size dependent so that nanostructured materials can be tuned controllably by adjusting the size and shape or extent of agglomeration[7].

Nanotechnology has also given birth to a promising research area called Nano fluidics. The term nanofluid was first used in 1995, by Choi [7] for a new class of heat transfer fluids, by definition [8] nanofluids are fluids which contain suspended nanometer sized metallic or nonmetallic particles or nanotubes. Nanofluids are used for the purpose of achieving better heat removal from micro devices. As devices shrink down to micro and even nano meter scale, heat can cause the device to fail, so cooling methods that use microchannels are being utilized to take away heat from the operating device. The idea behind the nano fluid in a micro channel is that the heat conductivity of the normal liquid with nanoparticles would increase and thus it would be a better method of removing heat.

In the development of energy-efficient heat transfer equipment, the thermal conductivity of the heat transfer fluid has a major role. By increasing the efficiency of heat transfer devices, it would be possible to; reduce the size of the devices, decrease the operating costs of the associated processes and increase the efficient work-life [9]. Heat transfer fluids such as water, oil, and ethylene glycol mixtures have been traditionally used despite their poor heat transfer abilities in such micro scale device structures. The development of advanced heat

2

transfer fluids with significantly higher thermal conductivities is still a challenging topic. It is well known that at room temperature, metals in solid form have orders-of-magnitude higher thermal conductivities than those of fluids [10]. On the other hand when the particle sizes are on the order of millimeters or micrometers, the mixtures are unstable, therefore, sedimentation occurs. This is a problem and these solid clusters of particles may erode the channel walls [11]. Also the presence of clusters of solid particles increases the pressure drop through the channel significantly, which increases the required coolant pumping power and associated operating cost [12]. A solution to this problem is to make the particles even smaller towards the sub-micron and nanometer scales.

As with micron or millimeter sized particles, by suspending nanoparticles in base fluids, the heat transfer performance of the fluid was seen to be significantly improved [13]. As was the case explained above, since solid materials have thermal conductivities much higher than fluids, such an attempt obviously results in a thermal conductivity enhancement [13] as the suspended nanoparticles increase the heat transfer surface area. The effective (or apparent) thermal conductivity of the fluid, the interaction and collision among particles as well as fluid-fluid and the fluid-flow passage surface interactions and the mixing fluctuation and turbulence of the fluid are all effective in the enhancement of the heat gathering capability of the nanofluid.

At the Mechanical Engineering Department, METU, Ankara, Turkey, Asst. Prof. Dr. Tuba Okutucu and her colleagues have been researching microchannel heat sink designs for chip cooling applications [14] and dimensional optimization of microchannel heat sinks[15].

The micro-channels used to cool down the devices scale with the device size, so that the channel widths are typically on the order of a few microns to tens of microns. In such dimensions it becomes important to be able to predict the motion of the nano-particle suspended solutions. Current techniques involve visible imaging of the nanoparticles as they traverse the channel. These techniques require transparent channels for observation, and even sometimes require the use of fluorescent molecules to be able to see the particles whose sizes can be as small as 10nm [16]. These methods become difficult when the channel is in a non-transparent semi-metallic substrate.

In this thesis the goal was to detect the particle concentration of nanofluids and thus detect particle dynamics in the channel by directly detecting the nanoparticle population homogeneity as they passed through the microchannels. In the process, undesired effects like sedimentation or aggregation could be quantified. However, unlike previous works which

utilized visible imaging methods to characterize the particle concentrations [17] our efforts were concentrated in using a novel method which uses terahertz radiation. By working with the Terahertz Research Laboratory located in the Physics Department at METU, led by Assoc. Prof. Dr. Hakan Altan, we formulated a characterization tool based on terahertz waves. One advantage of this method is that terahertz waves don't need optically transparent media around the channel (however it has to be non-metallic). Another advantage is that the terahertz systems we implemented in this thesis allowed for measurement of refractive indices. Thus, by examining the change in refractive index one can have an idea of the flow of nanoparticles though the microchannel. This way of understanding nanoparticle flow in a microchannel is completely novel (eliminates the use of fluorescent particles and optical detection methods) and to our knowledge has not been implemented before in the open scientific literature.

The terahertz system that was used utilized pulses of far-infrared radiation to probe the nanofluid systems. Terahertz Time-Domain Spectroscopy (THz-TDS) has evolved into an excellent tool for the investigation into the properties of bulk or even nanometer sized materials [18]. Even though the THz wavelength is much larger than the size of NPs, it can still be used to analyze a group of NPs since metals are near perfect reflectors in the far-infrared [18].

The interest in the THz range gained much attention in the early 1960's when researchers gave importance to the THz region of the electromagnetic spectrum [19]. In these years, there were few studies for generating and detecting THz radiation. By the late 1980's, with improvements in various laser technologies such as ultrafast lasers with femtosecond pulse durations generation and detection of coherent broadband THz radiation became probable. This method of generation has become commonly available and has spurred the development of novel THz generation techniques. By implementing generation and detection of THz pulses using photoconductive antennas based on optical rectification techniques, Auston and Cheung [20] developed the first THz-TDS system in 1985. After this step, many methods were developed for the generation and detection of THz radiation.

The THz region lies between the mid-infrared and the microwave frequency range. The frequency of 1 THz corresponds to photon energy of 4.1 meV, a wavelength of 300 μm or 0.3 mm, to a wavenumber of 33 cm^{-1}, time duration of 1 ps and a temperature of 48 K. THz fields have wavelengths extending from 3 mm (0.1 THz or 100 GHz) up to 30 μm (10 THz) [21]. Historically, this part of the electromagnetic spectrum is known as the "THz Gap" [21].

It has been a big challenge to combine optics and electronic techniques for generation and detection of THz radiation.

One of the major advantages of THz-TDS is that the transient THz electric field is measured and therefore, the constituent elements of the pulse which are the amplitude and phase that have connection with the absorption coefficient and the refractive index of the sample can be determined [19, 22]. Another advantage is that in this range wavelengths are long enough not to be absorbed by non-polar, non-metallic materials. The THz region is known for having absorption features (fingerprint spectra) of many materials [2].

Different types of materials have different optical properties in the THz region. Rotational and vibrational properties of highly absorptive materials can be determined using THz spectroscopy. THz is sensitive to dipole structures as polar molecules show high absorption in this frequency region. Metals are opaque due to their high reflectivity at THz frequencies. On the other hand, polymers (Teflon, TPX etc.), dielectrics (quartz, glass, plastics, paper, clothes, wood etc.) and semiconductors (silicon, germanium, gallium arsenide, etc.) are mostly transparent materials at THz frequencies [21]. It is also important to note that THz radiation is safe for humans due to its low photon energy and also is nondestructive to samples [23] and can be used safely for characterizing explosives [24] and flammable fluids [25].

In this thesis, a THz Time Domain Spectroscopy (THz-TDS) driven by a sub-20 fs Ti: Al_2O_3 laser source was constructed to investigate the properties of nanofluids. The system uses a photoconductive antenna for THz generation and a 2 mm thick <110> ZnTe crystal for THz detection based on the electro-optic method. Off-axis parabolic metal reflectors and TPX (polymethypenetene) lenses were used to focus and collimate the broad THz frequency range onto the sample which was a nanofluid suspended in a quartz cuvette. The nanofluid samples were created at the research laboratories of the National Nanotechnology Research Center (UNAM) located at Bilkent University, Ankara, Turkey. The reserach team led by Dr. Bülend Ortaç created the nanofluid suspensions using high energy per pulse laser beams focused on various bulk metals in 2-proponal liquid. Subsequently measurements were performed on these nanofluids placed in 2 mm path length quartz cuvettes. It was found that the THz pulsed radiation is shifted backward in time for certain nanofluid suspensions as compared to the propagation of the pulse through the liquid alone. The sensitivity of the THz pulse to these nanoparticles as seen in our measurements allowed us to estimate the particle concentration after modeling the dielectric function of the nanofluidic sample.

The outline of this thesis is as follows: In chapter 2, Terahertz Time Domain Generation and Detection Methodology is explained with a discussion on the challenges of detecting nano particles with THz waves. Furthermore, calculation of index of refraction and absorption of bulk materials are discussed.

In chapter 3, the system that was constructed and the experimental methods employed are explained in detail. The preliminary work done to select the base fluid for the nanofluid solution and the nanoparticle production methodology and the sample characterization techniques are also explained. Results are given for various metal nanoparticles in the base fluid chosen for THz studies. The observed negative shift of the THz pulse through certain samples is discussed. In chapter 4, the negative shift of the THz pulse is explained using theory based on the propagation of electromagnetic waves through dielectric and conducting interfaces. After modeling the dielectric function a method is developed to arrive at the particle concentration in the nanofluid sample. In the last chapter, the results observed for metal nanoparticle suspensions is summarized and challenges and fallbacks of this novel method is discussed.

CHAPTER 2

THz TDS GENERATION AND DETECTION METHODOLOGY

In this chapter, Terahertz Time Domain Generation and Detection Methodology is explained. In this thesis work we have constructed a photoconductive antenna generation-electro-optic crystal detection system for the investigation of nanoparticles in the THz region. In this chapter we will explain the THz generation and detection phenomena by focusing on photoconductive antenna (PCA) method based on GaAs for THz generation and electro optic (EO) method for THz detection based on <110> oriented ZnTe crystal.

2.1. THz TDS GENERATION and DETECTION TECHNIQUES

THz radiation generation techniques can be grouped into two as pulsed wave generation and continuous wave (CW) generation. Furthermore, both methods can be subcategorized into specific generation methods. Optical rectification is a technique which involves the mixing of like-high frequency components on an artifical or natural medium to generate a DC field-typically the THz field. This technique has been utilized with dielectrics, semiconductors and organic materials [26,27,28]. On the other hand, THz can also be generated using the controlled motion of free-carriers in semiconductor devices. Some notable examples include, transient photoconductive switching technique by using photoconductive antenna structures, surface depletion field method from semiconductor surfaces and by using tunneling effect of electron wave packets from quantum semiconductor structers [29, 30, 31]. Specifically CW generation methods have focused on photomixing by using photo conductive swtiching, difference frequency generation from nonlinear crystals, frequency multiplication of microwaves by use of Schottky barrier diodes are some examples as seen in the literature [32, 33, 34, 35].

The energy of THz waves are typically too low to measure directly using room-temperature detectors (RT~20°C~25meV or 6THz). That is why methods have been developed to measure the radiation indirectly (ie. its affect on another system is measured) or devices

have been constructed that is exteremely sensitive to these low energies and in most cases these devices work at cryogenic temperatures. In this effort to measure this radiation source with high accurascy many methods have been developed over the last 30 years.

THz radiation detection techniques can also be grouped into two as coherent detection where amplitude and phase of the incident radiation is detected and incoherent detection where only the intensity is measured. Coherent detection is the most widely used technique as the phase and amplitude has great importance in spectroscopy.

Free space electro-optic (EO) sampling, photoconductive switching for pulsed THz radiation and photomixing, heterodyne detection for continues wave THz radiation are the widely used for coherent detection techniques. On the other hand Bolometers, Golay cells, and pyroelectric devices are some examples for incoherent THz detectors [36, 37, 38].

2.2. PHOTOCONDUCTIVE ANTENNA METHOD FOR THz GENERATION

A PCA is a device based on a semiconductor that shows an increase in the electrical conductivity as it interacts with light. In a femtosecond time scale the interactions between optical pulse and the semiconductor cause generation and detection of THz pulses [39, 40].The general aim for generation of THz radiation is optical excitation in a semiconductor and changing the conductivity of the material. Once the THz field is generated the structure of the device should allow for the THz field to be collected and harnassed in the experimental set-up. To acoomplish this, the starting point is the formation of an antenna structure on a substrate material which will allow for the THz field to be generated solely by carriers confined within a small region. Once, generated the field is allowed to oscillate at a nominal frequency given by the width of the antenna structure and finally the point like generation of THz radiation needs to be collected, typically by an lens, from the structure. In summary, an antenna structure consists of a semiconductor substrate, metal electrodes in a dipole configuration, and a hemisphere typically made out of a material suitable for THz radiation to collimate the THz beam.

An example used typically is thedipole antenna and the coplanar transmission line which connects the dipole antenna to the contact pads that are all constructed on a semiconductor substrate that has a band-gap energy less than the photon energy of the visible excitation

pulse. The antenna typically has a small gap about a few μm at its center. The top view schematics of the basic structure of a photoconductive antenna is shown in the figure 2.1.
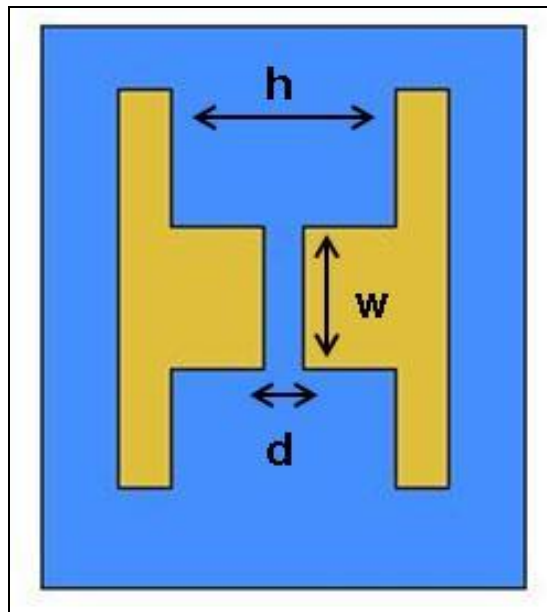
Figure 2.2.1. Top-view of the photoconductive antenna [41]

Here; h is the length of the antenna which varies from 10 to 200 μm for most of the antenna structures-in an ideal case it determines the peak frequency of the emitted radiation, w is the distance between the electrodes which forms the center gap (d) which is a few μm at its center. The center gap is related with the spot size of the optical pulse that is focused onto the gap [42,43].

The resistance of the antenna gap is expressed as $R(t) = \frac{w}{\sigma(t)A}$, where A is the crossectional area and σ is the conductivity [44]. When there is no optical pulse incident the resistance of the antenna structure is very high and can be on the order of mega ohms.

THz radiation is generated from a PCA as the photoconductive gap is illuminated by a femtosecond laser pulse where the photon energy equals to or greater than the band gap energy of the semiconductor material [45] as shown in Figure 2.2.
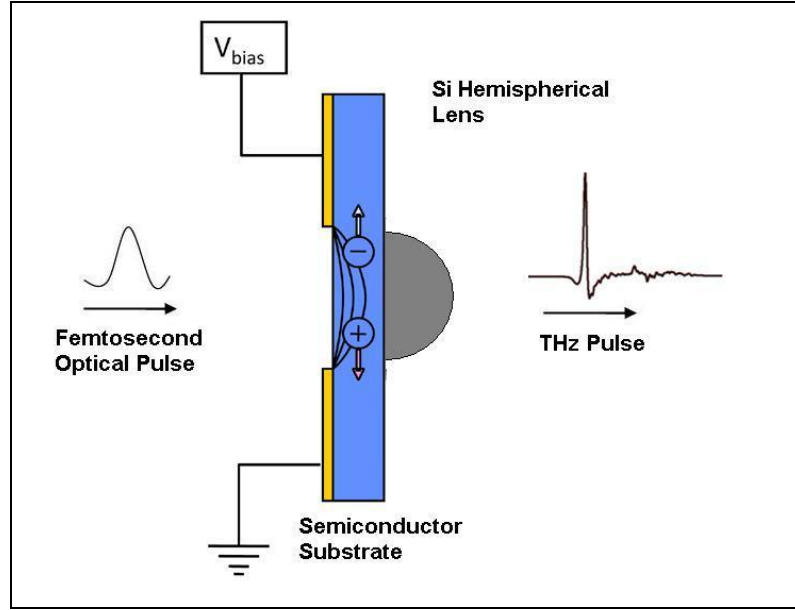
Figure 2.2.2. Schematic view of the photoconductive antenna

A bias voltage is applied on the metal electrodes. An electrone hole pair is formed in the conduction band of the substrate semiconductor as a femtosecond optical pulse focuses to the gap formed by the distance between the electrodes resulting in a photo current as a function of time in the dipole structure as the free carriers are accelerated by the applied bias voltage. The pulsed photocurrent amplitude depends on the applied bias voltage and the pump laser intensity and increases linearly. The radiation power also increases with the applied bias and pump power. The derivative of this photo current gives the resultant EM radiation in THz frequency range. To prove this, one can use a simplifed model where the radiation from this antenna stucture can be modeled as a Hertzian dipole. Thus, the electric field generation from a Hertzian dipole antenna can be formulated as;

$$E(r,t) = \frac{l_e}{4\pi\epsilon_0 c^2 r} \frac{\partial J(t)}{\partial t} \sin\theta \propto \frac{\partial J(t)}{\partial t} \qquad \textbf{2.1.}$$

Where $J(t)$ is the current in the dipole, l_e is the effective length of the dipole, ϵ_0 is used for the dielectric constant in vacuum, c is the velocity of light in vacuum and θ is the angle from the direction of the dipole and r is the distance from the dipole (r is greater than the emitted wavelength-far field) [46]. This entire process takes place in a subpicosecond time interval, proportional to the width of the excitation pulse. Optical pulse acts as a switch in the PC antenna. The carrier life time of the substrate is determined by the switch-off time where as the switch-on time relates the laser pulse duration to the substrate properties which are affected by carrier mobility [47]. High carrier mobility and high breakdown voltage play a

great role in a PC antenna [48]. Antenna structure geometry also affects the PC antenna quality. Stripline, dipole, offset dipole are some of the examples for antenna geometries [41, 49].

Depending on the wavelength of the excitation pulse different maetrails can be used as a substrate medium for the antenna structure. Low temperature grown gallium arsenide (LT-GaAs), radiation damaged silicon–onsapphire (RD-SOS), chromium-doped gallium arsenide (Cr-GaAs), indium phosphide (InP) are some of the commonly used substrates for PC antenna [50].

Finanlly the radiation is collected by a lens on the backside of the subcstrate material. The lens material has to work in the THz freuqency range and since the substrate material of the antenna is typically a semiconductor, the lens is also chosen from material with a similar refractive index so that reflective losses are at a minimum at the interface. Typically, a hemispherical Si lens with high resistivity is attached to the PC antenna to collimate the THz beam. Si is a good material as a collimating lens for its uniform refraction index and low absorption coefficient at THz frequencies. The emitter is attached in such that the focus of the lens concide with the emmiter zone so that the losses due to the internal reflection are minnimized. This substrate-lens design also minimizes the spherical aberration or coma diffects [51, 52].

2.3. DETECTION OF THz RADIATION BY USING ELECTRO OPTIC CRYSTAL

Detection of a THz-pulse beam with electro-optic crystals relies on the linear electro-optic effect which is based on non-linear interactions but the formulation scales linearly with the applied THz electric field. As the electric field is applied to the electro-optic crystal (isotropic crystal), the polarization of the crystal changes along a direction, altering the index of refraction as well along specific directions. This results in a phase difference between various components of the electric field vector for a visible beam propagating though the crystal. This effect is known as "linear electro-optic effect" (Pockel's effect). For detection of THz pulses, these processes are nonlinear optical techniques and occur only in crystals which are transparent to THz and optical pulses [53].

11

Depending on the wavelength of the exciting radiation, crystals such as GaSe, LiTaO3, GaP, ZnSe and ZnTe are some examples of widely used crystals for electro-optic detection[54].

For our system, the visible excitation (around Near IR or 800nm center wavelength) allowed for the use of <110> oriented ZnTe as the electro-optic detection crystal. ZnTe has a large electro-optic coefficient and that is why it is very effective in THz detection. Furthermore, its refractive index in the far IR is comparable to the near IR, so that the THz and NIR pulse travel at nearly same speed thus making this crystal very suitable for THz detection [55].

The process of detection is discussed in detail below:

Optical pulse and THz pulse are carefully aligned to propagate along the same direction though the crystal. As the linearly polarized optical beam passes through the electro-optic crystal with the THz beam, the electric field of the THz beam induces a change in the index of refraction which accounts to a rotation of the electric field of the optical pulse by an angle which is proportional to the applied field [56, 57]. In other words the birefringence due to the THz pulse on the crystal is sensed by the optical pulse such that the optical pulse changes its polarization. The minor and major components of the polarization are detected by photodiodes. The induced field birefringence is maximum when the THz electric field and the optical polarization is parallel on the [110] ZnTe crystal. The time duration of the optical pulse, second order susceptibility of the detector medium, transparency of the crystal at THz frequencies and optical frequencies are the limting factors in this detection method [58, 59].

After the electro-optic detection crystal, a quarter wave plate and a Wollaston prism is placed. A quarter wave plate converts the linearly polarization of the optical pulse into circular polarization then the Wollaston prism after the quarter wave plate splits the circularly polarized light into two components which are orthogonal and linearly polarized to each other and each component is detected by a balanced photo-receiver as shown in Figure 2.3.
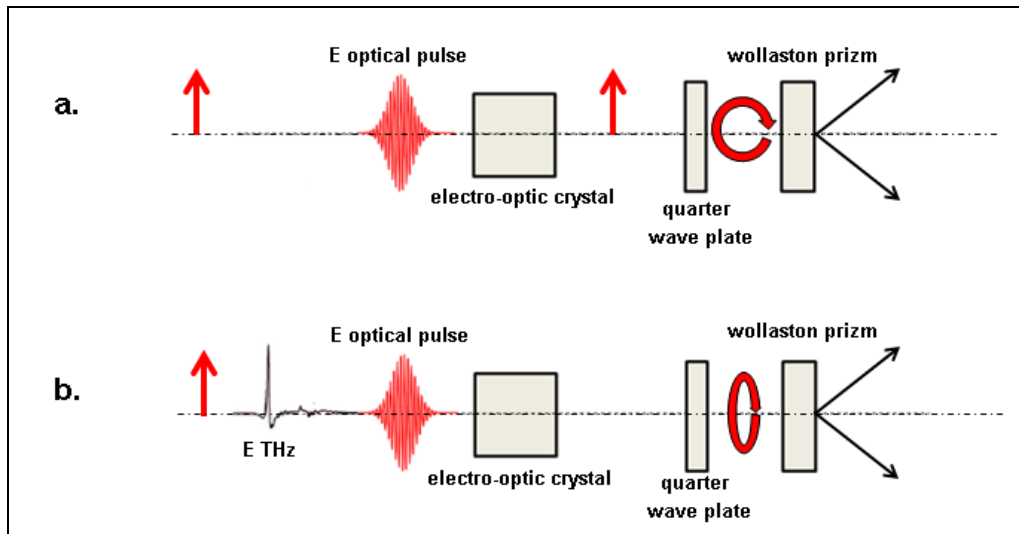
Figure 2.3.1. Electro-Optic Sampling.

2.3.1.a. In the absence of THz beam, the components of the polarized light become equal and the balanced photodiodes produce null current that the two modes of the propagating light are subjected to the same phase retardation.

2.3.1.b. The THz field induces birefringence in the electro-optic medium through the Pockel's effect and rotates the polarization of the optical pulse and a current which is proportional to the THz field and direction at the balanced photodiodes that the components of the optical beam propagating through the crystal are subjected to different phase retardations.

Photoconductive antenna method for THz generation and electro optic method for THz detection is a proven widely used broad band detection and generation scheme for that we have constructed an antenna-crystal system for the investigation of nanoparticles. The constructed system and the experimental methods employed are explained in detail in chapter 3.

CHAPTER 3

MEASUREMENTS ON NANOFLUIDS USING THz RADIATION

THz Time-Domain Spectroscopy is a useful technique to measure optical properties such as the absorption coefficient and refractive index of various materials.

In a time-domain THz measurement both amplitude and phase data is obtained by measuring the electric field in time. This helps us to calculate the absorption coefficient and refractive index of various materials. Nanofluids are liquids whose absorption coefficient as well as refractive index is thought to change with the addition of the nanomaterials or nanoparticles. In order to measure differences between the nanofluid and fluid without the nanoparticles we constructed a THz Time Domain Spectrometer where a photoconductive antenna was used for THz generation and a <110> ZnTe crystal was used in the electro optic (EO) method for THz detection.

In this chapter first a detailed description of the THz Spectrometer is given where we describe the experimental setup. Following the methods used to calculate the absorption coefficient and refractive index, experimental data and results are discussed. Here we give experimental results and investigate the transmission of THz pulses through a suspended nanomaterial solution. Finally the absorption coefficient and refractive index of various nanofluid samples are calculated and the results are analyzed.

3.1. THz TIME DOMAIN SPECTROMETER (THz-TDS)

We constructed the THz-TDS system in a class 10000 clean room located in the basement of the Physics department at Middle East Technical University, Ankara, Turkey. The system was constructed on a vibration isolated optical table and the room was air-conditioned to operate the system at a nominal temperature of 20 °C. Photoconductive antenna (PCA) method was used for THz generation and electro optic (EO) method was used for THz detection. From here on this system is referred to as "Antenna-crystal System".

The THz-TDS system consists of many optical and electronic components. Optical components are mirrors, lenses, filters, a wave plate and Wollaston prism. A function generator, balanced photodiode, lock-in amplifier and personal computer are the electronic components of the system. The System that was constructed is shown in a detailed schematic in Figure 3.1.1.
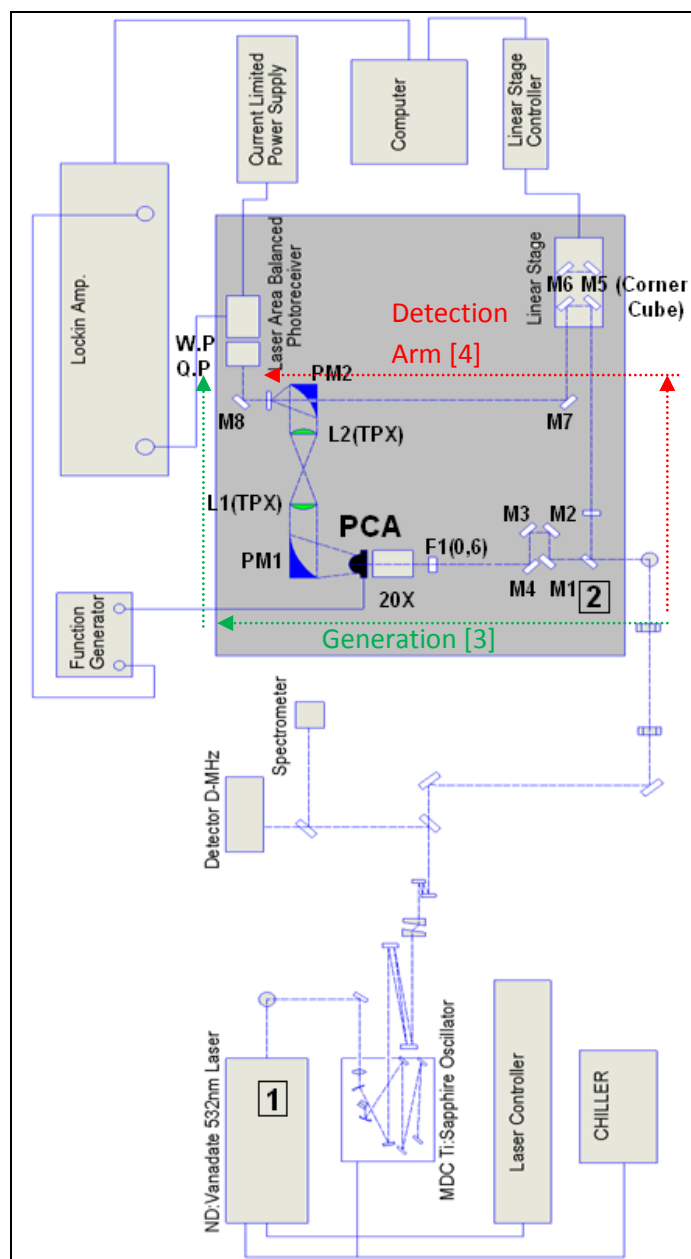
Figure 3.1.1. The Constructed THz-TDS System Schematic.1: Verdi V-5/2: Beam Splitter/ 3: Generation Arm/ 4: Detection Arm

The components shown in Figure 3.1.1. are listed below:

- 1.Ti: Sapphire Mode-Lock Laser (Coherent Verdi-V5 pumped Femtosource Femtolaser Scientific XL-Pro)
- 2.Beam splitter
- 3.Generation arm
    - M1, M2,M3,M.4: Mirrors/ F1: Attenuation filter (0,6)/MITUTOYO 20x objective (PLAN)/ Batop PCA-40-05-10-800 Photoconductive Antenna(PCA)/ PM1 – PM2: Off axis parabolic mirror (OAPM)/ L1 - L2 : Polymethylpentene (TPX) lenses with 50mm diameter and 100mm focal/ Function Generator
- 4.Detection arm
    - Attenuation filter (0.3)/ Corner Cube(M5,M6) and translation stage with motor controller Thorlabs BSC 103/ M7: Mirrors/ Lens with focal length 200 mm/ <110> cut ZnTe crystal
- 5.Data Acquisition components
    - M8: Mirrors/ Q.P : $\lambda/4$ Quarter wave plate/ W.P : Wollaston Prism/ New Focus 2307 Large-area Balanced Photoreceiver/ Stanford Research System SR830 Lock-in Amplifier/ Personal Computer with software

Below we give a more detailed explanation of the components listed above:

The Verdi V-5 laser is a compact solid-state diode-pumped, frequency doubled Nd: Vanadate (Nd: YVO4) laser that provides single-frequency green (532nm) output at power levels greater than 5 watts. The laser head is mounted on water cooled heat sink which is connected to a chiller.

This diode pumped Nd: Vanadate laser is used to pump a mirror-dispersion-controlled Ti-Sapphire oscillator. Approximately 4W of green pump power results in a beam with a center wavelength near 800nm with an average power of roughly 300mW. The cavity is tuned to emit pulses at a repetition rate of 75MHz. This corresponds to a cavity length of roughly 4m. Each visible pulse is compressed to minimize dispersion using chirped mirrors. Outside the oscillator extra dispersion compensation is performed to minimize the effects of the output coupler. Each pulse spectrum and width is measured. The spectrum of each pulse is measured with a polychromatic visible spectrometer connected to a laptop computer (Figure 3.1.2.a). The pulse width of each pulse is measured with the Femtometer PC-DAQ pulse characterization system. These pulses are measured by using a dispersion minimized broad-band auto-corellator. (Figure 3.1.2.b).

16
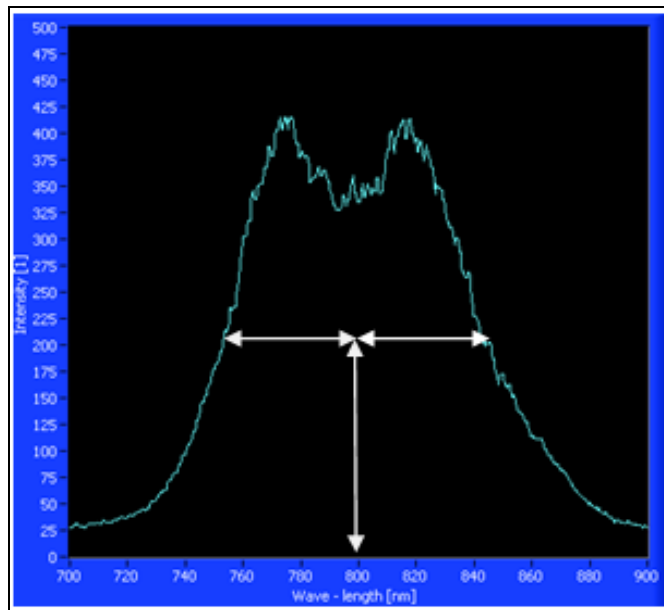
Figure 3.1.2.a. The spectrum of each pulse measured with a polychromatic visible spectrometer, the center of the spectrum is shown by arrows and the intersection point corresponds to the center wavelength of 800nm.
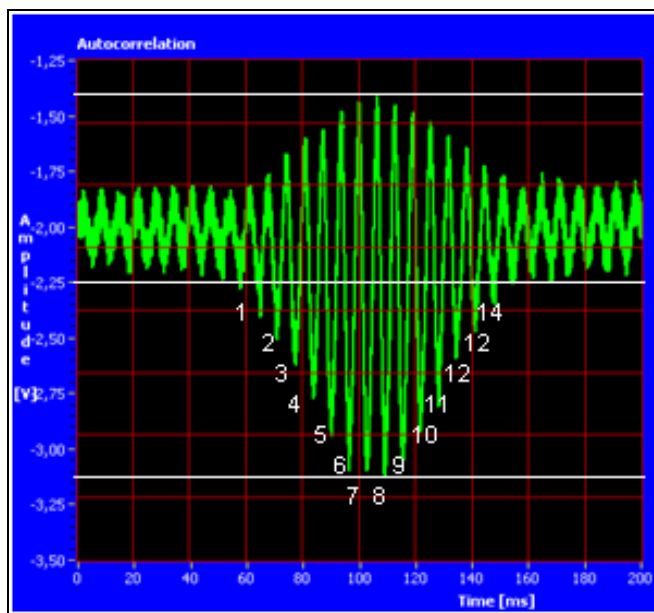
Figure 3.1.2.b The autocorrelation data measured by dispersion minimized broad-band auto-corellator, the number of fringes above 50% line are noted with numbers from 1 to14.

Below we give a detailed analysis of how one obtains the pulse width. We note that calculating the pulse width from the spectrum of the pulse is not as reliable a method as the autocorrelation method for a number of reasons: The multi-mode fiber used to collect the

17

light from the laser will introduce loss and different wavelengths will couple differently to the spectrometer. An example calculation is shown below. Typically, the pulse width of the Ti: Sapphire oscillator used to pump the THz-TDS system is around 20fs.

Evaluation of the Fringe Distance $\Delta\tau$:

From the center of the gravity of the spectrum λ_0 the fringe spacing $\Delta\tau$ can be estimated. $\Delta\tau = \lambda_0 / c$ in the spectrum the center wavelength amount to 800nm; therefore the fringe spacing is 2.669 fs.

Estimation of the number of fringes:

The total number of fringes N is estimated by counting the number of fringes above 50% line. Linear interpolation can be used to determine the percentage of the fringe –period at the 50% line. N = 0.05+14+0.15=14.2

Evaluation of the pulse duration:

The de-convolution factor assuming a sech^2 pulse shape B = 1.897
Pulse Duration (FWHM)= N* $\Delta\tau$ / B = 14.2*2.669/1.897 = 20 fs

The given specifications of the mirror-dispersion-controlled Ti-Sapphire oscillator and the diode pumped Nd: Vanadate laser are listed in Table 3.1.1. and Table 3.1.2.

Table 3.1.1. Specifications of the mirror-dispersion-controlled Ti-Sapphire oscillator

MDC Ti:Sapphire Oscilator	
Femtosource Scientific	sPRO
Pulse Duration	<12fs
Spectral width	>75nm
Output Power	>300mW
Output Energy @ 75 MHz	>4nJ
Pump Beam Diameter	2mm(1/e^2), TEM$_{00}$
Pump Power @ 532nm	5W
Cooling Water	18-22 °C, 10W

Table 3.1.2. Specifications of the diode pumped Nd: Vanadate laser

Verdi V-5 laser	
PARAMETER	SPECIFICATION
Output Power	5 Watts
Wavelength	532nm
Beam Diameter	2.25mm±10%
Beam Divergence	<0.5mrad
Power Stability	± 1 %
Noise	>0.02 %rms
Polarization	<100:1, vertical, linear
Linewidth	<5MHz rms
Point Stability	<5μrad/ºC

We note that the values listed above are expected values, and due to day to day operation of the system we obtain different values. For all the measurements outlined in this thesis, the Ti:Sapphire oscillator average laser power was near 330mW, at a repetition rate of 75MHz and pulse duration was near 20fs.The center wavelength of each pulse was near 800nm.

The laser beam is transported through a couple of steering mirrors and two irises to a beam splitter. The steering mirrors and irises allow us to direct the laser beam consistently into the THz-TDS system. Since there are many optical components in a Ti: Sapphire oscillator, day-to-day operation of the laser will result in minute deviations of the beam. Over large distance this can be an important factor.

To negate this we use two mirrors and two irises so that the beam always travels along the same path before entering the THz-TDS system. The beam splitter is a 25/75 split, where the most power is directed towards the generation arm. Generation and detection paths are shown in Figure 3.1.3. :
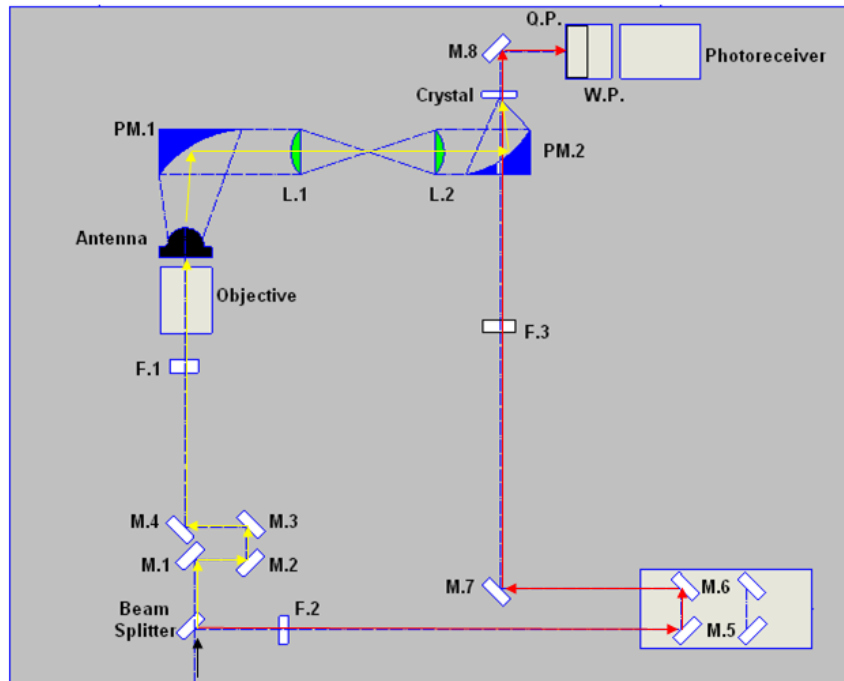
Figure 3.1.3. Schematic: The Generation Path (yellow arrows) and the Detection Path (red arrows) schematic of the constructed THz-TDS system. Laser pulse is divided into two paths by using a 25:75 beam splitter; one arm is for the generation and the second arm is for the detection: Generation arm follows the path which is shown with yellow arrows from the beam splitter to the generation antenna and then the generated THz wave is focused to the crystal by using the parabolic mirrors. Detection arm follows the path which is shown with red arrows from the beam splitter to the crystal.

In order to detect the THz radiation, the visible and the THz beam should reach the detector (electro-optic crystal) at the same time. Four mirrors (M1, M2, M3 and M4 in figure 3.1.3) were placed in the generation arm to equate the path length with the detection arm.

In the generation arm, after these four mirrors, the incoming power of the laser beam was reduced to the optimum operation conditions of the PC antenna by an absorptive natural density filter which absorbs 75% of the incoming beam. This way we insured that we would not damage the PC antenna. Incident laser pulse was focused to the antenna gap with a 20x objective (MITUTOYO NIR ACHROMAT OBJECTIVE). PC antenna was placed on a xyz translation stage for precisely aligning the focused beam and to compensate laser fluctuations.

Butterfly type photoconductive antenna which is mounted on a Batop PCA-40-05-10-800 is used for THz Generation. The electrodes along with the substrate form a square chip which

is glued on hyper hemispherical silicon lens made of high resistivity float zone silicon (HRFZ-Si) that transmits the signal independent of frequency which shown in Figure 3.1.4. Silicon lens also reduces the divergence of the radiated pulse.

Figure 3.1.4(a)	Figure 3.1.4(b)	Figure 3.1.4(c)
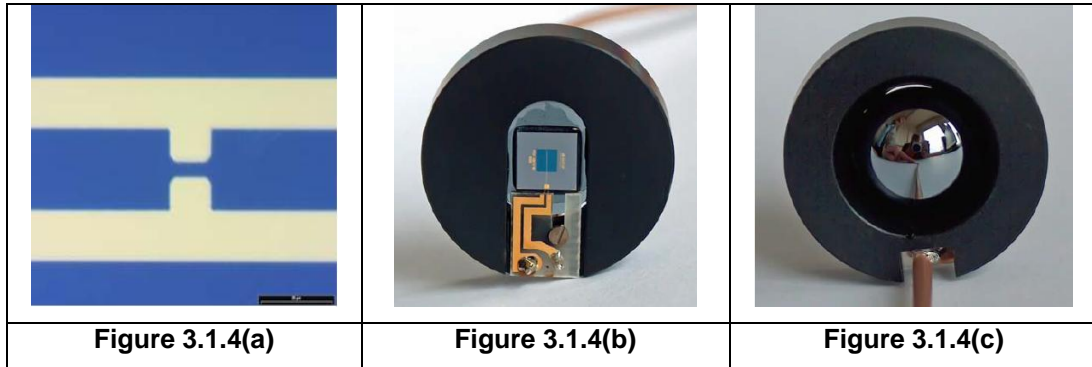
Figure 3.1.4. The antenna gap structure (a) and the square chip (b) which is glued on hyper hemispherical silicon lens(c)

For the THz Generation; peak to peak 15V Sine wave with 1 kHz frequency was applied to the antenna from the function generator. A reference signal was also connected to the lock-in amplifier so that phase sensitive voltage measurements could be performed.

The radiation is collimated(PM.1, 50mm diameter, 50mm focal distance 90 degree off-axis parabolic mirror) from the antenna and focused(PM.2, 62,5mm diameter and 119,4mm focal distance off-axis parabolic mirror) on to the ZnTe crystal(2mm thick <110> orientation) by off-axis electro-formed nickel parabolic reflectors. In the detection arm, the reflected beam from the beam splitter is directed to the corner cube (M5 and M6) which is placed on a computer controlled translation stage for the delay line. This delay line uses a stage and controller obtained from THORLABS, with a scan distance of 50mm and minimum step size of 1 micrometer.

This delay line provides time and path difference between optical and THz beam in order to profile the THz waveform.

In the detection arm, after reflecting through M7. the beam is focused on to the ZnTe crystal by a 200mm focal lens and passes through the drill hole which is parallel to the focusing axis of the reflector PM.2. This hole in PM.2 results in a loss of power in the collimated THz beam, however this is necessary so that the THz pulse and visible detection pulse travel the same distance in the detection crystal. After the ZnTe crystal the beam is directed by M8. to

the Balanced Photo Diode after passing through the Quarter Wave Plate (Q.P) and the Wollaston Prism (W.P.).

The electro-optic detection crystal is isotropic, and when the THz field is incident on the crystal it is birefringent. The quarter wave plate changes the polarization of the optical beam and the Wollaston prism separates the polarization into its components.

The QWP ensures that when the THz pulse is not present on the crystal, the visible detection pulse will be circularly polarized after the detection crystal. Thus the horizontal and vertical components of the beam will cancel each other out in intensity on the balanced detector. This means that when the THz pulse is not present and we see no signal.

If the optical beam and the THz beam are both incident on the crystal, then the polarization after the crystal will be elliptical. The QWP just adds a 90 degree phase shift to this polarization. Now the horizontal and vertical components of the polarization have different intensity. This difference is detected by the balanced photodiode.

Since the electric field of the THz waveform is changing on a time scale of picoseconds and the visible detection pulse is 20fs, we can effectively probe the changes in the THz electric-field by varying the delay between both pulses with the aid of the motor controlled translation stage. The motor controlled translation stage is connected to the personal computer and the signal from the balanced photo detector is measured with the lock-in amplifier. THz field is amplitude modulated with the aid of the AC bias from the function generator. This allows us to reduce effects of noise and detect the signal from the balanced photo detector with the lock-in amplifier. As the stage is stepped and the path-difference between the generation and detection arm is varied on a scale of 1-20 microns per step we measure the strength of the THz electric-field as voltage data points collected with a personal computer running LabView software as shown in Fig.3.1.5.:
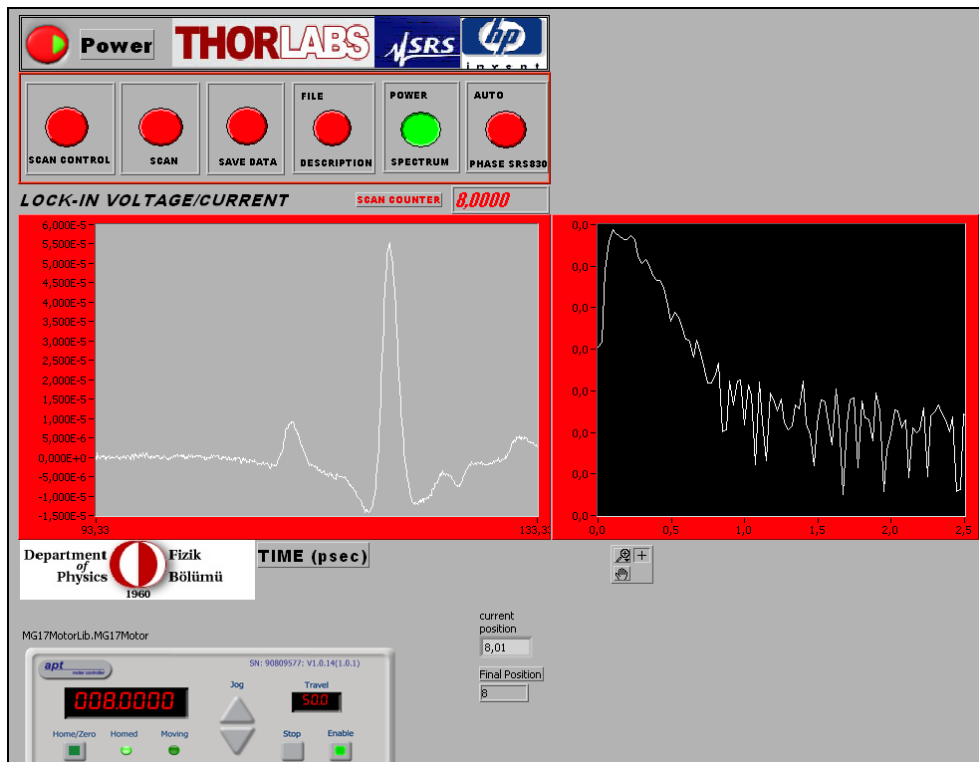
Figure 3.1.5.a. The LabView code user interface is shown above is used to manage the step size, time duration, and the scan distance. Program reads the voltage measurements from the lock-in as we move the stage in steps and plots the time domain data (the plot on the left) and plots the frequency domain (the plot on the right) by applying a FFT to the time-domain data set.
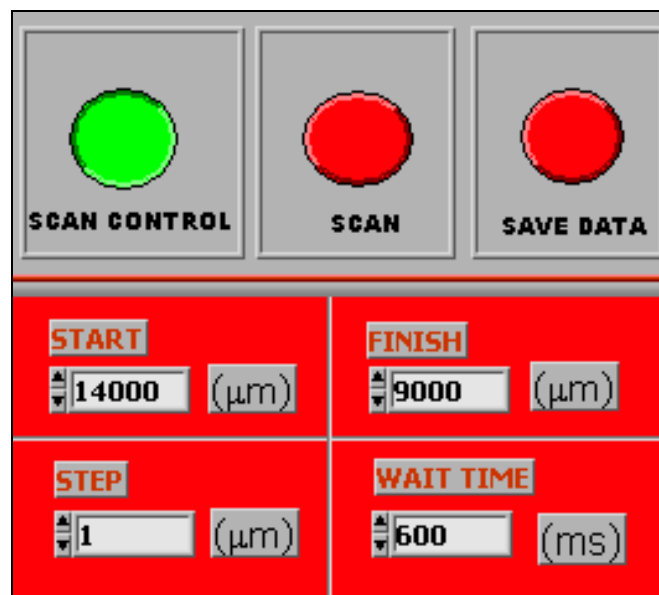
Figure 3.1.5.b. The LabView code user interface scan control parameters window.

23

The LabView code that was written controls the motor controller through a user interface and reads the voltage measurements from the lock-in as we move the stage in steps. This code helps us to manage the step size, time duration, and the scan distance which are put in by using the Scan Control Window as shown in Figure 3.1.5.b.

.

Step size is the measure of the distance travelled by the translation stage in one motion. This path difference also results in the time difference of the optical pulse which travels near the speed of light through air. The step size also tells us the maximum frequency we can detect after applying a Fourier transform to the time-domain data set (we actually perform a Fast Fourier Transform-FFT-as can be seen in fig 3.1.5).

Time duration is the amount of time that the motor delays between two consequent moves. It helps to synchronize the motor and the lock-in amplifier to prevent data losses. Basically, we ensure that we always take a measurement after the stage comes to a complete stop, this way our data is reproducible.

Scan distance is the length of distance travelled by the translation stage. The step size and scan distance give the total time of the motion. The scan distance also gives us a measure of the spectral resolution.

The voltage values gathered from the balanced photodiode are plotted with respect to the scan-time which gives the THz waveform in the time-domain. The code allows us to save the data in both ASCII and MS Excel file formats. Typically after the data is recorded we analyze the results using either Origin software or Matlab software.

To look at samples whose diameter is less than the collimated beam diameter of our THz beam (50mm coming from PM.1) we focus the beam using special lenses that are used to focus the THz radiation. In the experiment due to its transparency at THz frequencies two polymethylpentene (TPX) lenses with 50mm diameter and 100mm focal length are placed in between the off-axis parabolic reflectors to focus the THz pulse as shown in Fig. 3.1.6. This figure shows how we place the sample (quartz cuvette that houses liquid and liquid + nanoparticle) near the focus of the THz beam. It is important to note that at 1 THz (300 µm) the transmittance of TPX lens is 85%. The spot size of the THz beam was less than 1cm at the focus.
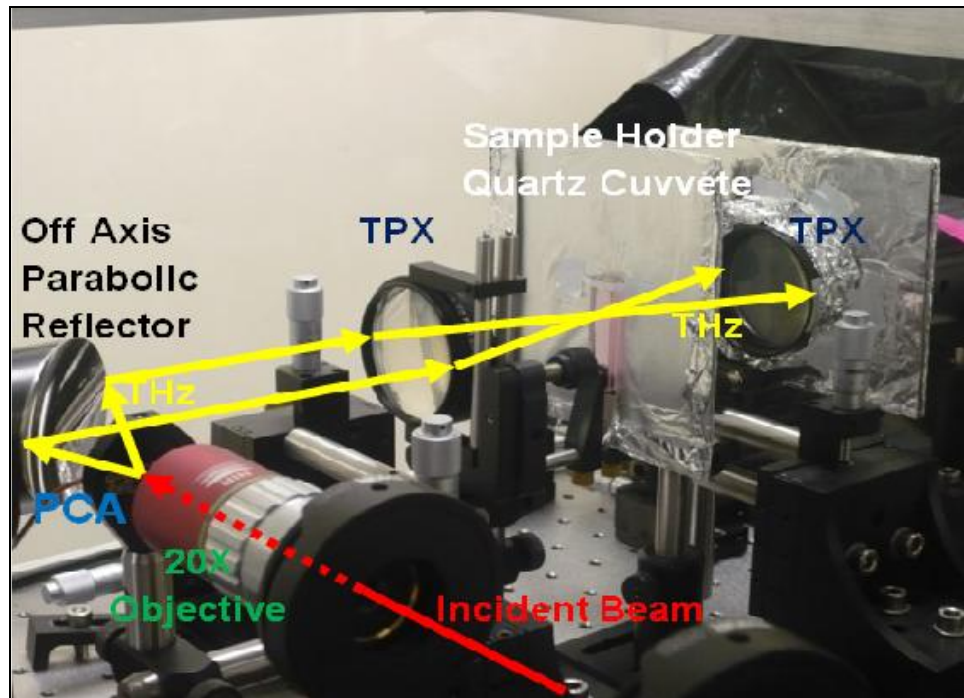
Figure 3.1.6. THz pulses are generated by PCA method. Two polymethylpentene (TPX) lenses are used to focus the THz pulse to the mid part of the quartz cuvette (Sample Holder) in between the off-axis parabolic reflectors. The area around the quartz cuvette was shielded with aluminum to block any unwanted THz radiation from the receiver system.

3.2. ANALYSIS OF THE TIME DOMAIN THz MEASUREMENTS

Measured time domain data can be analyzed by applying a Fourier Transform. Time domain data is basically the THz waveform, which is the detected electric field with respect to the delay time. The time dependence of the electric field can be converted into frequency dependence by Fourier Transform. Thus, the frequency dependent electric field can be expressed as;

$$E(\omega) \equiv A(\omega)e^{-i\phi(\omega)} = \int dt E(t)e^{-i\omega t} \qquad \textbf{3.2.1.}$$

where A (ω) is amplitude of the electric field in frequency domain, and ø (ω) is the phase of the electric field in frequency domain. As can be seen from the formula, Fourier Transform provides the frequency dependent amplitude (and thus the spectral power density) and phase information that are characteristic to THz Time Domain Spectroscopy. By using these parameters the absorption coefficient and the refractive index can be calculated.

In Figure 3.2.1. we show how the time-domain measurements are converted to the frequency domain by use of the Fourier Transform.
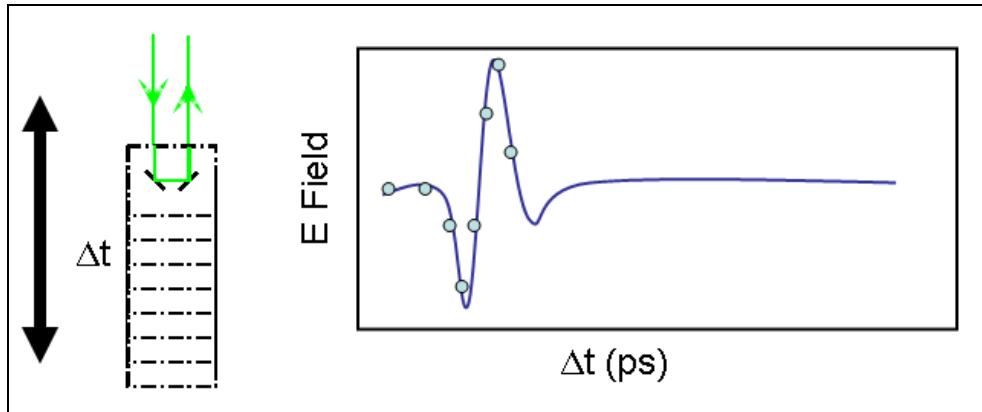
Figure 3.2.1. The Translation stage schematic on the left indicates the change in the optical path which is referred to as delay time. The measured E Field versus the time interval (Δt) plot is shown on the right [60].

Spectral range of the Fourier analysis is determined by the delay time. The amount of time it takes for the optical beam to travel 300 μm is approximately 1 ps. Thus, the change in the optical path can be referred to as delay time. The time interval (Δt) between each measurement defines the sampling rate (f=1/Δt). Spectral range starts from (-f/2) and ends at (+f/2). The spectrum is symmetric at the center frequency (f=0). Bandwidth of the THz system can be obtained from this analysis.

By applying Fourier Transform (FT) to the time domain data (both reference and sample waveform), spectral information is obtained, such as phase and amplitude. The comparison of the phase and amplitude within each reference FT and sample FT provides optical properties of the materials studied. Phase difference in general results in the refractive index, where power ratio results in power absorption coefficient.

Figure 3.2.2. Time domain data of the transmitted THz pulse which was calculated by zero padding the data. Zero Padding the data causes the following Fourier transform to apply an interpolation in frequency domain [82].

Figure 3.2.3. spectral information (unwrapped phase and amplitude) is obtained by applying Fourier Transform (FT) to the time domain data

The refractive index for a sample is complex and is composed of real and imaginary parts. n_r is real part and n_i is the imaginary part of the complex refractive index where k is the wave vect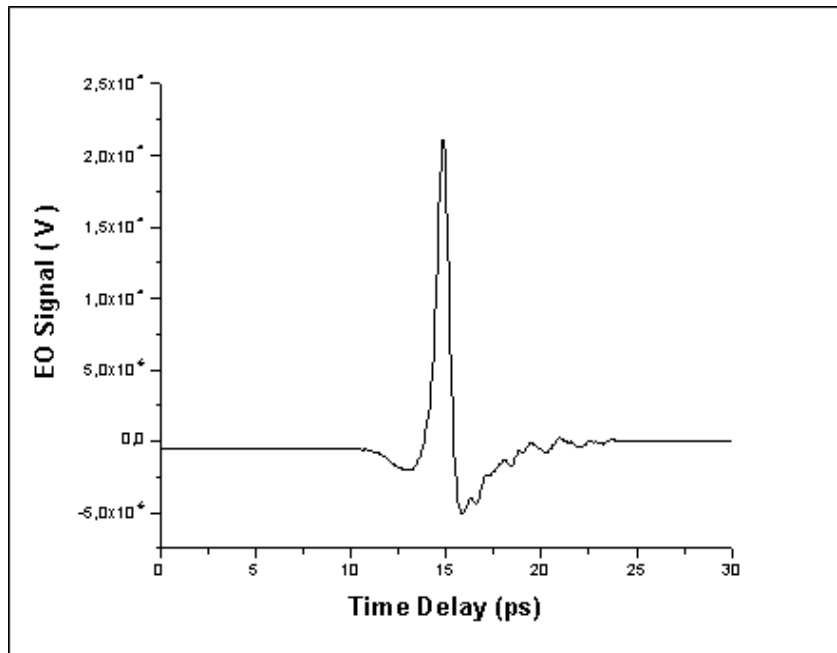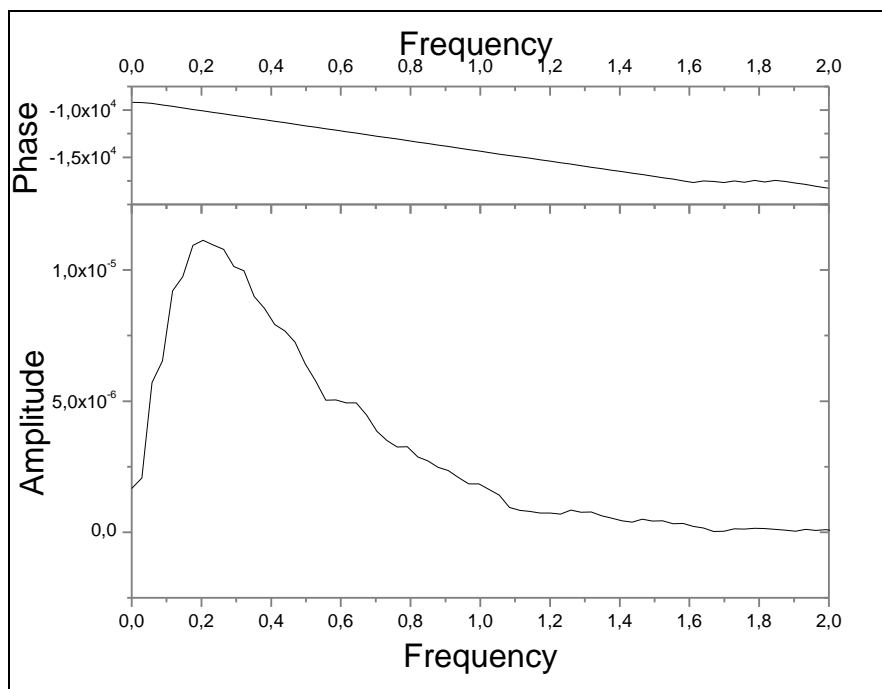or, l is the sample thickness, and $\varphi(\omega)$ is the phase. Here, the real part gives the delay through the sample and the imaginary part typically gives the absorption coefficient.

$$\tilde{n}(\omega) = n_r(\omega) - i n_i(\omega) \tag{3.2.2.}$$

And

$$E(\omega) = |E(\omega)| e^{i\varphi(\omega)} \tag{3.2.3.}$$

Then,

$$n_r = \frac{1}{kl}(\varphi(\omega,l) - \varphi(\omega)) \tag{3.2.4.}$$

$$n_i = -\frac{1}{kl}\left(\ln\left(\frac{E(\omega,l)}{E(\omega)}\right)\right) \tag{3.2.5.}$$

When the sample is present in the spectrum, it usually takes more time to travel through the sample for the THz pulse. As a result, when compared to the reference pulse, THz pulse that passes through the sample appears later. This causes the time difference in the waveform. This time difference results in the phase difference in the frequency domain. Typically this phase difference can be used to calculate the refractive index; this was the motivation behind studying nanofluids. The presence of a material in the fluid was expected to increase the refractive index. From these results one can obtain the contribution of the nanomaterial to the refractive index of the host medium and extract important parameters important to characterize the nanofluid. As will be shown in the following measurements, for some samples, instead of a positive delay with respect to the reference scan we see a negative delay which suggests superluminal propagation of the THz pulse when the sample is present. Furthermore, the positive delay that is observed for other samples is much less than expected. We discuss this phenomenon in chapter 4. Below the experimental results are given for various nanofluid samples. First the best base fluid for THz transmission measurements is determined. Second, the base fluid is used in forming suspensions of various metal nanoparticles. Afterwards, THz-TDS measurements are performed to obtain the power absorption coefficient and refractive index as discussed above.

3.3. NANOFLUID MEASUREMENTS

3.3.1. Determining the Base Fluid for THz Measurements

THz field interacts with polar molecules. Polar liquids tend to absorb the THz intensity, thus when studying such liquids researchers typically use very thin samples [61] Since we are trying to analyze nanoparticles in a host fluid it is important that we use a liquid that does not affect the THz pulse as much as it passes through. While this is an advantage due to THz transmission it can also be disadvantages for nanofluid suspensions, since the use of polar liquids tend to stop aggregation in such suspensions [62]. To choose the right polar liquid we performed measurements on a variety of liquids and tried to determine the best possible host before THz transmission measurements. Measurements were performed using a 2mm path length quartz cuvette whose width was 1cm. Measurements were taken for Ethanol (99,5%), Ethylene glycol(99%), 2-propanol (99,5%) (Isopropanol), methanol (95%) and distilled water.

Results are Shown Below:
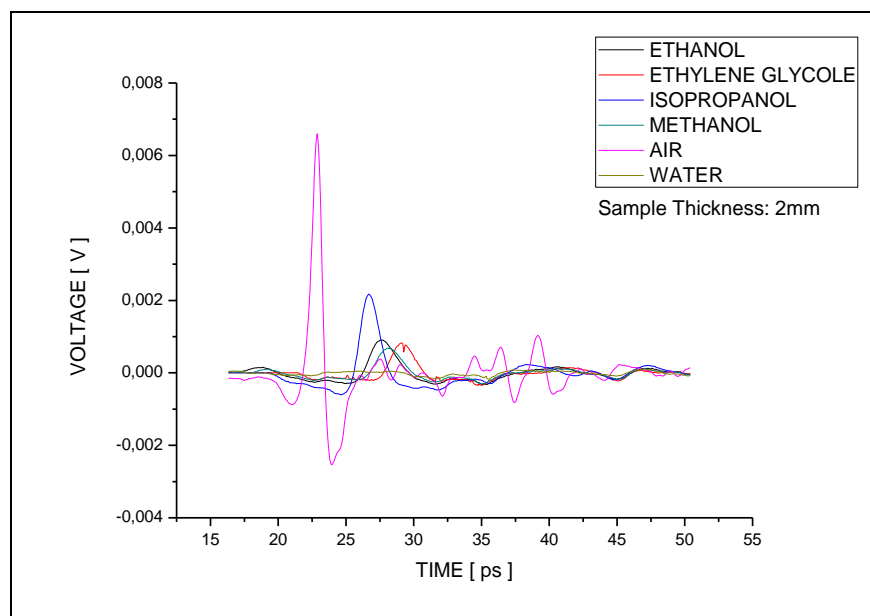
Figure 3.3.1.1.a. Time Domain Data for possible polar host fluids. As seen above 2-propanol has the maximum intensity when compared to other possible hosts.
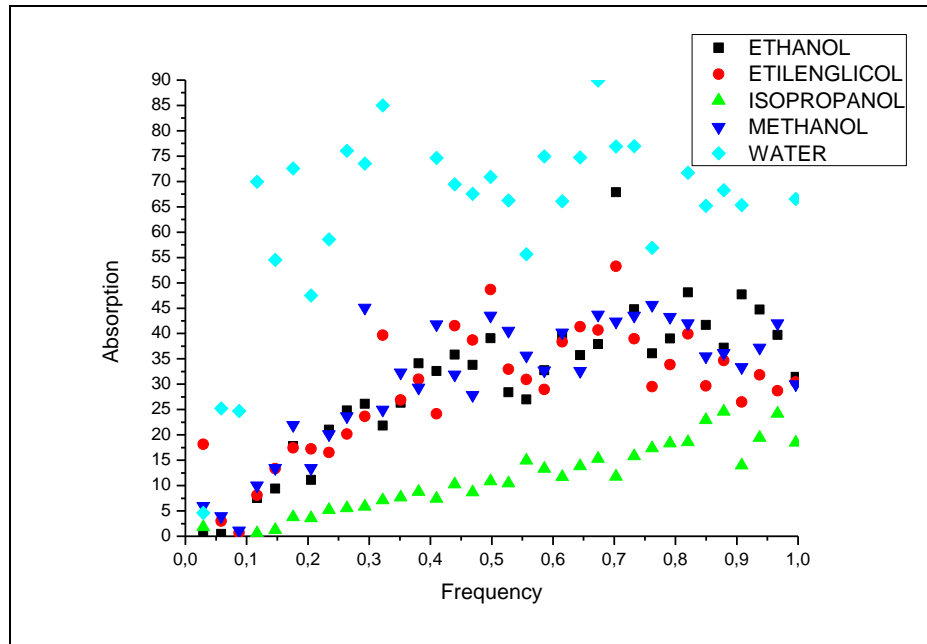
Figure 3.3.1.1.b. Power Absorption Data for possible host polar fluids. As seen above 2-propanol has the lowest absorption when compared to other possible hosts.

Table 3.3.1.1. Refractive Index and Transmission Data

SAMPLE	ΔV Peak to peak	Transmission %	ΔT±0.0333	Refractive Index	n-max	n-min	Δn
QUARTZ CUVETTE	0.0091257	n.a.	0	n.a.	n.a.	n.a.	n.a.
ETHANOL	0.0012163	13.32798287	4.76842	1.71526306	1.72527	1.70526	±0.01
ETHYLENE GLYCOLE	0.0010574	11.58745471	6.265137	1.93977052	1.94978	1.92977	±0.01
ISOPROPANOL	0.0027808	30.47173819	3.808126	1.571218945	1.58122	1.56121	±0.01
METHANOL	0.00094	10.30031463	5.262237	1.789335505	1.79934	1.77933	±0.01
WATER	0.0002414	2.645191935	3.736052	1.560407845	1.57041	1.5504	±0.01

As can be seen from the table above 2-propanol has the best transmission. We obtained the time-domain data sets with a step size of 20 microns which result in an error of +/- 0.0333ps per step. This standard deviation in step size can give us an idea of how precisely we can measure the refractive index of a medium. Since the 2-proponaol liquid has a positive delay

with respect to the quartz cuvette, by measuring the delay of the peak of the THz waveform we can gain an idea about how precisely we can measure the refractive index of the liquid.

By measuring the peak displacement in time and using the following formulas:

$$n = 1 + \frac{\Delta t \cdot c}{d} \qquad \textbf{3.3.1.1.}$$

$$n_{max} = 1 + \frac{(t + \Delta t) \cdot c}{2\pi d} \qquad \textbf{3.3.1.2.}$$

$$n_{min} = 1 + \frac{(t - \Delta t) \cdot c}{2\pi d} \qquad \textbf{3.3.1.3.}$$

$$\Delta n = \frac{n_{max} + n_{min}}{2} \qquad \textbf{3.3.1.4.}$$

We calculate the maximum and minimum refractive index for 2-proponol liquid. These numbers suggest that we cannot measure any changes in refractive index of a medium to less than 0.01 when using a step size that corresponds to 20μm of path difference in the scan. This implies that the nanofluid or fluid with nanomaterial has to show a change larger than 0.01 for us to be able to observe the effect on refractive index of the liquid. This also gave us an idea that if we want to observe smaller changes we need smaller steps. That is why typically a step size of 2μm was chosen to observe changes as small as 0.001 in the refractive index. The other method to improve this resolution is to decrease the step-size.

3.3.2. Production of Nanofluids

The samples measured in these studies were manufactured at Institute of Materials Science and Nanotechnology (UNAM- Bilkent University) by the Bülend Ortac laser group using pulsed laser ablation from a bulk metal sample placed in a liquid. Pulsed Laser Ablation Method is a new and unique method for generating nanocrystals in a host liquid and is a conventional method used for thin-film deposition [63]. Among these studies Laser Ablation Synthesis in Liquid Environment is a proven method of generating nanoparticles by removing

31

material from bulk surface in various solutions [64]. There are many parameters which should be taken into consideration while generating nanoparticles. These are laser wavelength, pulse energy, pulse duration, repetition rate, and the host liquid environment [65].

For these studies a variety of materials were chosen to observe the best possible change in refractive index from the THz measurements. Our preliminary analysis showed that both the concentration of particles and refractive index of the particles are important to see an observable change in the THz transmission (i.e. An appreciable delay in the time-domain pulse). Since the refractive index of the nanoparticles is not well known in the THz range, we used the known bulk refractive index to choose the best particles. This is not uncommon, and since the wavelength of the THz radiation is much larger than the particle diameter bulk refractive index can be a good estimate for these samples. Typically heavy metals have a very large refractive index in the THz range. For this reason, and through discussions with the research group at UNAM, we chose to measure copper, palladium and silver nanoparticles in 2-proponaol liquids.

To manufacture these samples the following items were used:

Bulk Palladium wafer (99.95%, Kurt J. Lesker Company), bulk Copper wafer (99.99%, Kurt J.Lesker Company), bulk silver wafer (99.99%, Kurt J.Lesker Company) and organic liquid-isoproponal (>99%, Sigma-Aldrich) were purchased commercially. For preparation, the materials were used without any purification. Palladium, copper and silver wafers were washed with acetone via an ultrasonic cleaning system.

Table 3.3.2.1.a. Index of refractions of commercially available metals at THz frequencies[66, 67, 68, 69, 70, 71]

ω(1/cm)	n (Al)	n (Fe)	n (Ti)	n (W)	n (Al2O3)	n (Ge)	n (Si)	n (Cu)	n (Au)	n (Pb)	n (Ag)	n (Co)	n (Pd)
50.0	437.0	183.4	120.0	242.1	3.8	4.0	3.4	*	399.0	159.0	*	*	*
300.0	109.0	24.9	20.9	44.2	*	4.0	3.4	*	62.8	*	47.8	*	*
500.0	60.7	12.1	17.3	17.5	*	*	*	31.6	28.2	*	20.1	15.2	11.4

Table 3.3.2.1.b. Reflectivity measurments of variuous metals at THz frequencies [78].

Metals	Reflectivity at 0,58THz	Reflectivity at 2,55 THz
Silver (Ag)	0,996	0,995
Copper (Cu)	0,997	*
Gold (Au)	0,994	0,994
Aluminium (Al)	0,995	0,994
Nickel (Ni)	0,994	0,991
Chromium (Cr)	0,993	0,974

The index of refraction of Silver (Ag) for frequencies close to 1 THz is not well determined in the literature, we calculated the index of refraction of Ag from the given reflectivity measurements [78] at 0.5 THz. The index of refraction can be calculated from reflectivity by using the well known Fresnel equations, for normal incidence at the interface of air to sample which takes the form: $R = \left(\frac{n-1}{n+1}\right)^2$ such that the index of refraction of Ag at 0,54THz is calculated to be 997,99 for a given reflectivity of 0,996.

The generation of colloidal stable nanocrystals of Palladium, Copper and Silver was carried out using a commercial nanosecond pulsed ND:YLF laser (Empower Q-Switched Laser, Spectra Physics) operated at 527 nm with pulse duration of 10 ns, average output power of 16 W at a pulse repetition rate of 1 kHz corresponding to a pulse energy of 16 mJ. The laser beam was focused on the wafer target placed in the glass vessel containing 3 ml of pure isoproponal medium by using a plano-convex lens with a focal length of 50 mm. The laser ablation was carried out for time duration of ~15 min.

To understand the distribution of particle size, Zeta Potential Analyze Method [72] is used for the size distribution characterization of the nanoparticles as shown:
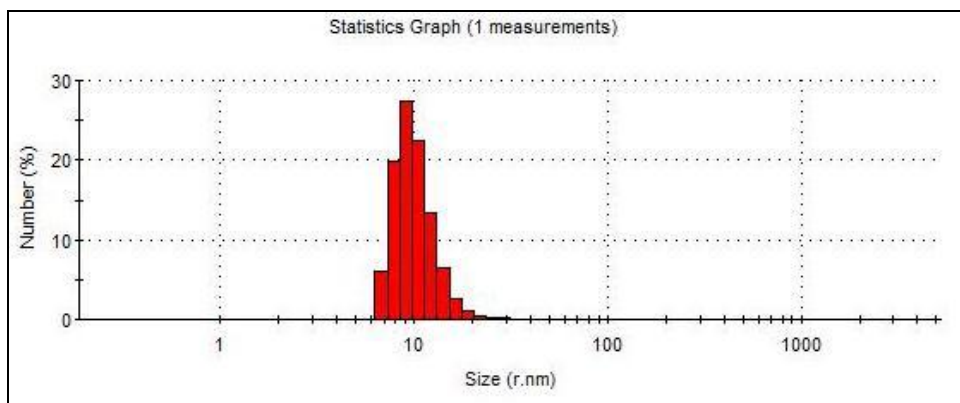
Figure 3.3.2.2.a. Zeta Potential Analyze Data for the Ag nanoparticle suspension
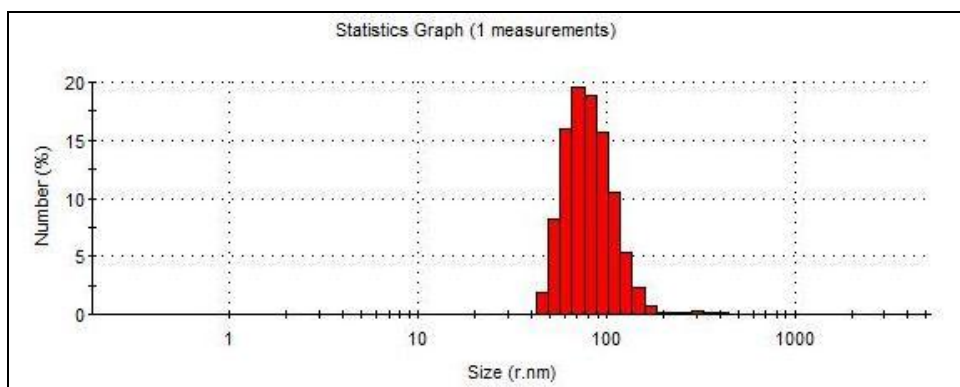

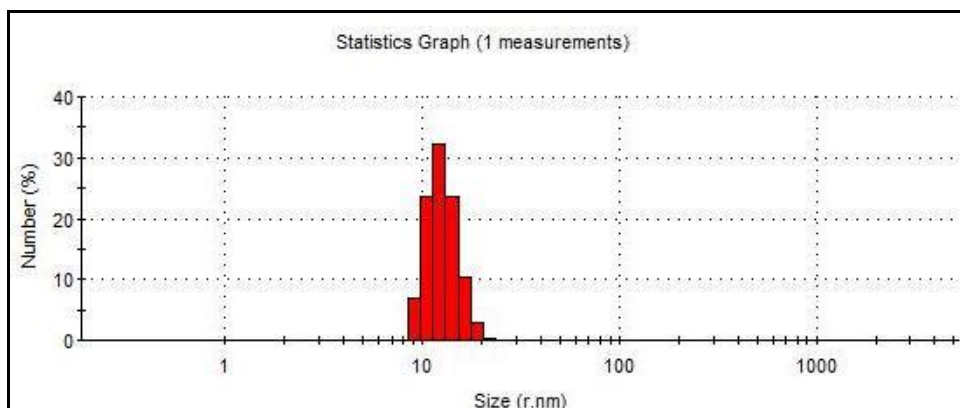**Figure 3.3.2.2.b.** Zeta Potential Analyze Data for the Pd nanoparticle suspension

Figure 3.3.2.2.c. Zeta Potential Analyze Data for the Cu nanoparticle suspension

3.3.3. THz TDS Measurements

Measurements were performed using a 2mm path length quartz cuvette whose width was 1cm. Measurements were taken for 2-proponol solutions with and without the Cu, Ag and Pd Nano Particles. We expected the THz pulse to experience both amplitude and phase change upon passing through the nanoparticle suspension. For this reason measurements were performed for different concentrations of Cu, Ag and Pd nanoparticles in 2-proponol. Measurements are repeated after up to 7 days to control the sedimentation of particles.

There can be possible effects such as possible changes in the chemistry of the isopropanol as a result of the interaction of the alcohol with the metal nanoparticle which can be further aided by the heat treatment during laser ablation process for the production of nanoparticles. For example, alcoxides (conjugate bases of alcohols) may have formed after interaction with the metal nanoparticle [73]. All these effects can affect the analysis of the THz measurements. That is why the different concentrations of nanoparticles were analyzed for diluted samples only. Additional heating or cooling was implemented to change the concentration of the nanoparticles in the host fluid.

To summarize, we analyzed the nanofluid samples for different nanoparticle concentrations which were only prepared by diluting with pure (99.5%) isopropanol. This has another advantage in that the measurements are compared to the base fluid which was not in contact with the metal nano particles during the laser ablation process. With this method we formed various concentrations and typically diluted the nanofluid to concentrations of 1X, 2X and 3X. For the sample denoted as 3X, this was prepared by pouring one fourth by volume of the pure isopropanol into three fourths of nanoparticle solution by volume. For the sample denoted as 2X, half to half volume of mixture was prepared. And finally for the sample denoted as 1X, three fourths of pure isopropanol was poured into one fourth of nanoparticle dispersion.

A series of measurements were taken:

In the first series measurements were performed on the Ag nano particles of various concentrations (1X, 2X and 3X) in 2-propanol host with the following measurement parameters: the scan distance from 14mm to 8mm (this is the travel range of our stage) with 20µm step size. The time domain data is shown in Figure 3.3.3.1.a.
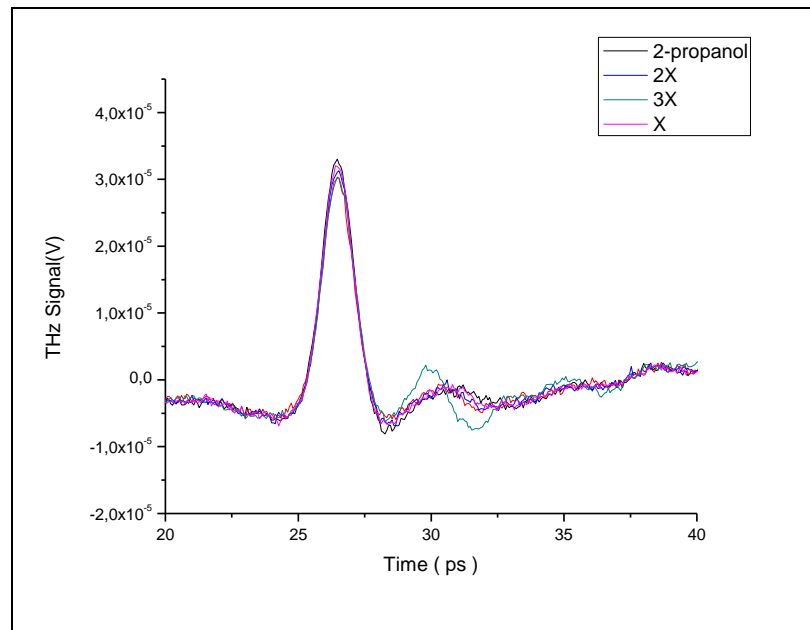
Figure 3.3.3.1.a. Time Domain data plot of 3X,2X and 1X Ag nanoparticles suspensions.

In order to identify the time shift and the intensity changes we replotted the magnified data of the main peak as shown in figure 3.3.3.1.b.
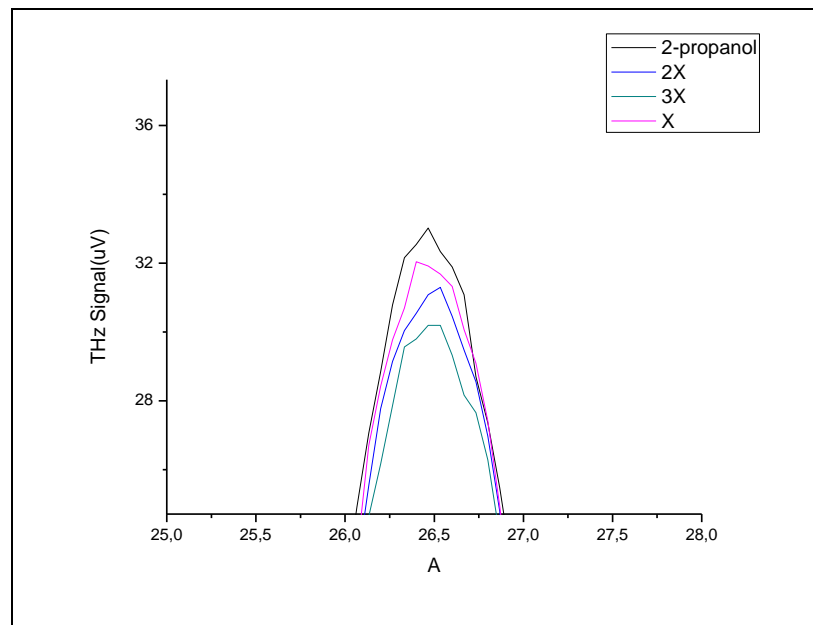
Figure 3.3.3.1.b. The main THz peak magnified data plot of the Time Domain data of 3X, 2X and 1X Ag nanoparticles suspensions.

Upon first observation, as seen from the plot in figure 3.3.3.1.b, the intensity increases as the concentration decreases.

A slightly positive time shift is observed for the highest concentration of the suspension but no analysis can be done since the time shifts in between the differently concentrated suspensions are beyond our resolution limit.

In order to increase the resolution we decreased the scan distance from (14mm to 8mm) to (10,5mm to 9,5mm) and decreased the step size from 10μm to 1μm step size. And to control the aggregation and sedimentation we repeated the measurements after up to 7 days.

The results are shown below for Ag nanoparticles in isopropanol host fluid before sedimentation/aggregation control:
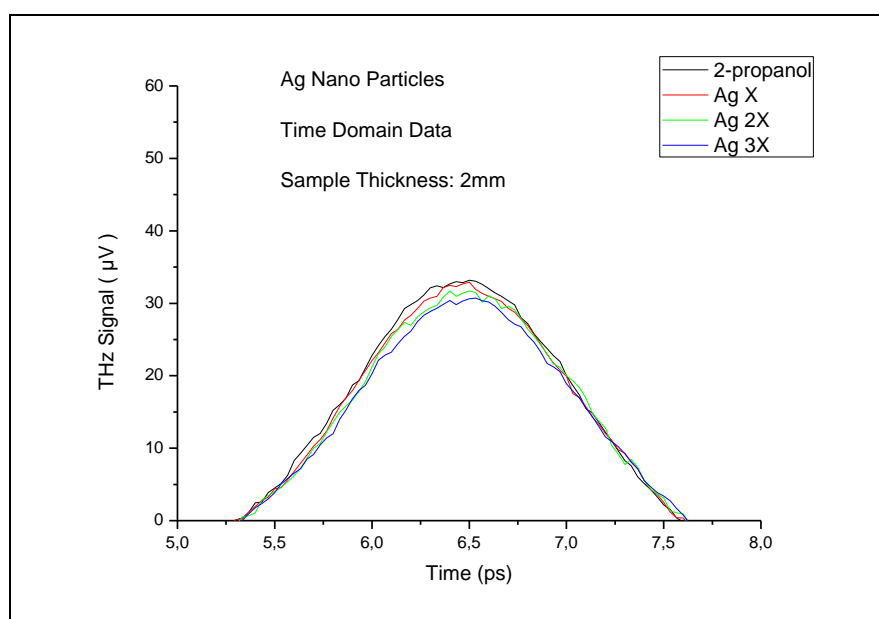
Figure 3.3.3.2.a. THz Time Domain Data. A slightly time shift and an intensity change is observed. And it is also observed that the intensity is decreasing as the concentration increases.
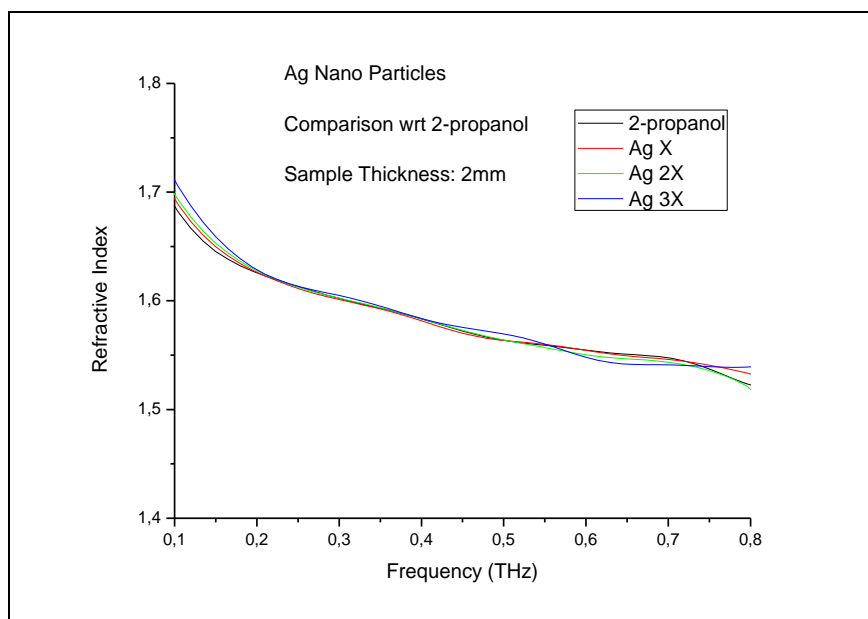
Figure 3.3.3.2.b. Refractive Index Data. No discernible difference is observed in between various concentrations.
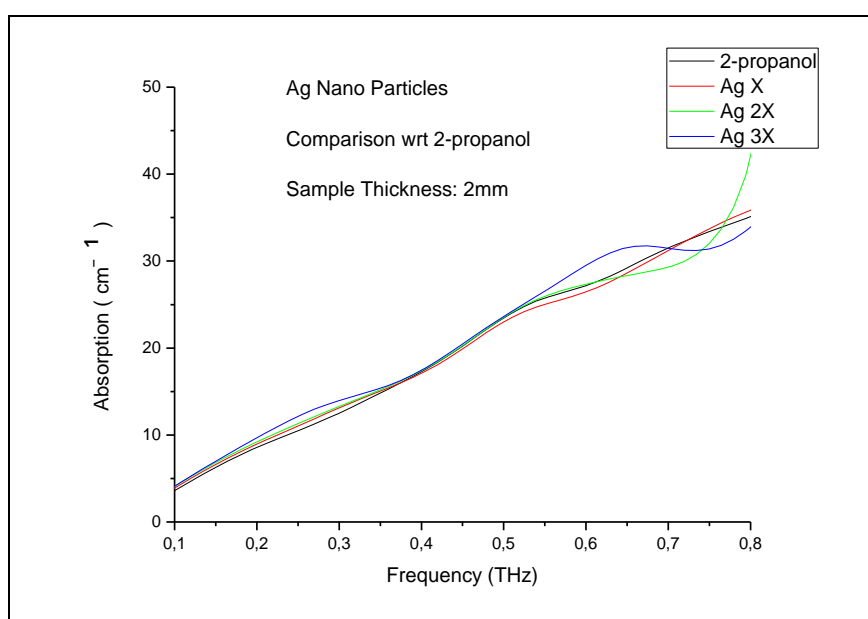
Figure 3.3.3.2.c Absorption Data. No difference is observed in between various concentrations.

The results are shown below for Ag nanoparticles in isopropanol host fluid 12 days after initial measurements. This was done to check for sedimentation and aggregation:

Figure 3.3.3.3.a. THz Time Domain Data. The data matches with the host fluid which is thought to be caused by sedimentation/aggregation. No distinct difference is observed.

Figure 3.3.3.3.b. Refractive Index Data. No distinct difference is observed.

Figure 3.3.3.3.c. Absorption Data. No distinct difference is observed.

In the second series, measurements were performed on the Pd nano particles of various concentrations (1X, 2X and 3X) in 2-propanol host with the following measurement parameters: the scan distance from 10,5mm to 9,5mm and 1µm step size. The time domain data is shown in Figure 3.3.3.4.a.

The results are shown below for Pd nanoparticles in isopropanol host fluid before sedimentation/aggregation control:
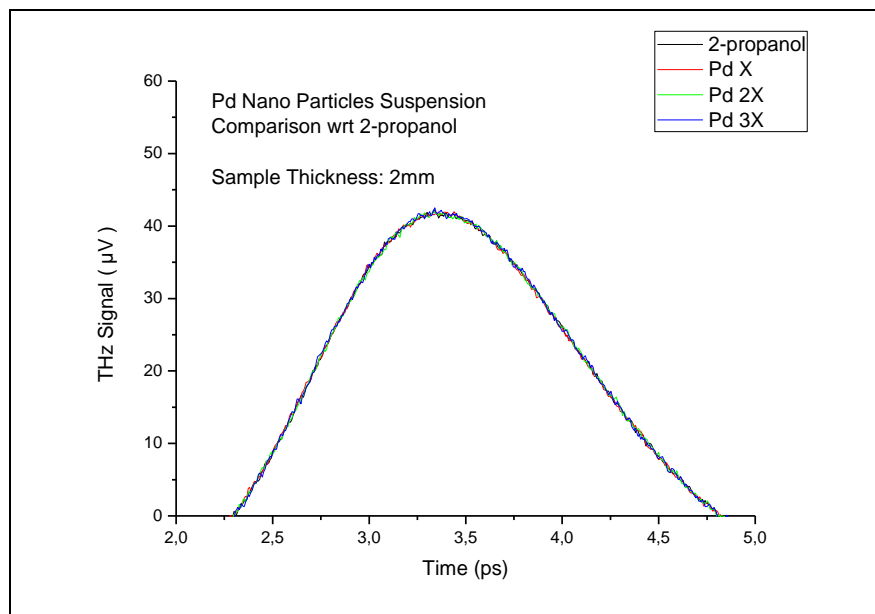
**Figure 3.3.3.4.a.** Time Domain Data. All datas match with the host fluid which is thought to be caused by sedimentation/aggregation or that the concentration of nanoparticles was insufficient. No distinct difference is observed.

Figure 3.3.3.4.b. Index of refraction Data. No distinct difference is observed.
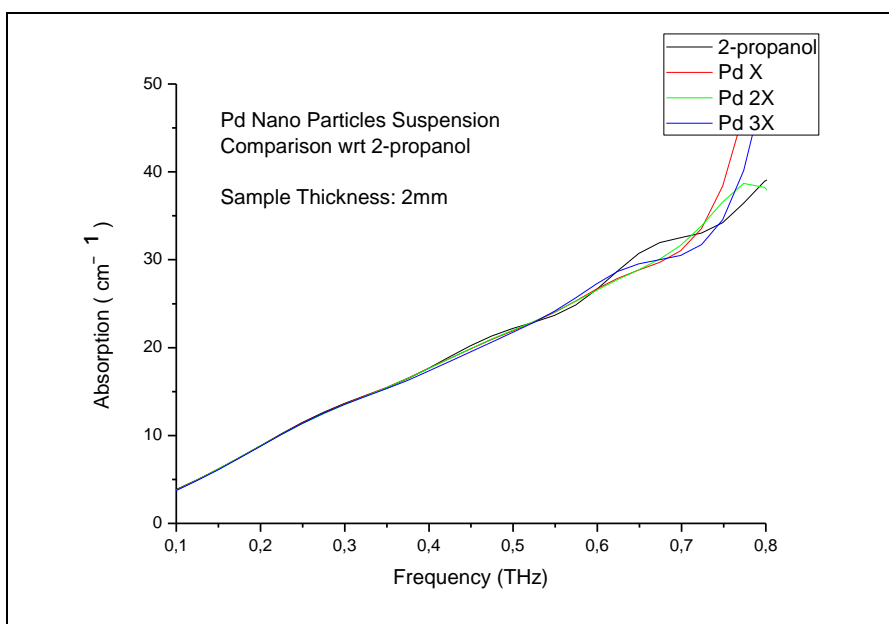
Figure 3.3.3.4.c. Absorption Data. No distinct difference is observed.

The results are shown below for Pd nanoparticles in isopropanol host fluid 2 days after initial measurements. This was done to check for sedimentation and aggregation:
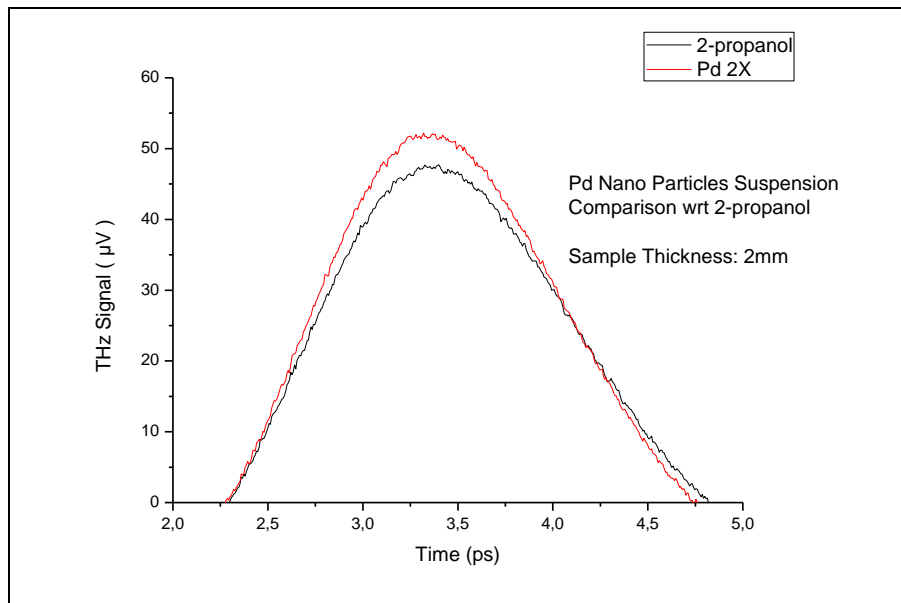
Figure 3.3.3.5.a. Time Domain Data. As a different and interesting result from the first day data this time a slightly negative time shift was observed and an increase at the intensity was observed for Pd 2X.

.
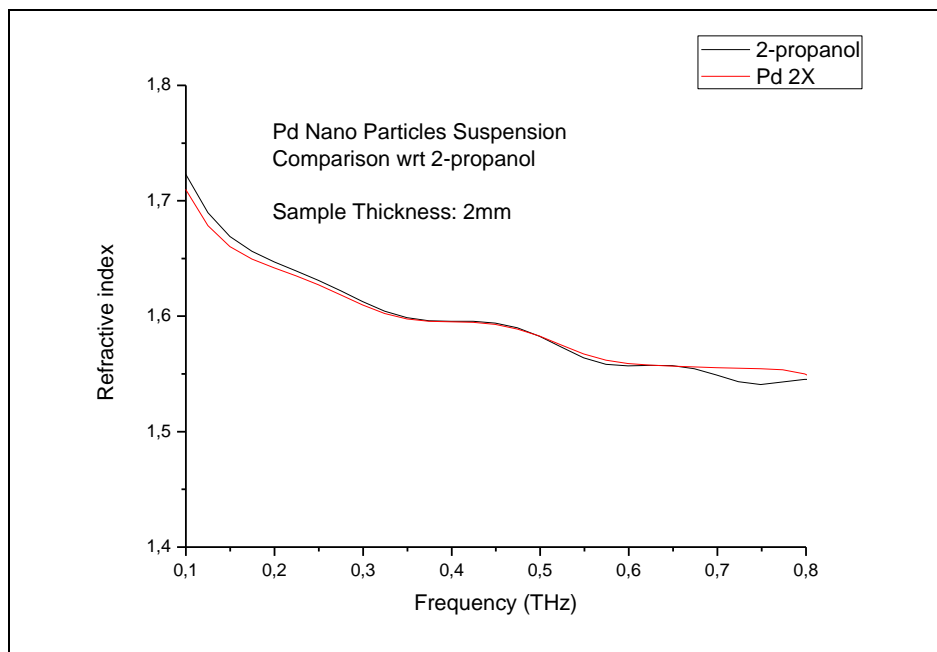
Figure 3.3.3.5.b. Index of Refraction Data. No distinct difference was observed.
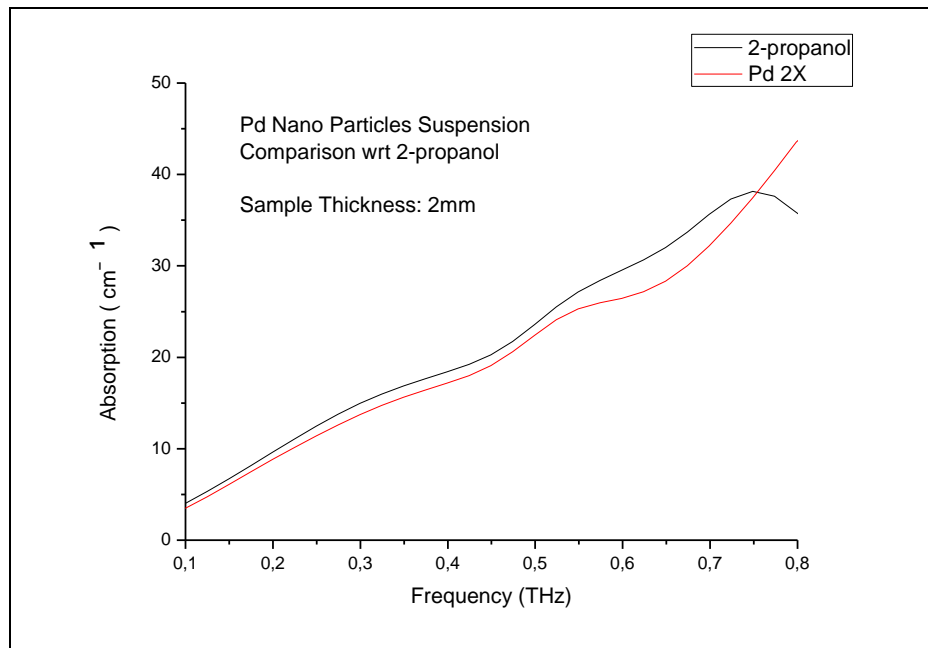
Figure 3.3.3.5.c. Absorption Data. No distinct difference was observed.

The results are shown below for Pd nanoparticles in isopropanol host fluid 7 days after initial measurements. This was done to check for sedimentation and aggregation:
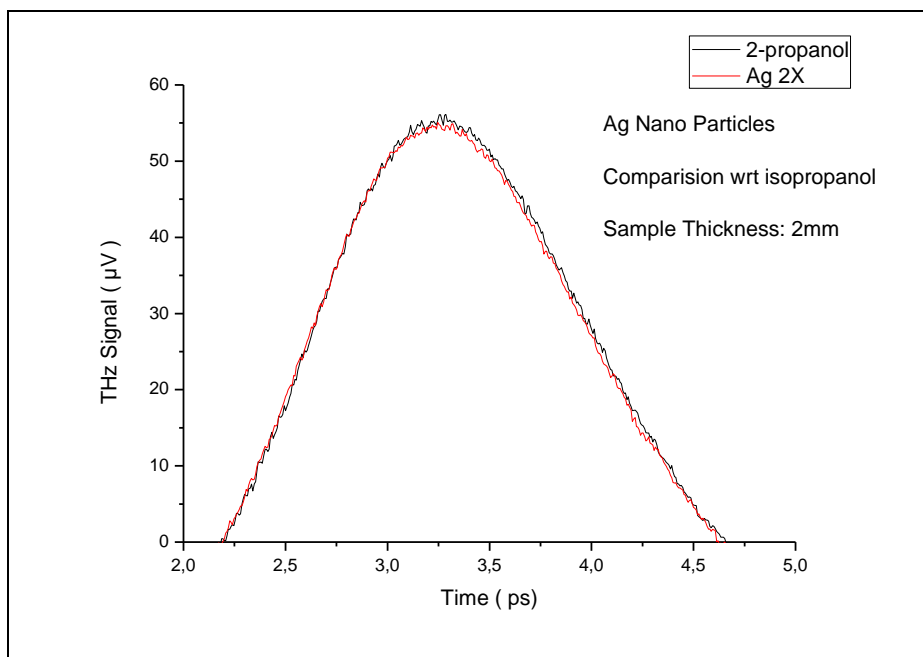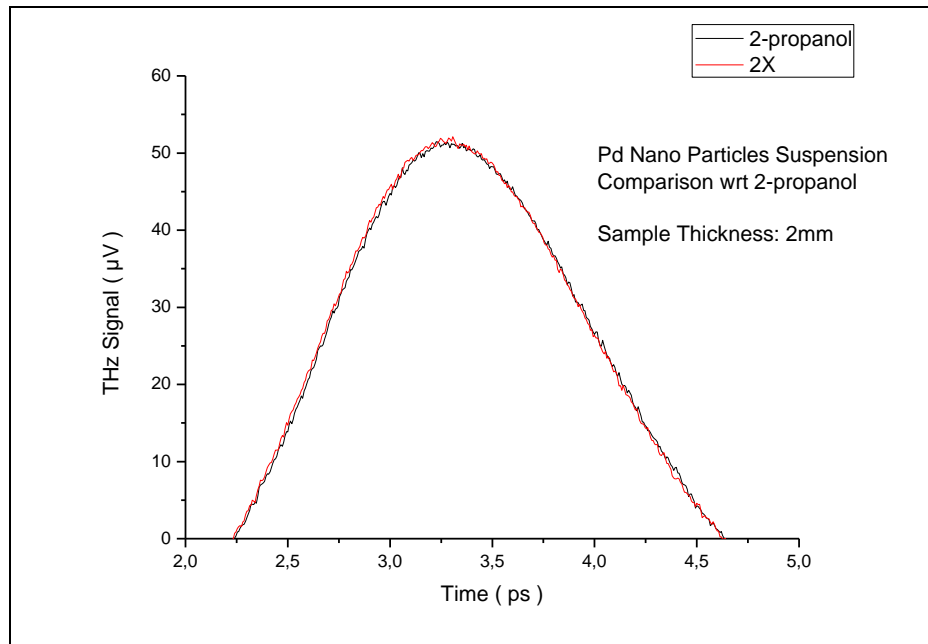

Figure 3.3.3.6.a. Time domain Data. Pd 2x data matches with the host fluid which is thought to be caused by sedimentation.
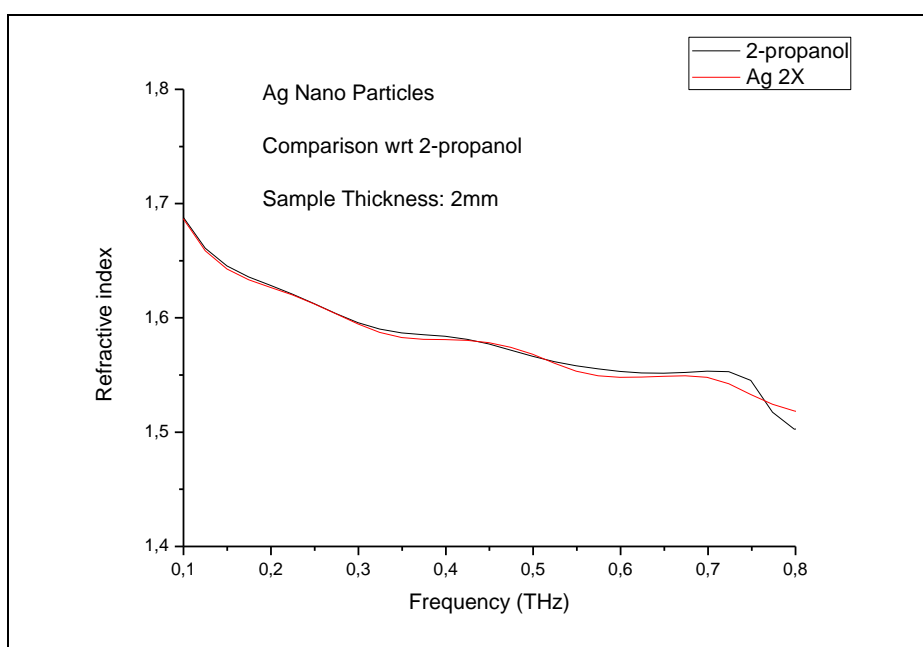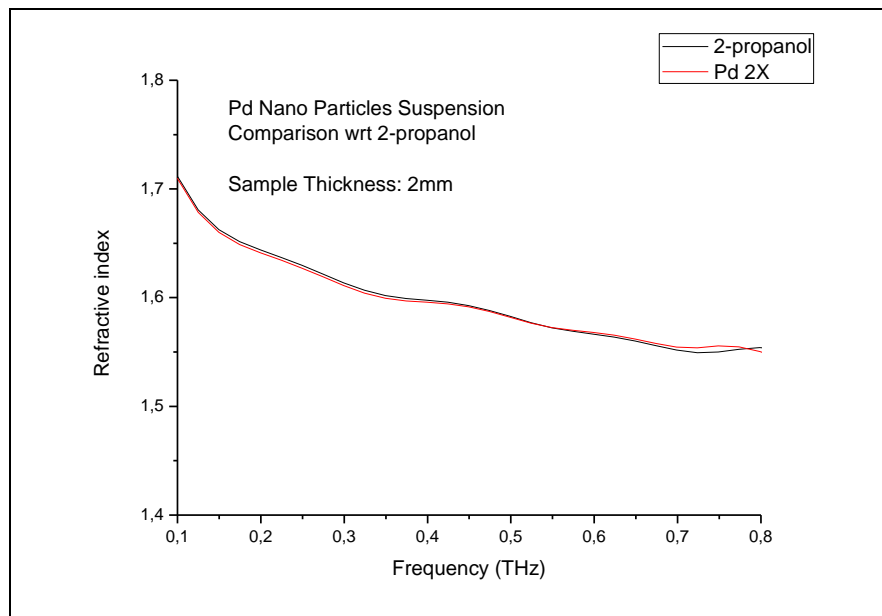
Figure 3.3.3.6.b. Index of Refraction Data. No distinct difference was observed.
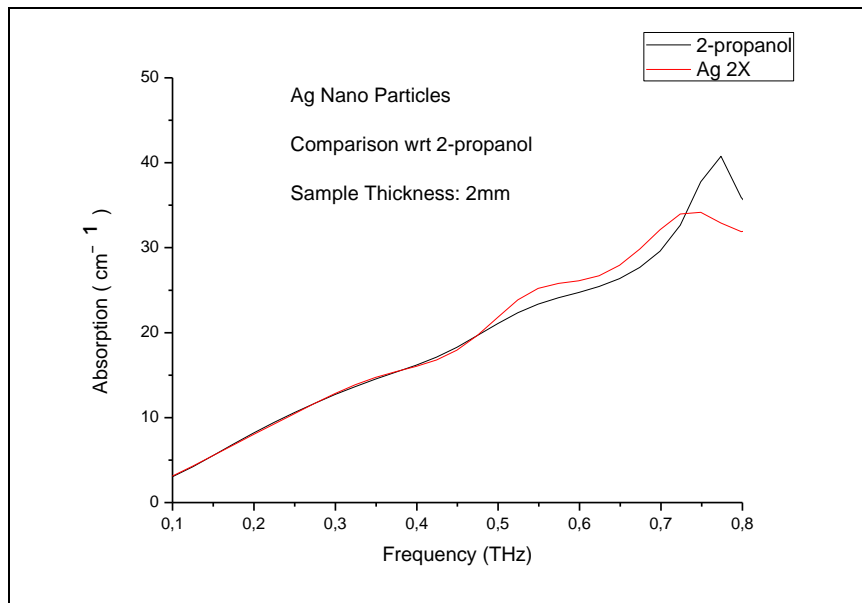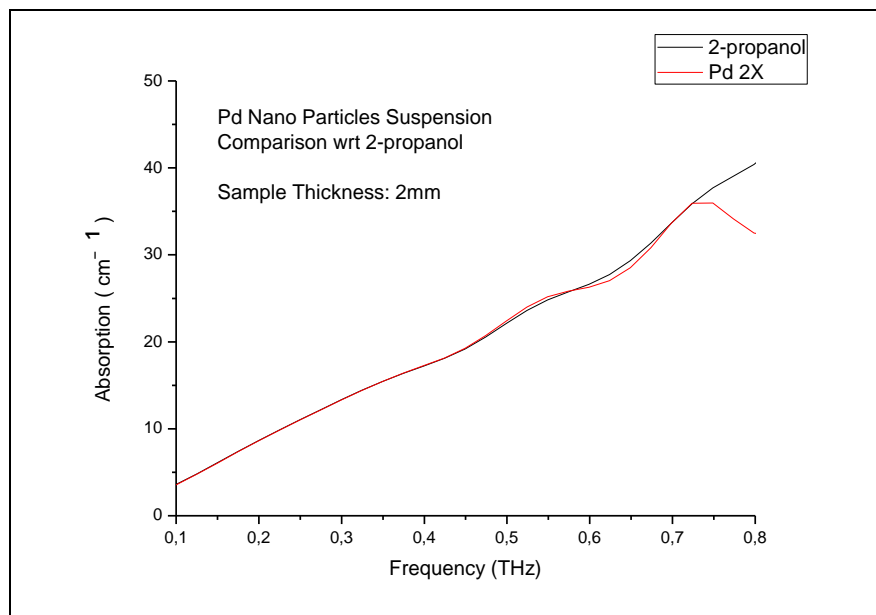

Figure 3.3.3.6.c. Absorption Data. No distinct difference was observed.

In the third and final series, measurements were performed on the Cu nano particles of various concentrations (1X, 2X and 3X) in 2-propanol host with the following measurement parameters: the scan distance from 10,5mm to 9,5mm and 2μm step size. The time domain data is shown in Figure 3.3.3.4.a.

The results are shown below for Cu nanoparticles in isopropanol host fluid before sedimentation/aggregation control:
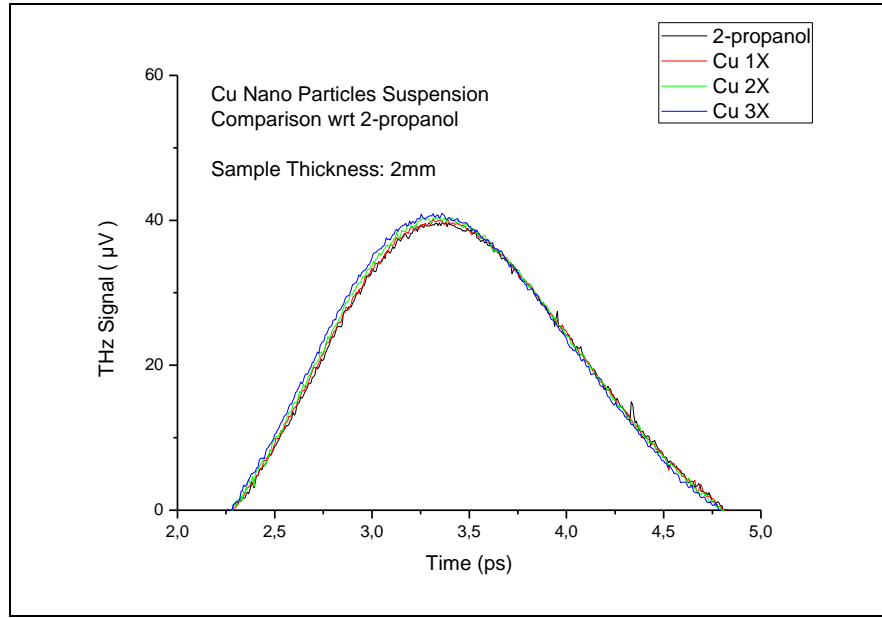
**Figure 3.3.3.7.a.** THz Time Domain Data. As an interesting result, negative time shift and an intensity (increase) change was observed as the concentration increases
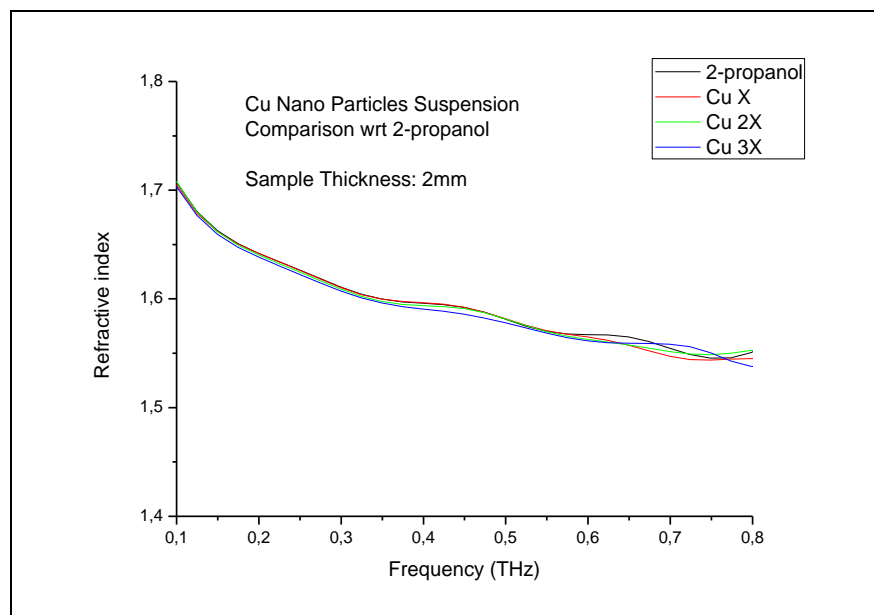
Figure 3.3.3.7.b. Index of Refraction Data. No distinct difference was observed.
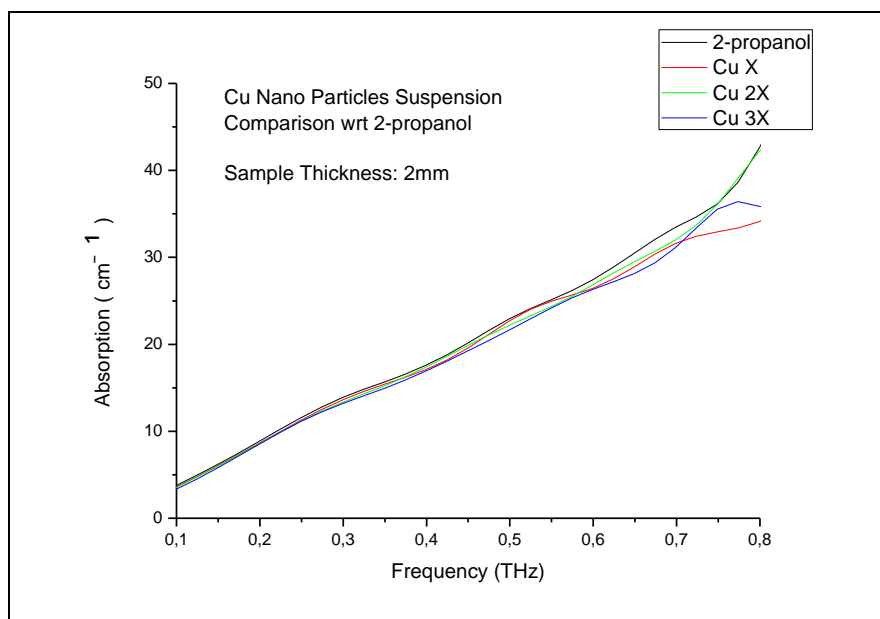
Figure 3.3.3.7.c. Absorption Data. No distinct difference was observed.

The results are shown below for Cu nanoparticles in isopropanol host fluid 6 days after initial measurements. This was done to check for sedimentation and aggregation:
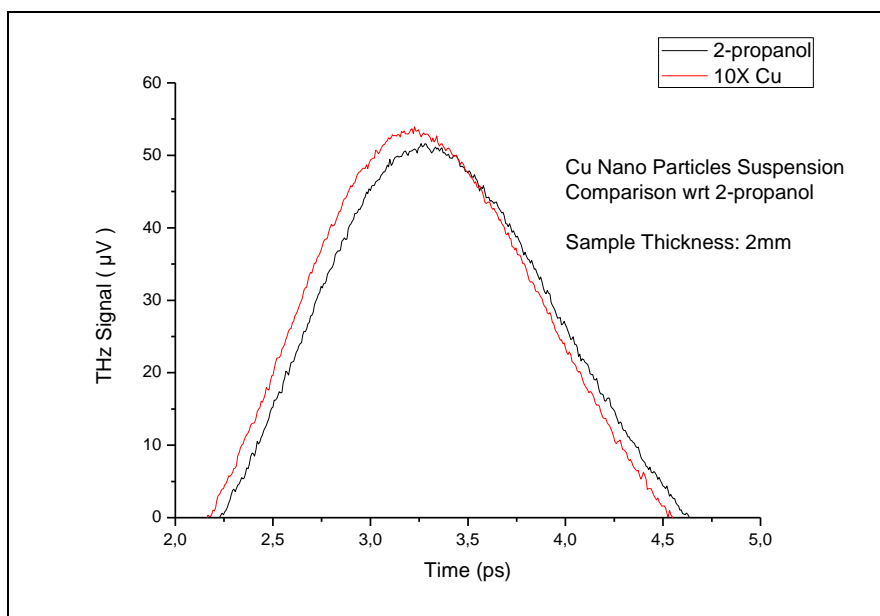
Figure 3.3.3.8.a. Time Domain Data. A negative time shift and an intensity change was observed with suggests no aggregation and sedimentation due to the similarity with previous measurements.
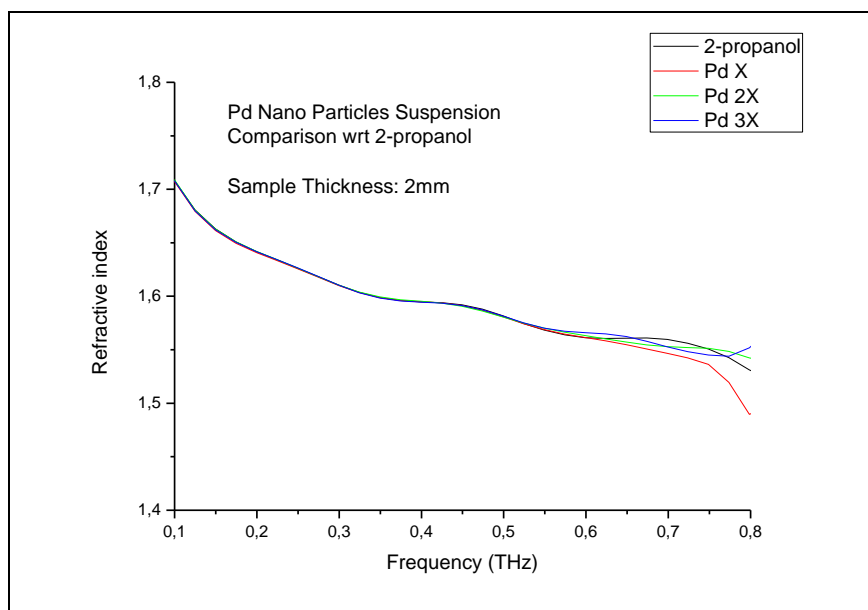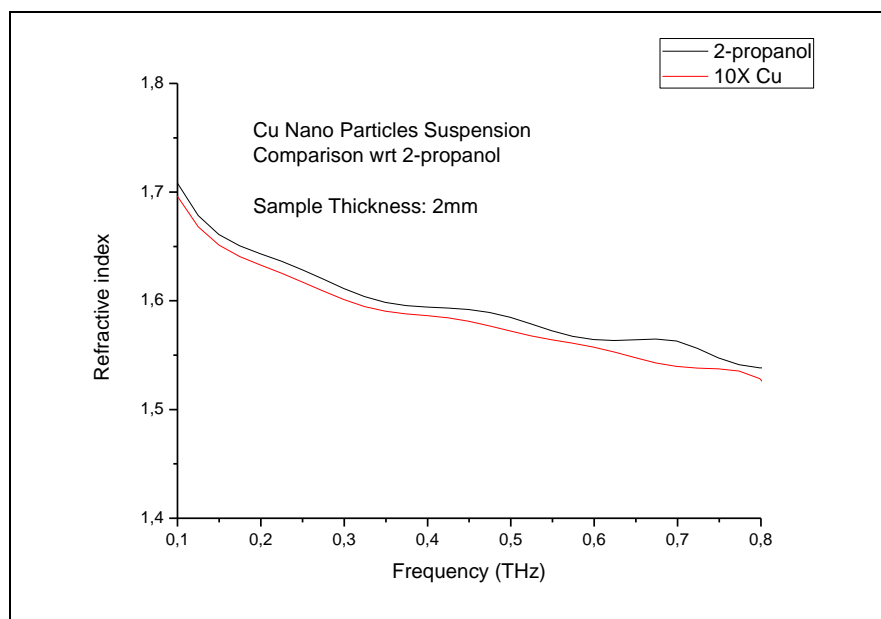
Figure 3.3.3.8.b. Index of Refraction Data. No distinct difference was observed.
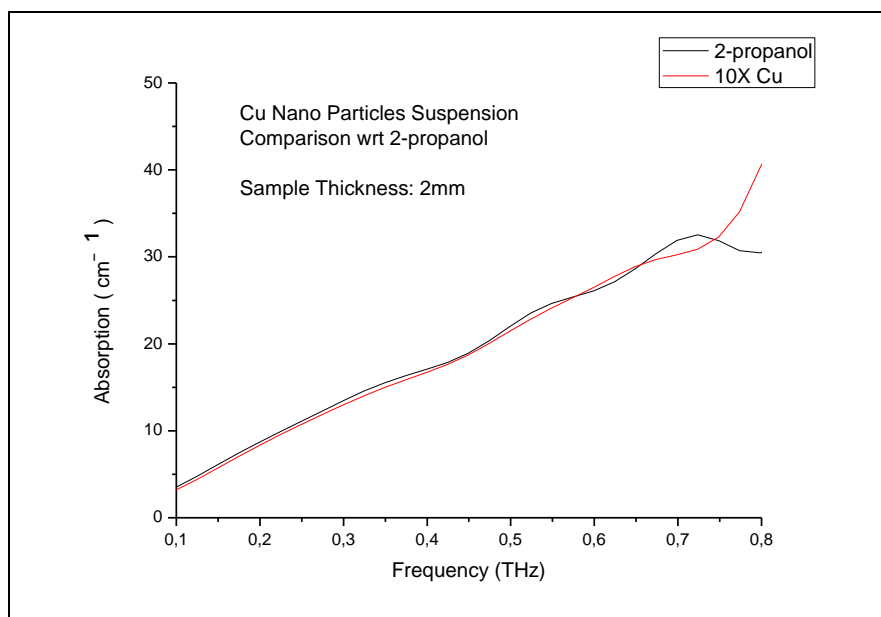
Figure 3.3.3.8.c. Absorption Data. No distinct difference was observed.

3.3.4. Results

We expected the THz pulse to experience both amplitude and phase change upon passing through the nanoparticle suspension. For this reason measurements were performed for different concentrations of Cu, Ag and Pd nanoparticles in 2-proponol. Measurements were repeated after up to 7 and in one case 12 days to control and check the sedimentation/aggregation of the metal nanoparticles.

No distinctive difference was observed in the frequency domain measurements (Index of Refraction and Absorption) in any of the different concentrations of nanoparticle suspensions.

For Ag suspensions, in the first day measurements show a slight time shift and an intensity change that was observed to decrease as the concentration increased. For the measurements taken after waiting 12 days, all datas matched up with the host fluid which is thought to be caused of sedimentation/aggregation or even can be due to chemical changes in the host fluid, thus no distinct difference was observed.

For Pd suspensions, in the first day measurements showed that all datas matched up with the host fluid which can be due to sedimentation or can be possibly due to a low concentration of nanoparticles. As was observed in the particle size distribution tests, the Pd particle size distribution was about 10 times larger than Ag or Cu particles. For the second day measurements, an interesting negative time shift was observed with an increase in the intensity for Pd 2X concentration. Pd 1X and Pd 3X concentrations were not tested. Lastly, for the seventh day measurement set, for the Pd 2X suspension, the time shift and intensity change did not recur in the THz profile, but similar to the first day measurement data it matched up with the host fluid.

For the first day measurement, no shift or change in amplitude was observed, this is thought to be a result of either the sedimentation/aggregation of the particles in that the THz beam which goes through a spot size of roughly 8mm in diameter does not see many particles; or the concentration of the Pd particles is not dense enough for THz detection as was the case for Ag and Cu particles. This can be explained by the fact that the Pd particles were much larger than the Ag or Cu particles. However, on the second day there was a negative shift and increase in intensity which would suggest that most probably the absorption and refractive index of the nanofluid changed, Afterwards, on the seventh day, results were

obtained which match the first day measurement, which could be indicative of sedimentation or aggregation. As will be clear in the next chapter it is difficult to say whether the absorption increased or decreased, or whether the refractive index increased or decreased since the THz pulse is not only passing through the nanofluid but it is also passing through the quartz cuvette holder. These arguments on the behavior of change in time for Pd nano particle solutions are left as a future study.

For Cu suspensions in the first day measurements showed a slight negative time shift and an increase in the intensity was also observed. The negative time shift and intensity change was observed as the concentration increases which is very interesting and results were the same for the seventh day measurements as well. Upon first examination of the measurements one can conlude that there were no aggregation and or sedimentation in the Cu nanoparticles suspensions for various concentrations, however as was stated earlier the effect of the quartz cuvette structure, the interaction of the alcohol with the metal particles, any chemical changes in the ablation process all need to be analyzed separately to effectively decipher the measurements.

3.4.   SUMMARY AND DISCUSSION

THz Time-Domain Spectroscopy is a useful technique to measure the absorption coefficient and refractive index of various materials. We constructed a THz Time Domain Spectrometer to probe the dynamics of metallic nanoparticle suspensions.

It is known that the use of polar liquids tend to stop aggregation in such suspensions but polar liquids tend to absorb the THz intensity thus we made a series of measurements with various polar liquids. As a result of the fluids measurements it was seen that isopropanol is the best host for the nanoparticle suspensions.

The samples measured in these studies were manufactured by using pulse laser ablation from Pd, Ag and Cu materials in 2-propanol host and characterized by Zeta Potential Analyzer. We expected the THz pulse to experience both amplitude and phase change upon passing through the Nanoparticle suspension but as was shown frequency dependent quantities such as power absorption coefficient and refractive index showed no discernible

49

difference between the host fluid (isopropanol) and the various concentration nanofluid systems (Ag, Pd, Cu for 1X, 2X and 3X).

However, the time-domain profiles showed interesting slight difference when high resolution scans were acquired (2μm step size). For example we observed slight shifts in time and slight changes in intensity.

We expected to observe positive time shifts, and possibly an increase in amplitude since the refractive index of quartz (about 2.1 in the THz range, [74]) is much higher than the refractive index of the isopropanol. Thus when nanoparticles were added the increase in refractive index will allow for a better index match between quartz and nanofluid resulting in an increase in amplitude upon transmission, with the requirement that the absorption did not change. According to our expectations, we observed a positive time shift for Ag nanoparticles but a decrease in amplitude, which can be indicative of an increase in absorption. This positive delay with respect to the reference scan is analyzed in detail in Chapter 4.

Furthermore, we observed a negative time shift in Pd and Cu nanoparticle suspensions with slight changes in intensity. These measurements changed over long time scales possibly due to sedimentation or aggregation in these samples.
Especially in Cu nano particle suspensions a strong negative time shift was observed. Upon first examination, this observed negative time shift instead of a positive delay with respect to the reference scan (through just isopropanol) would suggest superluminal propagation of the THz pulse. This is actually not the case, and this negative shift can be explained by examining the phase change occurred at the interface between the quartz and the nanofluid sample. We discuss this phenomenon in chapter 4.

CHAPTER 4

ANALYSIS OF THE TIME-DOMAIN MEASUREMENTS

In this chapter, the time-domain measurements of the THz pulse profiles through the nano particle suspensions is explained by using theory based on the propagation of electromagnetic waves through dielectric and conducting interfaces. In our THz_TDS system we placed various nanofluid (Cu, Pd, Ag in 2-pronanol) samples in a quartz cuvette of 2mm path length. First, the theory behind propagation through the layers that make up this sample holder is explained within the framework of stratified media. Then the total transmission and the phase shift coefficients of the THz pulse are obtained from the fitting curve analyses of the experimental data for Ag and Cu nanoparticle solutions.

The absorption of various concentrations of Ag nanofluid are estimated and the index of refraction data are calculated.

After modeling the dielectric function based on Maxwell-Garnett theory, a method is developed to arrive at the particle concentration in the nanofluid sample, in which the obtained result well agrees with the commercially available nanofluid solutions.

4.1. SAMPLING SYSTEM AND THEORITICAL FORMULATION

A medium whose properties are constant throughout each plane perpendicular to a fixed direction is called a stratified medium [1]. The theory of stratified media is of considerable importance in optics, in connection with multilayers.

The derivation of the differential equations starting from the well known, Maxwell's equations for a time-harmonic electromagnetic wave propagated through a stratified medium and the most conventional expression of various theorems related to stratified media are given as a characteristic matrix in details in Reference [75].
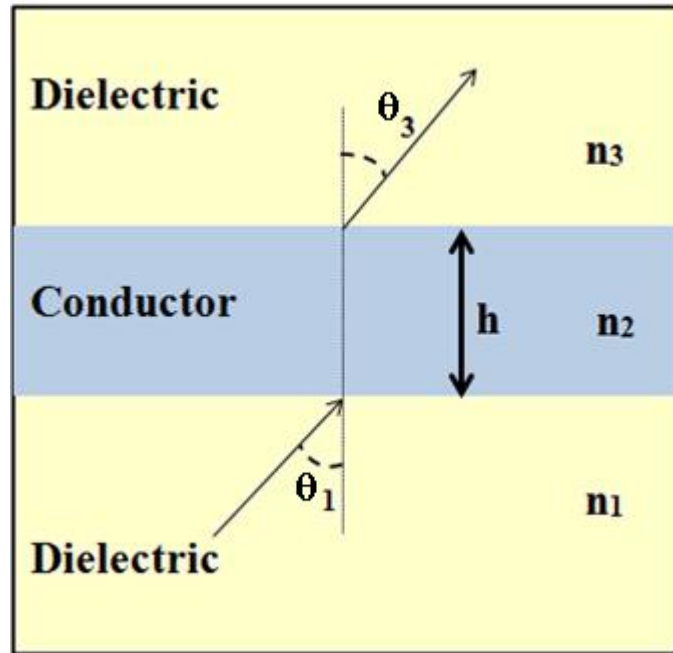
Figure 4.1.1. An absorbing film situated between two dielectric media.

A plane wave of angular frequency ω is transmitted over a plane parallel absorbing film with thickness h and index of refraction n_2 is situated in between two dielectric media with refractive indices n_1, n_3 and field absorption coefficients as α_1, α_2 respectively as is illustrated in figure 4.1.1.

The field transmission amplitudes t_{12}, t_{23} and phase shifts χ_{12}, χ_{23} at first and second interfaces respectively are given by [76] :

$$t_{12}^2 = \frac{(2n_1 \cos\theta_1)^2}{(n_1 \cos\theta_1 + n_2)^2 + \left(\frac{\alpha_1 c}{\omega}\right)^2}$$ **4.1.1.**

$$\tan\chi_{12} = -\frac{\frac{\alpha_2 c}{\omega}}{n_1 \cos\theta_1 + n_2}$$ **4.1.2.**

$$t_{23}^2 = \frac{4\left(n_2^2+\left(\frac{\alpha_2 c}{\omega}\right)^2\right)}{(n_3\cos\theta_3+n_2)^2+\left(\frac{\alpha_2 c}{\omega}\right)^2}$$

4.1.3.

$$\tan\chi_{23} = \frac{\frac{\alpha_2 c}{\omega}n_3\cos\theta_3}{n_2^2+\left(\frac{\alpha_2 c}{\omega}\right)^2+n_2 n_3\cos\theta_3}$$

4.1.4.

Here the subscript 12 refers to the first interface as the electromagnetic wave propagates from dielectric to conducting medium, and with the similar notation the subscript 23 refers to the second interface from conducting medium to dielectric medium.

As shown above that the frequency dependent phase shift at the first interface account for the observed negative shift. A negative phase shift of the field is caused by the dielectric-conductor interface as an electromagnetic field is transmitted into an absorbing medium.

In our experiment a plane wave of angular frequency ω is transmitted at normal incidence over the consecutive interfaces of air, quartz and NF sample as shown in figure 4.1.2.
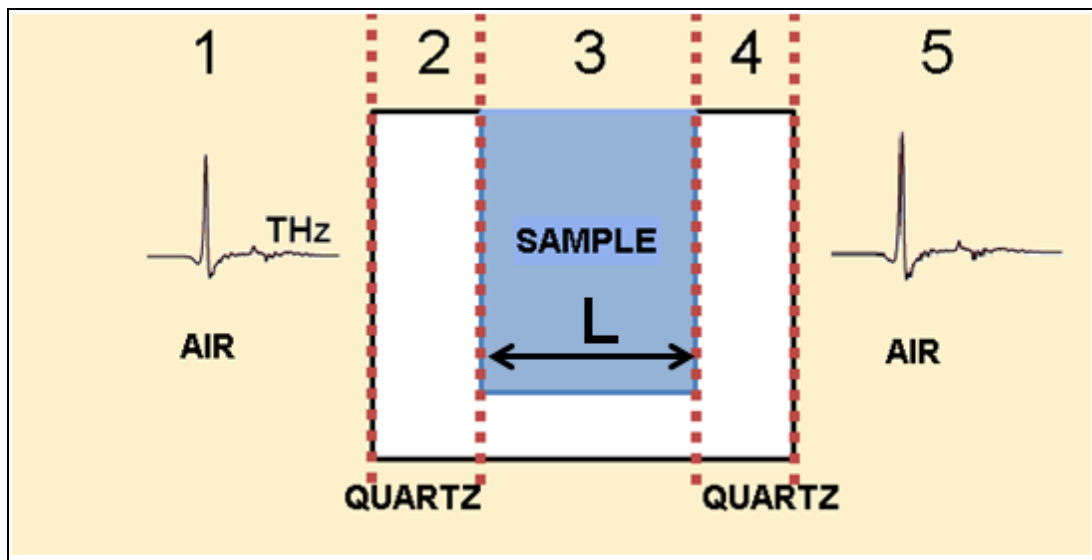
Fig. 4.1.2. Illustration of the sample holder used in the THz TDS experiments as the THz Field propagates through the quartz cuvette containing the sample.

The 1, 2, 3, 4, and 5 quantities refer to the mediums of air, sample holder and the sample of thickness L consecutively.

In terms of Total Transmission amplitude t_m and total phase change φ_m, the ratio of nanofluid (sample pulse) E_{NF} to isopropanol solution (reference pulse) E_{iso} in the frequency domain can be described by:

$$\frac{E_{NF}}{E_{iso}} = t_m e^{-i\varphi_m}$$

4.1.5.

In our case the ratio of the sample pulse to reference pulse is described as [60]:

$$\frac{E_{NF}}{E_{iso}} = \frac{\frac{2\,n_Q}{n_Q + \widetilde{n_{NF}}} e^{-i\,\widetilde{n_{NF}}\,kL}\,\frac{2\widetilde{n_{NF}}}{n_Q + \widetilde{n_{NF}}}}{\frac{2\,n_Q}{n_Q + \widetilde{n_{iso}}} e^{-i\,\widetilde{n_{iso}}\,kL}\,\frac{2\,\widetilde{n_{iso}}}{n_Q + \widetilde{n_{iso}}}}$$

4.1.6

Here, the relative Fresnel transmisson coefficients are given through the interfaces 2 to 3 and 3 to 4 only as can be seen in Figure 4.1.2. The other coefficient cancel out because they appear for both transmisson through the nanofluid sample holder and the host fluid sample holder. In addition, the wave aquires a phase that is proprotional to the complex index of the medium. Since both media are absorbing both refractive indices are complex. By rearanging the equation in the form, $\frac{E_{NF}}{E_{iso}} = \mathcal{Z} e^{\Upsilon}$ where Υ contains both the argument and the loss, we get:

$$\frac{E_{NF}}{E_{iso}} = \frac{\widetilde{n_{NF}}\,(n_Q + \widetilde{n_{iso}})^2}{\widetilde{n_{iso}}\,(n_Q + \widetilde{n_{NF}})^2}\,e^{-\alpha_{NF}\,L}\,e^{\alpha_{iso}\,L}\,e^{-i(n_{NF} - n_{iso})kL}$$

4.1.7

Here, $k = \frac{w}{c}$ and as seen from the above equation, $\mathcal{Z}$ is given as:

$$\widetilde{\mathcal{Z}} = \frac{\widetilde{n_{NF}}\,(n_Q + \widetilde{n_{iso}})^2}{\widetilde{n_{iso}}\,(n_Q + \widetilde{n_{NF}})^2}$$

4.1.8.

54

Complex index of refractions of isopropanol base fluid, $\widetilde{n_{iso}}$ and the nanofluid solution, $\widetilde{n_{NF}}$ are given as:

$$\widetilde{n_{NF}} = n_{NF} - ik_{NF} \qquad\qquad \textbf{4.1.9.}$$

$$\widetilde{n_{iso}} = n_{iso} - ik_{iso} \qquad\qquad \textbf{4.1.10.}$$

The field absorption coefficients of the base fluid and the nanofluid are given as:

$$\alpha_{NF} = \frac{\omega}{c} k_n \qquad\qquad \textbf{4.1.11.}$$

$$\alpha_{iso} = \frac{\omega}{c} k_{iso} \qquad\qquad \textbf{4.1.12.}$$

By implenting the equations 4.1.9 through 4.1.12 to the equation 4.1.8. and and for simplicity rearanging, $\widetilde{Z}$ in the form $\widetilde{Z} = \frac{a - ib}{c - id}$

Where:

$$a = n_{NF}n_Q^2 + n_{NF}n_{iso}^2 - n_{NF}k_{iso}^2 + 2n_Q n_{iso} n_{NF} - 2k_{NF}n_{iso}k_{iso} - k_{NF}n_Q k_{iso} \qquad \textbf{4.1.13.}$$

$$b = -i(2n_{NF}n_{iso}k_{iso} + 2n_Q n_{NF}k_{iso} + k_{NF}n_Q^2 + k_{NF}n_{iso}^2 - k_n k_{iso}^2 + 2k_{NF}n_Q n_{iso}) \qquad \textbf{4.1.14.}$$

$$c = n_{iso}n_Q^2 + n_{iso}n_{NF}^2 - n_{iso}k_{NF}^2 + 2n_Q n_{iso} n_{NF} - 2k_{iso}n_{NF}k_{NF} - 2k_{iso}n_Q k_{NF} \qquad \textbf{4.1.15.}$$

$$d = -i(2n_{iso}n_{NF}k_{NF} + 2n_Q k_{NF}n_{iso} + k_{iso}n_Q^2 + k_{iso}n_{NF}^2 - k_{iso}k_{NF}^2 + 2k_{iso}n_Q n_{NF}) \qquad \textbf{4.1.16.}$$

The Argument of a complex number $\widetilde{z} = x - yi$ is given as,[60] by definition:

$$\text{Arg}\,\widetilde{z} = \arctan\left(-\frac{y}{x}\right) \qquad\qquad \textbf{4.1.17.}$$

55

Then $\text{Arg } \widetilde{Z}$ becomes:

$$\text{Arg } \widetilde{Z} = \arctan\left(\frac{bc-ad}{ac+bd}\right)$$

4.1.18.

The Modulus of a complex number $\widetilde{z} = x - yi$ is given as,[76] by definition:

$$|\widetilde{z}| = (x^2 + y^2)^{1/2}$$

4.1.19.

Then the modulus of $\widetilde{Z}$, $|\widetilde{Z}|$ becomes:

$$|\widetilde{Z}| = \left(\frac{a^2+b^2}{c^2+d^2}\right)^{1/2}$$

4.1.20.

Finally, the ratio of sample pulse to reference pulse in the frequency domain is equated as:

$$\frac{E_{NF}}{E_{iso}} = |\widetilde{Z}| \, e^{(\alpha_{iso}-\alpha_{NF})L} \, e^{-i\,\varphi_m}$$

4.1.21.

The total transmission amplitude and total phase change are found to be :

$$t_m = \left(\frac{a^2+b^2}{c^2+d^2}\right)^{1/2} e^{(\alpha_{iso}-\alpha_{NF})L}$$

4.1.22.

$$\varphi_m = \arctan\left(\frac{bc-ad}{ac+bd}\right) + \Delta n \frac{\omega}{c} \, L$$

4.1.23.

Where $\Delta n = n_{NF} - n_{iso}$, and L is the length of the nanofluid or host fluid, and ω is the THz frequency.

The frequency dependent field absorption coefficient $\alpha_{iso}(\omega)$ can be calculated from the above equation by using the power transmission, T, which is computed from the FFT analaysis of isopropanol with respect to quartz [77]:

$$\alpha_{iso} = -\frac{1}{2L} \ln\left[\left(\frac{(n_{iso}+n_Q)^2}{4\,n_Q n_{iso}}\right)^2 \cdot T\right]$$

4.1.24.

56

The field absorption is corrected for reflective losses between the quartz and sample fluid index mismatch. The index of refraction $n_{iso}(\omega)$ is calculated from the experimental data and the index of refraction of quartz is n_Q=2.1 in this frequency range. The phase shift (φ_m) is calculated by taking the experimental data of the time domain scan though isopropanol and applying an appropriate phase shift until the isopropanol data match the nanofluid time-domain data. Then once φ_m is determined by using this fitting procedure, and n_Q as well as $n_{iso}(\omega)$ is also calculated experimentally, we assume that α_{iso} is very similar to α_{NF} which is justified since the measurements as shown in chapter 3 show that the absorption through the nanofluid and hot fluid is not much different. After these steps, then the index of refraction of nanofluid n_{NF} can be calculated by using equation 4.1.23. Once the index of refraction is calculated we check the transmission amplitude (equation 4.1.22) with the measured transmission amplitude to see what the absorption coefficient of the nanofluid is actually. After we obtain this result we place it back into equation 4.1.23 to calculate α_{NF} once again. This iterative procedure gives an estimate for the error in calculating the nanofluid refractive index. The next section explains the fitting procedure to obtain the phase shift in detail.

4.1.1 FITING CURVE ANALYSES

Above φ_m was used to describe the phase shift, here in this section we call this shift χ'. Thus, χ' is used to refer to the phase shift obtained from the fitting curve analyses of the experimental data.

The THz time-domain wave forms were all analyzed using OriginPro8 SR1 program. This program edition FFT function (8.0) was verified with MatLab software to be working properly. Fast Fourier Transformation(FFT) and Inverse Fast fourier Transformation (IFFT) functions were used to modify the isopropanol time-domain THz waveform data sets.

Since this is a complex procedure checks were performed to ensure the inverse tranbsformation gave the correct result. Thus, we confirmed for different time-domain data sets that the IFFT transforms the FFT result back to its original time-domain data set when no phase shift was applied.

This is explained in detail as follows:
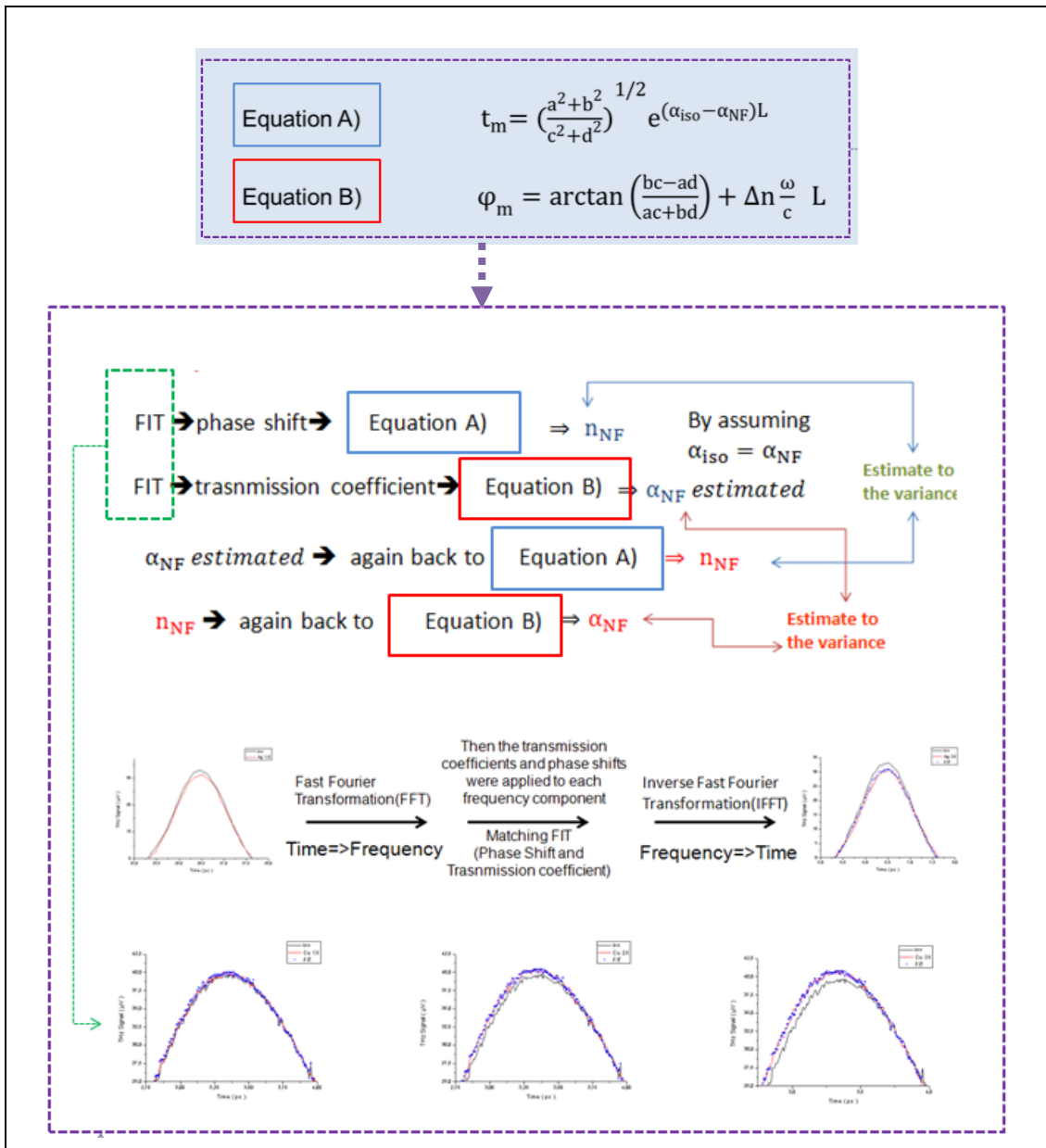
Figure 4.1.3. The Fitting curve analyses flow chart. Total transmission amplitude and total phase change Equations 4.1.22 and 4.1.23. are symbolized as equation A and B. First we calculated the index of refraction (Equation A) of nanofluid by assuming that the absorption coefficients of isopropanol and nanofluid sample are to be equal. Then by using Equation B the absorption coefficient of nanofluid is calculated and by implanting this calculated value back to equation A we calculated the index of refraction of nanofluid sample the difference in between the two calculated index of refraction values gives the estimate of variance. By using the same methodology we implanted index of refraction value which is calculated at

the second interval in to the equation B in order to estimate the variance of absorption coefficient.

In the following figures there will be three data sets: Black lines will represent the data points of the reference pulse in the time-domain (typically this is the host fluid measurement—isopropanol), the red line is the actual data set of the THz pulse through the nanofluid solution with either a positive or negative time shift and change in amplitude. The blue squares represent the fit that was obtained after IFFT was applied to the data set which was obtained after shiftting the phase of the data set that was obtained after FFT was applied to the black line (isopropanol data set).

The blue dots were obtained by applying the following steps: First, the time domain data of the reference pulse obtained from the experimental analysis of isopopanol was transformed to frequency domain by appliying Fast Fourier Transformation(FFT). Then the transmission coefficients and phase shifts were applied to each frequency component till the matching fit was obtained. After obtaining the matching phase shift and the total transmission coefficient, the resultant spectrum was transformed back to the time domain by Inverse Fourier Transformation (IFFT).

First, results are shown for Ag nanoparticle suspensions. These data sets show a slight positive phase shift which can be well explained by the theory as described in the previous section. While we expect the conducting medium to give a negative phase shift when the THz pulse travels from the quartz into the nanofluid, the path length of the quartz cuvette itself (2mm) when considered will negate this effect resulting in an overall positive phase shift. The Ag nanoparticle suspension data fits this picture well as shown below. The Ag analysis initially was done for a scan step size of $20\mu m$ (will be referred to as low resolution from here on afterwards), as stated in chapter 3 this results in a refractive index resolution of 0.01.

Figure 4.1.4. THz Time domain Spectrum of Ag nanofluid solution of 1X concentration versus isopropanol reference data and the matching fitting curve plots.

Figure 4.1.5. THz Time domain Spectrum of Ag nanofluid solution of 2X concentration versus isopropanol reference data and the matching fitting curve plots

Figure 4.1.6. THz Time domain Spectrum of Ag nanofluid solution of 3X concentration versus isopropanol reference data and the matching fitting curve plots.

After these measurements the Ag analysis was also done for a scan step size of 2μm (will be referred to as high resolution from here on afterwards), as stated in chapter 3 this results in a refractive index resolution of 0.001.

Figure 4.1.7. THz Time domain Spectrum of Ag nanofluid solution of 1X concentration versus isopropanol reference data and the matching fitting curve plots.

Figure 4.1.8. THz Time domain Spectrum of Ag nanofluid solution of 2X concentration versus isopropanol reference data and the matching fitting curve plots.

Figure 4.1.9. THz Time domain Spectrum of Ag nanofluid solution of 3X concentration versus isopropanol reference data and the matching fitting curve plots.

Second, results are shown for Cu nanoparticle suspensions. These data sets show a slight negative phase shift which can be well explained by the theory if we only consider the first interface (1 to 2 or quartz to nanofluid) to dominate the transmission of the THz pulse as described in the previous section. Further analysis needs to be performed to understand the effects in Cu nanofluidic solutions. In addition, Pd nanoparticle solutions also show either no phase shift or negative phase shift. As was explained previously, since the pathlength in the quartz cuvette is so long (2mm) this should negate any negative phase shift, and we should observe a positive phase shift. The reason that we do not may be attributed to dynamics within the nanofluid which was not evident for the Ag nanoparticle solutions.

Here we fit the Cu nanoparticle suspension time-domain data to show the magnitude of the negative phase shift which occurs when the THz pulse traverses these samples. The Cu analysis was done for a scan step size of 2μm, as stated in chapter 3 this results in a refractive index resolution of 0.001.
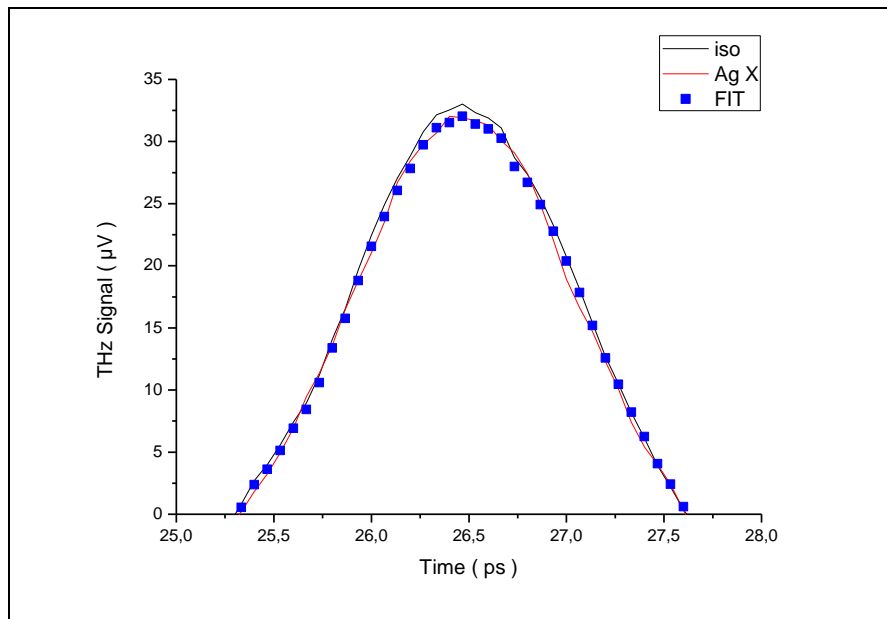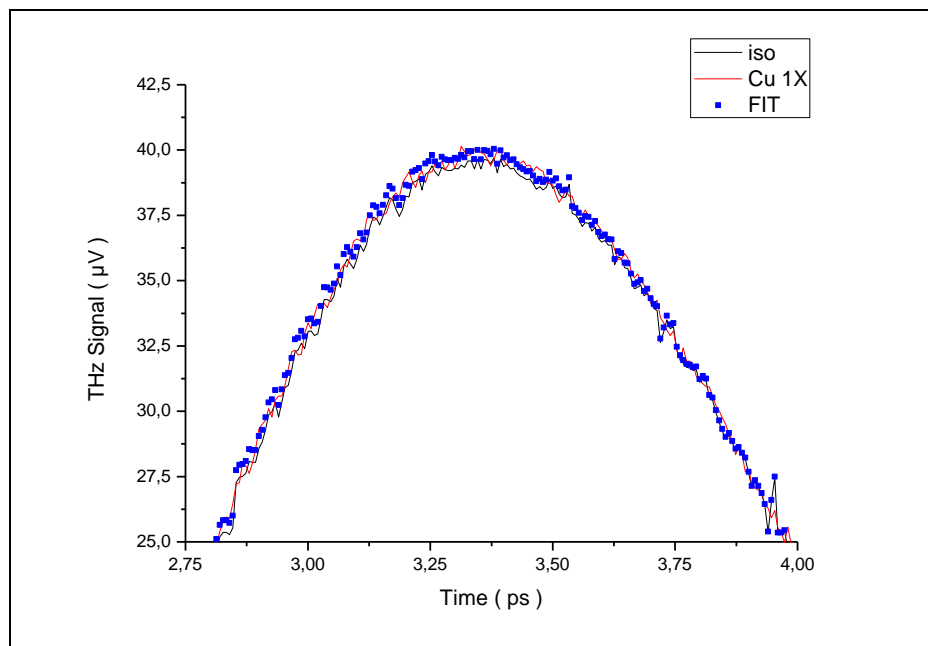

Figure 4.1.10. THz Time domain Spectrum of Ag nanofluid solution of 1X concentration versus isopropanol reference data and the matching fitting curve plots.
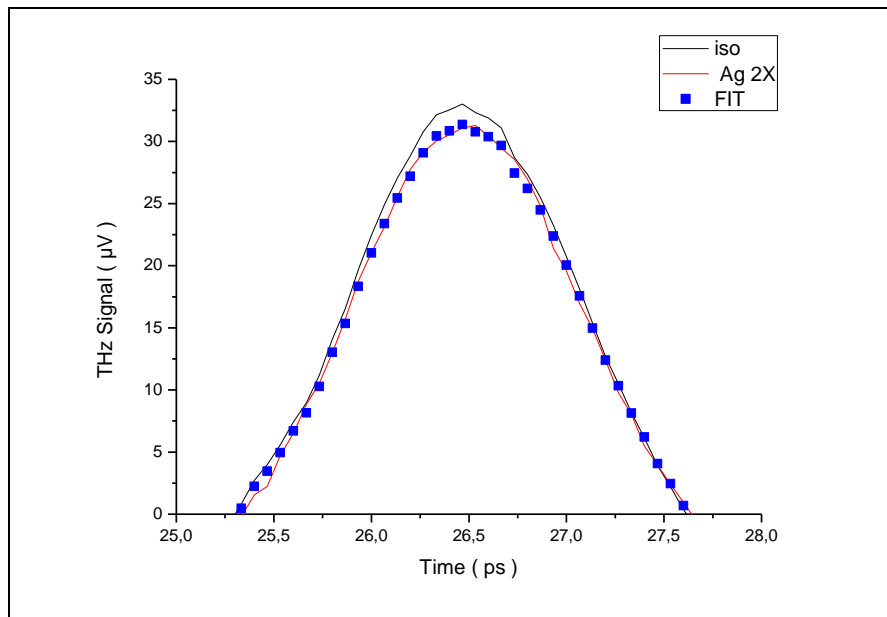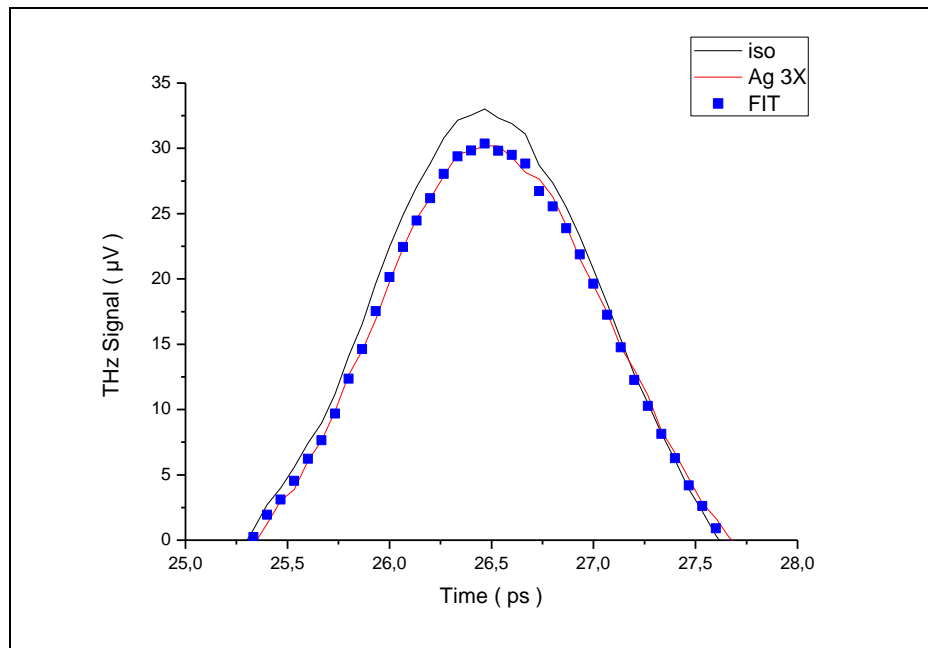
63
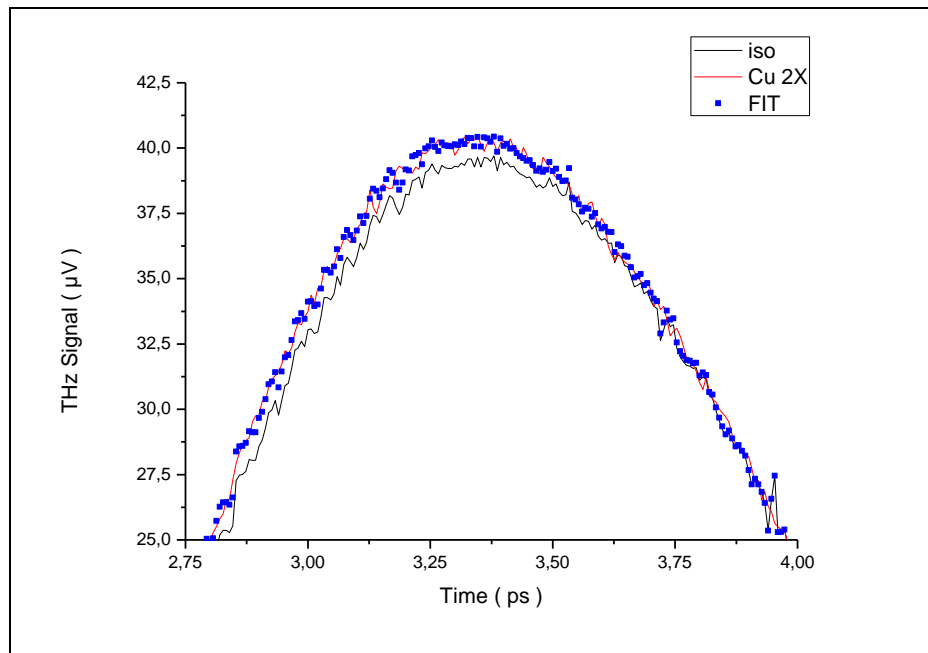
Figure 4.1.11. THz Time domain Spectrum of Ag nanofluid solution of 2X concentration versus isopropanol reference data and the matching fitting curve plots

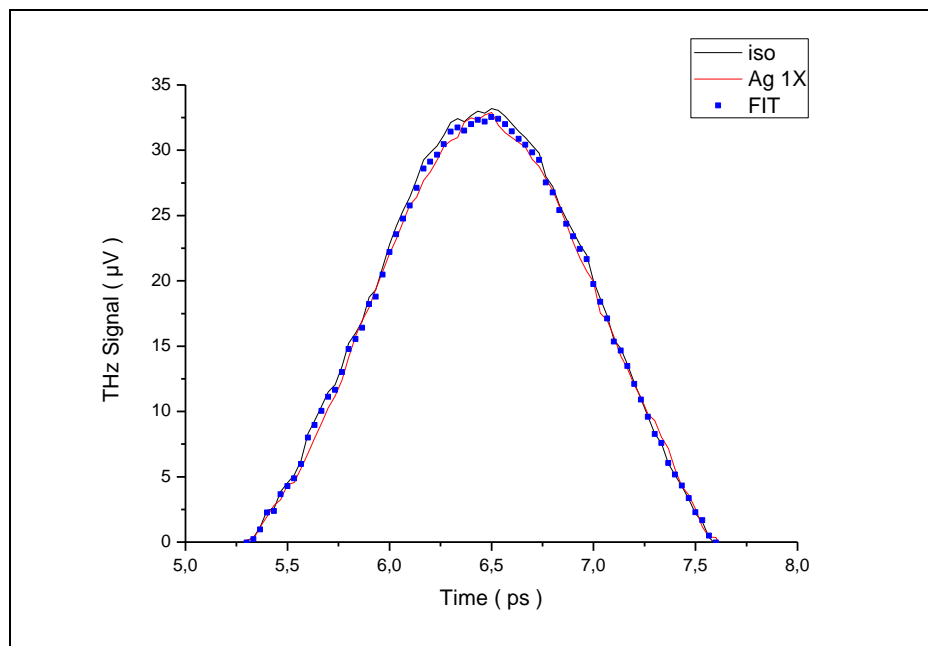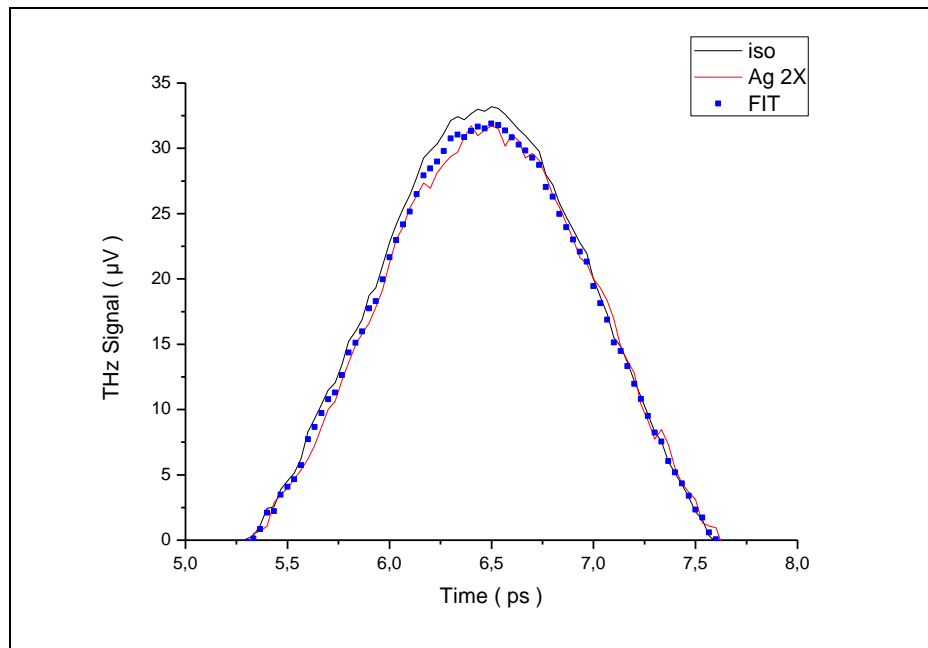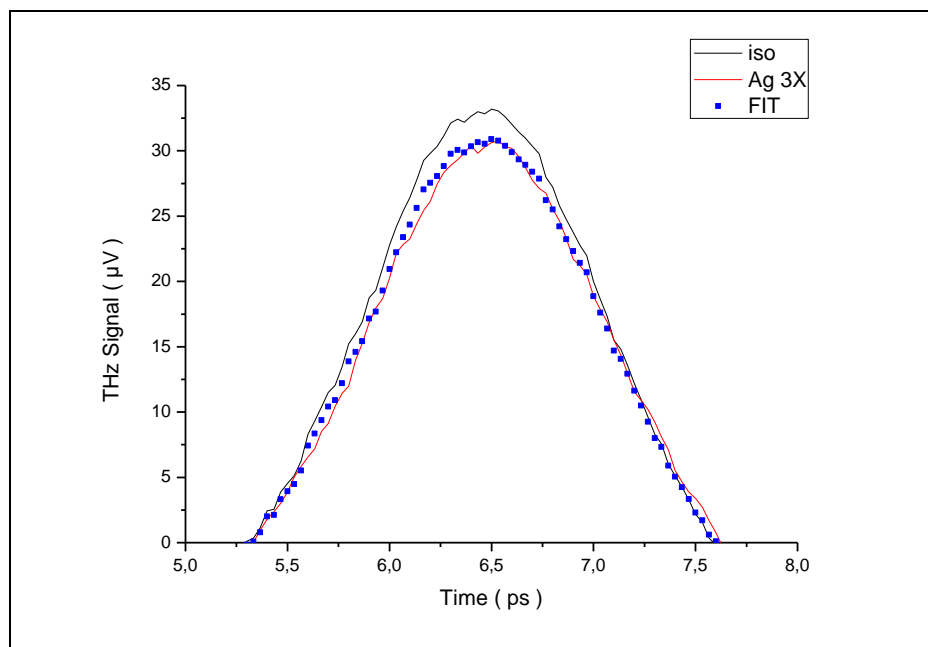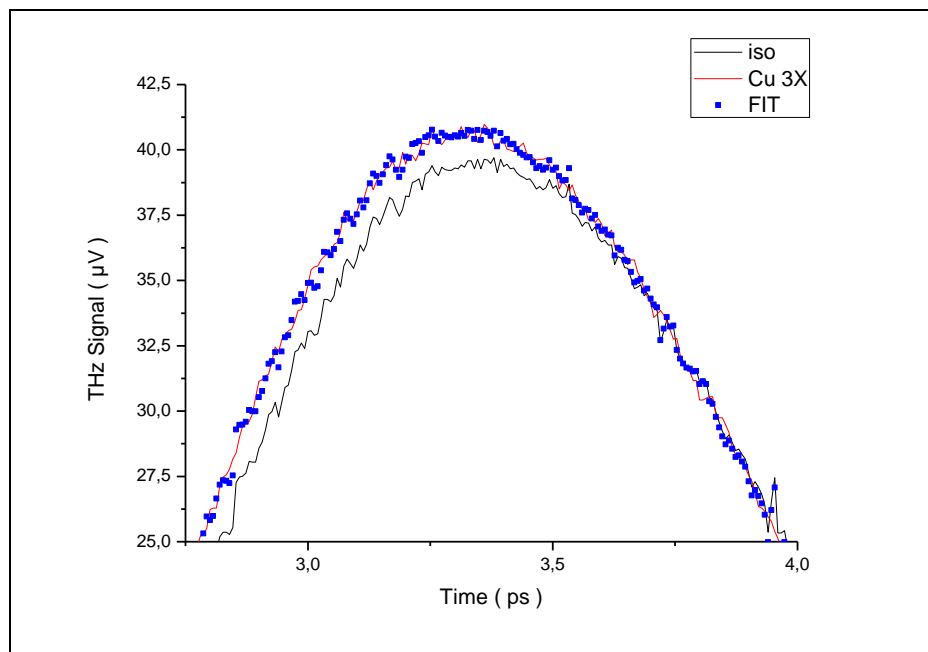**Figure 4.1.12.** THz Time domain Spectrum of Cu nanofluid solution of 3X concentration versus isopropanol reference data and the matching fitting curve plots.

4.1.2. CALCULATION RESULTS

For the low resolution scan for the Ag Nanoparticles, from the fitting curve plots given in chapter 4.1.1. , the phase shift χ' and total transmission coefficient t_m was found to be;

Table 4.1.1. Total transmission amplitudes calculated from the time domain data fit for the low resolution scan.

Low Resolution Scan	t_m
Ag 1X	$0,97 \pm 0,01$
Ag 2X	$0,95 \pm 0,01$
Ag 3X	$0,92 \pm 0,01$
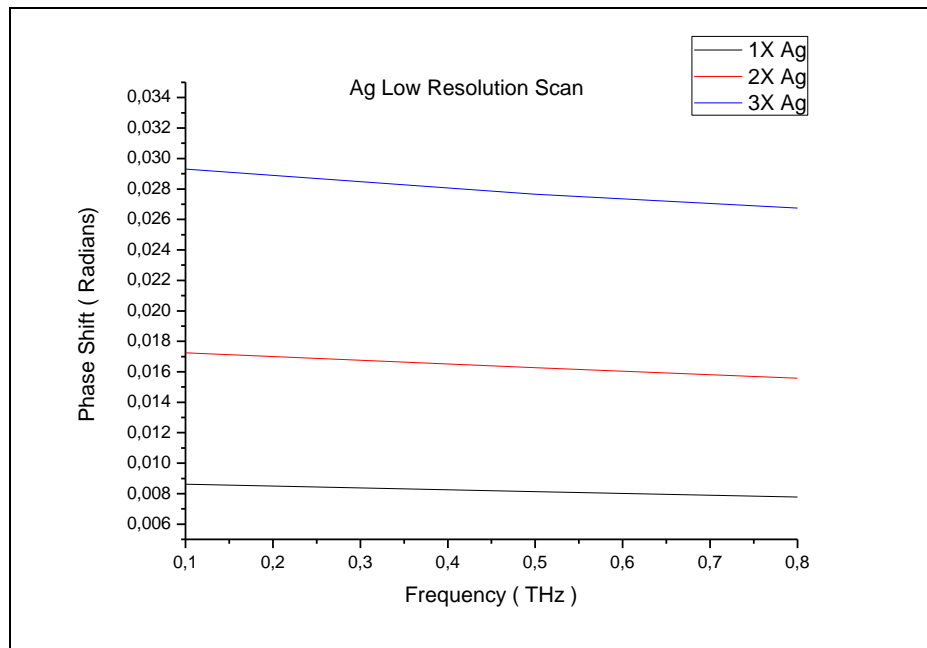
Figure 4.1.13. The phase shift χ' calculated from the time domain data fit for the low resolution scan.

As stated previously to calculate the index of refraction of the nanofluid we performed two iterative steps. First we used the equation 4.1.23. to calculate the index of refraction of n_{NF} by assuming: $\alpha_{iso} \cong \alpha_{NF}$ and then we estimated the α_{NF} by using equation 4.1.22 and comparing the t_m amplitude we obtained from the actual data to the calculated one using our initial n_{NF} result. Afterwards, we used this new α_{NF} (ratio with respect to α_{iso} is given in table

4.1.2) in equation 4.1.23 and calculated index of refraction of the nanofluid once again. The difference between them gives an estimate to the variance of the nanofluid refractive index and its dependence on the absorption coefficient. These results are given in Table 4.1.3.

Table 4.1.2. The estimated absorption ratio of Ag nanofluid 1X concentration to isopropanol for the given THz frequencies.

THz	$\frac{\alpha_{NF}}{\alpha_{iso}}$ for Ag 1X	$\frac{\alpha_{NF}}{\alpha_{iso}}$ for Ag 2X	$\frac{\alpha_{NF}}{\alpha_{iso}}$ for Ag 3X
0,1	1,08370	1,08400	1,08440
0,5	1,03495	1,03497	1,03500
0,8	1,02020	1,02027	1,02029

Table 4.1.3. The index of refraction data calculations of the given Ag nanoparticle suspensions.

THz	Refractive Index isopropanol	Ag X	Ag 2X	Ag 3X
0,1	1,70754	1,70942±0,00005	1,71138±0,000048	1,71413±0,000052
0,5	1,57506	1,57533±0,00005	1,57571±0,000048	1,57626±0,000048
0,8	1,56127	1,56348±0,00099	1,56168±0,000046	1,56199±0,000023

In the same manner as the previous discussion, for the high resolution scan for the Ag Nanoparticles and from the fitting curve plots given in chapter 4.1.1. , the phase shift χ' and total transmission coefficient t_m was found to be:

Table 4.1.4. Total transmission amplitudes calculated from the time domain data fit for the high resolution scan.

High Resolution Scan	t_m
Ag X	0,98±0,01
Ag 2X	0,96±0,01
Ag 3X	0,93 ±0,01
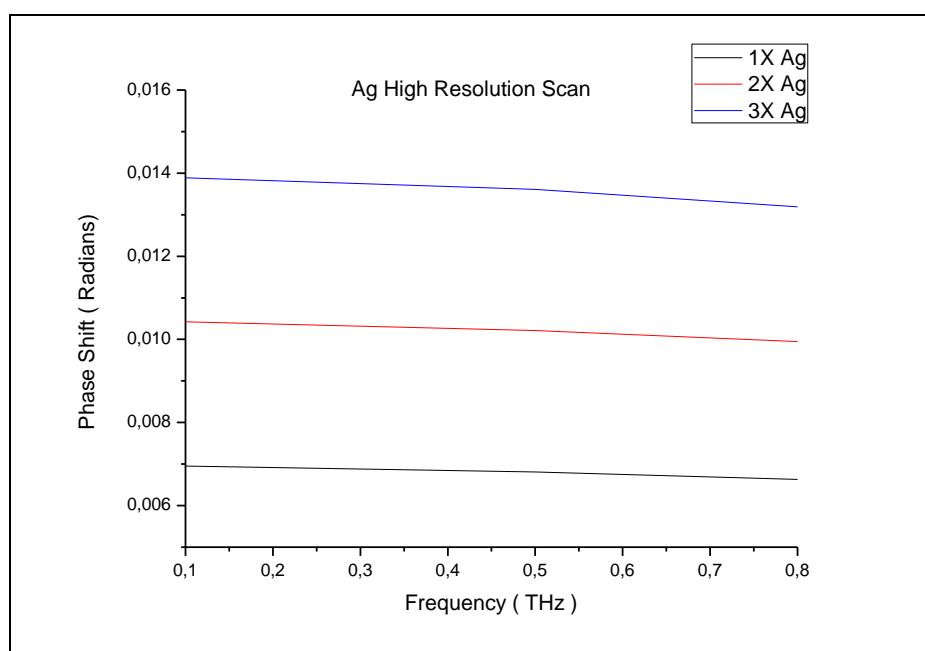
Figure 4.1.14. The phase shift χ' calculated from the time domain data fit for the high resolution scan.

As described above the ratio of the absorption coefficients and calculated refractive indices of the Ag nanofluids are given in Table 4.1.5 and Table 4.1.6 respectively.

Table 4.1.5. The estimated absorption ratio of Ag nanofluid to isopropanol for the given THz frequencies for the high resolution scan.

THz	$\frac{\alpha_{NF}}{\alpha_{iso}}$ for Ag 1X	$\frac{\alpha_{NF}}{\alpha_{iso}}$ for Ag 2X	$\frac{\alpha_{NF}}{\alpha_{iso}}$ for Ag 3X
0,1	1,03355	1,03362	1,03368
0,5	1,01757	1,01758	1,01758
0,8	1,01560	1,01561	1,01561

Table 4.1.6. The index of refraction data calculations of the given Ag nanoparticle suspensions for the high resolution scan.

THz	Refractive Index of isopropanol	Ag X	Ag 2X	Ag 3X
0,1	1,66273	1,66360±0,00012	1,66416±0,00012	1,66471±0,00012
0,5	1,59234	1,59263±0,000011	1,59278±0,000011	1,59294±0,000011
0,8	1,56127	1,56145±0,0000046	1,56155±0,0000047	1,56164±0,0000047

Finally, to show the relative negative phase shift, we analyzed the Cu nanoparticle solution datasets as given in section 4.1.1. From the fitting curve plots the phase shift χ' and total transmission coefficient t_m was found to be;

Table 4.1.7. Total transmission amplitudes calculated from the time domain data fit for the high resolution scan.

10,5-9,5 mm Scan	t_m
Cu 1X	$1,0085 \pm 0,0005$
Cu 2X	$1,018 \pm 0,0005$
Cu 3X	$1,025 \pm 0,0005$
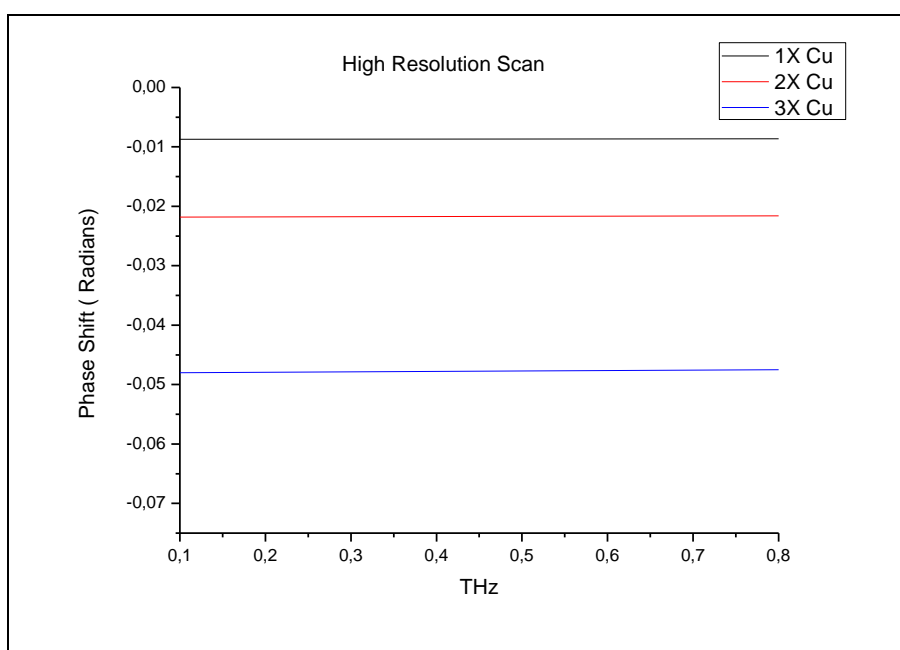
Figure 4.1.15. The phase shift χ' calculated from the time domain data fit for the high resolution scan.

4.2. A NEW METHOD FOR NANO PARTICLE CONCENTRATION CALCULATION

As explained in Chapter 3.2.2. the index of refraction of Ag at 0,5 THz is found to be 997,99 which is much greater than the index of refraction of the base fluid (isopropanol) used. As we have predicted the additon of Ag nanoparticles to 2-propanol solution increases the index

refraction of the solution. A method is developed to predict the particle concentration in the nanofluid.

The Maxwell-Garnett theory is one of the most widely used effective medium theories which describes the optical properties of heterogeneous materials in terms of effective dielectric constants. It is used to describe the effective dielectric of a heterogeneus medium where there are includions of conducting particles in a deielctric host.

Dielectric constant of nanofluid suspension ϵ_{NF} that was found in the previous section is the effective dielectric constant since spherical Ag nanoparticles of radius r are suspended in 2-propanol solution as a host medium of dielectric constant ϵ_{iso}. For sphere sizes much smaller than the wavelength of the incident radiation, Maxwell-Garnet [79] model can be employed in an explicit form as shown in equation 4.2.1.

$$\epsilon_{NF} = \epsilon_{iso} \frac{\epsilon_{NP}(1+2f) - \epsilon_{iso}(2f-2)}{\epsilon_{iso}(2+f) + \epsilon_{NP}(1-f)} \qquad \textbf{4.2.1.}$$

where,

$$f = \frac{4\pi}{3} na^3 \qquad \textbf{4.2.2.}$$

f is the volume fraction of the embedded particles of radius a and n is the particle number density

Dielectric constant is the square of refractive index given as:

$$\epsilon = n^2 \qquad \textbf{4.2.3.}$$

Such that;

$$\epsilon_{NF} = n_{NF}^2 \quad , \qquad \epsilon_{NP} = n_{NP}^2 \quad , \qquad \epsilon_{iso} = n_{iso}^2$$

Using the results in the previous section for the high resolution scans where the dielectric constants were found for the nanofluid, and isopropanol host fluid as well as the literature value for the refractive index of Ag (assumed to be same as for Ag nanoparticles), the fill factor is calculated for 0,5THz as follows.

$$\epsilon_{iso} = 1{,}59234^2 = 2{,}53555 \qquad \text{at 0,5THz}$$

$$\epsilon_{NP} = 997{,}99^2 = 995984 \qquad \text{at 0,5 THz}$$

$$\epsilon_{NF} = 1{,}59263^2 = 2{,}53647 \qquad \text{at 0,5 THz for 1X Ag Concentration}$$

And **f** is calculated from equation 4.2.1. as shown in below table :

Table 4.1.8. Fill factor of Ag nanoparticles for 1X, 2X and 3X concentrations.

f for 1X Ag	$0{,}00012037 \pm 0{,}0000048$
f for 2X Ag	$0{,}00018503 \pm 0{,}0000048$
f for 3X Ag	$0{,}00024991 \pm 0{,}0000048$

f is the volume fraction of the embedded particles and contributes to the total nanoparticle area in the THz Path as shown in figure 4.2.1.

Area of THz   Area of Box   Nano Particle Area
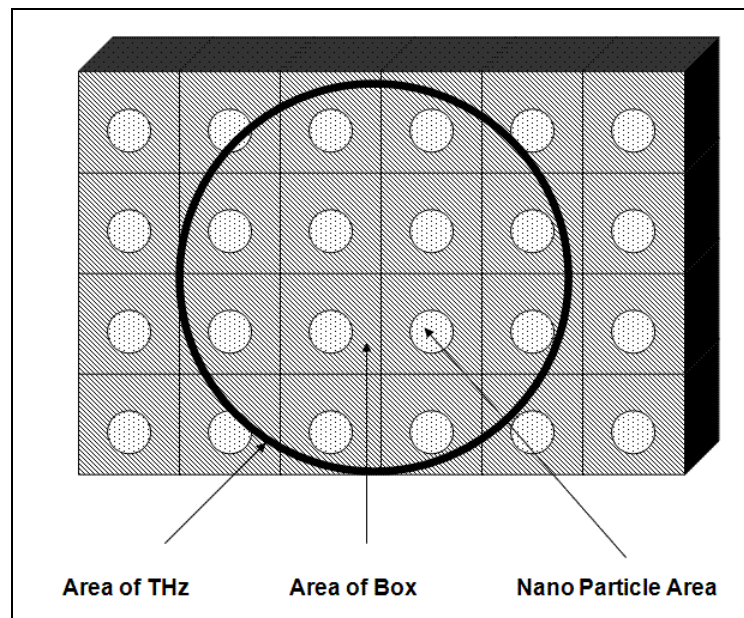
Figure 4.2.1 Illustration of the total nanoparticle area in the THz Path intersecting with the assumed unit particle surroinding cubes.

Using equation 4.2.2 for the Ag nanoparticle radius of 5nm, we can estimate the total nanoparticle presence in the THz beam path as:

Table 4.1.9. Ag nanoparticle concentrations for 1X, 2X and 3X concentrations.

NP Concentration for Ag 1X	$2,29562 \cdot 10^{14} \pm 0,092 \text{ particle}/cm^3$
NP Concentration for Ag 2X	$3,53555 \cdot 10^{14} \pm 0,092 \text{ particle}/cm^3$
NP Concentration for Ag 3X	$4,77543 \cdot 10^{14} \pm 0,092 \text{ particle}/cm^3$

The calculated Ag nano particle concentration well agrees with commercially available (although we note that these commercially available nanoparticles were not manufactured using laser ablation based technqiues) 10nm Biopure[TM] Silver [80] nanoparticles products sold by Nanocomposix Company Inc. based in San Diego, 4878 Ronson Court. The size distrubutions of their available products are in between 8 nm to 10 nm and the concentrations are differing according to the surfactants and the solvents used, from $3,8 \cdot 10^{14}$ to $4,9 \cdot 10^{14} \text{ particles}/ml$ for a mass concentration of 1mg/ml. Higher concentrations could lead to aggregation, so our results seem to agree within an order of magnitude with commercially available nanofluids.

4.3. SUMMARY AND DISCUSSION

In this chapter the sample holder system that consisted of of 5 multiple layers of air, quartz and nanofluid sample interfaces was modeled as a plane wave of angular frequency ω is transmitted over a plane parallel absorbing film with known thickness and index of refraction which is situated in between two air-quartz and quartz-air (dielectric) media.

The ratio of sample pulse to reference pulse in the frequency domain is described in terms of total transmission amplitude and total phase change. These were modeled based on Fresnel transmission coefficients between dielectric and conducting media [75]. In order to determine the nanofluid refractive index the other parameters were obtained as follows: Using the index of refraction of quartz at these THz frequencies with the index of refraction of the 2-propanol base fluid along with the estimation of the phase shift between reference (2-propanol) and nanofluid (Ag nanoparticles in 2-propanol) the nanofluid refractive index was determined at certain frequencies (0.1, 0.5 and 1 THz).

In addition, the transmission amplitudes in the frequency domain were obtained from the fitting curve analyses of the experimental data as well as the total phase shifts.

To fit the data these steps were followed: the time domain data of the reference pulse optained from the experimental analyses of isopopanol was transformed to frequency domain by appliying FFT and then the reference signal was manipulated by appliying transmission coefficients and phase shifts which fit the nanofluid time domain data. The resultant spectrum was obtained by transforming the modified FFT spectrum back to the time domain by IFFT.

Our results suggest that both the absorption and refractive index of the base fluid changed with the addition of the nanoparticles. A method was developed to arrive at the particle concentration in the nanofluid sample in which the calculated nano particle concentration well agreed in magnitude with commercially available nanoparticles products.

The mathematical theory we used for the calculation of index of refraction truly satisfied the transmission and absorption values obtained for Ag nanoparticles on the other hand our theory did not hold for Cu or Pd nanoparticles.

For Cu nanoparticles we modeled the phase shift and saw that it was negative, which suggests that the Cu nanofluid fluid system is highly absorptive. However, the amplitude did not decrease upon transmission but increased which suggests that over the 2mm pathlength absorption did not change much when compared to the host fluid It is noted in light of reference [81] that the observed negative shift in Cu nanoparticles are not associated with superluminal propagation. The frequency dependent phase shift at the first interface (quartz to absorbing Cu nanofluid sample) can account for the observed negative shift. However, the pathlength of 2mm is too large and would surely negate this effect. In addition upon transmission back to the dielectric interface a positive shift would have occurred. Thus, we can only conclude two things, either,

- The Cu nanoparticles are concentrated near the first interface in a very thin layer,

or

- The host fluid chemistry has been altered somehow with the inclusion of Cu nanoparticles. This change in chemistry could result in a decrease in refractive index however this would not explain the increase in amplitude.

72

CHAPTER 5

CONCLUSION

In this thesis, we constructed a THz Time Domain Spectrometer (THz-TDS) to examine the effects of nanoparticles in host fluids that can be used for cooling purposes in microchannel heatsinks. Using this technique, optical properties such as the absorption coefficient and refractive index of nanoparticle solutions were measured in the THz region. Using the change in refractive index between host fluid, which was isopropanol, and the nanofluid which was metal nanoparticles in isopropanol, we were able to calculate the concentration of Ag nanoparticles for various concentrations. Throughout the measurements a photoconductive antenna was used for THz generation and a <110> ZnTe crystal was used in the electro optic (EO) method for THz detection.

At first, a series of measurments using a 2 mm path length quartz cuvette on various polar liquids which are used in nanoparticle suspensions for their tendency to stop aggregation in such suspensions were investigated. 2-propanol (99.5%) is found to be the best base fluid to be used for the nanoparticle suspensions for its weak THz absorptivity when compared to the other polar fluids such as Ethanol (99.5%), Ethylene glycol (99%), methanol (95%) and distilled water.

Ag, Cu and Pd nanoparticle solutions were manufactured at Institute of Materials Science and Nanotechnology (UNAM- Bilkent University) by the Bülend Ortac laser group using pulsed laser ablation from a bulk metal sample placed in a liquid and the size distribution of nanoparticles were determined by Zeta Potential Analyze Method. The diameter distributions of nanoparticles are measured to be as: 10 nm for Ag nanoparticles, 12 nm for Cu nanoparticles and 75 nm for Pd.

We prepared nanofluids samples of various concentrations of 1X, 2X and 3X for different nanoparticles of Ag, Cu and Pd which were only prepared by diluting with pure (99.5%) isopropanol in order to cancel possible effects of possible changes in the chemistry of the isopropanol as a result of the interaction of the alcohol with the metal nanoparticle which can be further aided by the heat treatment during laser ablation process.

Table 5.1. Time Domain and Frequency Domain measurement results are given for easy comparison.

	Time Domain Data	Refractive Index Data	Absorption Data
	a.	b.	c.
Figure 3.3.3.2.			
Figure 3.3.3.3.			
Figure 3.3.3.4.			
Figure 3.3.3.5.			
Figure 3.3.3.6.			
Figure 3.3.3.7.			
Figure 3.3.3.8.			

Nanofluids are fluids whose absorption coefficient as well as refractive index is thought to change with the addition of the nanomaterials or nanoparticles. To investigate the nanofluids we have taken a serious of measurements which were taken for 2-proponol solutions with and without the Cu, Ag and Pd nanoparticles, in order to control sedimentation and aggregation of nanoparticles we repeated the measurments after up to 7 days to control the sedimentation of particles.

As a first result of the measurements, the frequency dependent quantities such as power absorption coefficient and refractive index showed no discernible difference between the isopropanol host fluid and the nanofluid samples of Ag, Pd and Cu. On the other hand the time-domain profiles showed interesting differences such that we observed shifts in time and in intensity.

We observed a positive time shift for Ag nanoparticles but a decrease in amplitude which is a result of an increase in absorption. The mathematical theory we used for the calculation of index of refraction truly satisfied the transmission and absorption values obtained for Ag nanoparticles. This theory was based on the propagation of a beam through various layered conducting and dielectric media.

We observed a negative time shift in Pd and Cu nanoparticle suspensions with changes in intensity. The observed negative shift in Cu nanoparticles are not associated with superluminal propagation as thought to be at first glance.

For Cu nanoparticles we modeled the phase shift and saw that it was negative, which suggests that the Cu nanofluid fluid system is highly absorptive. The frequency dependent phase shift at the quartz to absorbing Cu nanofluid sample interface is found to be a possible explanation for the observed negative shift. On the other hand since the path length of sample holder being 2mm is too large a positive shift was expected. We conclude in two possible results that either the Cu nanoparticles are concentrated in a very thin layer or the host fluid chemistry has been altered somehow with the inclusion of Cu nanoparticles as this change in chemistry could result in a decrease in refractive index.

Finally, our results suggest that both the absorption and refractive index of the base fluid changed with the addition of the nanoparticles. For the Ag nanoaprtcile solutions for which a positive shift occurred we developed a method to calculate the particle concentration in the nanofluid sample based on effective medium theory. Maxwell-Garnett model was to explain the inclusion of metal spherical particles in a host medium. This allowed for the estimation of

the nano particle concentration which agreed in magnitude with commercially available nanofluid products.

In conclusion, we have investigated metal nanoparticles with different particle sizes and concentrations by using a THz TDS system. We observed that the THz transmission through a static solution with and without these metal nanoparticles show differences which suggest that this method can be used to probe the dynamics of nanoparticles in nanofluids. We also observed that the absorption and refractive index of the base fluid changes with the addition of the nanoparticles. We developed a method to calculate the particle concentration in the nanofluid sample based on the change in the refractive index further more for a NF sample of given geometry and the concentration the particle size can also be calculated. Using refined techniques this method can be further developed to monitor the particle flow in THz non-opaque micro channels which can aid in future development of nanofluid cooling systems for micro device applications. The dynamics of the aggregation and sedimentation problems of nanofluids with in the micro channels would also be investigated as a future work.

REFFERENCES:

[1] Richar Feynman, "There is plenty of room at the bottom"December 29th 1959 at the annual meeting of the American Physical Society at the California Institute of Technology (Caltech)

[2] I. Jones, T. J. Rainsford, B. Fischer and D. Abbott " Towards T-ray spectroscopy of retinal isomers: A review of methods and modelling" Vibrational Spectroscopy, 41, 144-154 (2006)

[3] Benning and Rohrer, Scannin tunnelin Microscopy /Volume 126, Issues 1–3, 2 March 1983, Pages 236–244

[4] Foster LE. Nanotechnology. New York: Prentice Hall; 2006.

[5] .http://www.nobelprize.org/nobel_prizes/physics/laureates/1986, last visitted May 2012

[6] Guozhong Cao, Nanostructures and Nanomaterials, 2nd edition, Imperial College Press in 2004

[7] Choi, U. S., 1995, "Enhancing Themxd Conductivity of Fluids with Nanoparticles, " Developments and Applications of Non-Newtonian Flows, eds. D. A. Siginer and H. P. Wang, The American Society of Mechanical Engineers, FED-VO1. 23 VM.D VO1.66, pp. 99-105.

[8] Suranjan Sarkara_ and R. Panneer Selvam/Molecular dynamics simulation of effective thermal conductivity and study of enhanced thermal transport mechanism in nanofluids/ Computational Mechanics and Nanotechnology

[9] G.r.Blackwell , "Thermal Management" The Electronic Packaging Handbook Boco Raton CRC Press LLC,(2000).

[10] Touloukian, Y. S., Powell, R. W., Ho, C. Y., and Klemens, P. G., 1970, Thermophysical Properties of Matter, VO1.2, Plenum Press, New York.

[11] D. Wen and Y. Ding, Experimental Investigation Into Convective Heat Transfer of Nanofluids at the entranceRegion Under Laminar Flow Conditions, Int J Heat Mass Transfer (2004),pp,5181-5188

[12] Y. Xuan, Q. Li, Int. J. Heat and Fluid Flow 21 (2000) 58-64

[13] S. Lee, S.U.S. Choi, S. Li and J.A. Eastman, Measuring Thermal Conductivity of Fluids Containing Oxide Nanoparticles, ASME J Heat Transfer 121 (1999), pp.280-289

[14] Göker Türkakar, Tuba Okutucu-Özyurt, Dimensional optimization of microchannel heat sinks with multiple heat sources, International Journal of Thermal Sciences, in press, available online 23 January 2012.

[15] Aziz Koyuncuoğlu, Tuba Okutucu, Haluk Külah, A CMOS Compatible Metal-Polymer Microchannel Heat Sink for Monolithic Chip Cooling Applications, proceedings of the International Heat Transfer Conference IHTC14 August 8-13, 2010, Washington, DC, USA

[16] Terahertz microscopy with sub micrometer resolution, Roland Kersting, Hou-Tong Chen, Nicholas Karpowicz and Gyu Cheon Cho, J. Opt. A: Pure Appl. Opt. 7 (2005) S184–S189

[17] Optical properties of the metals in the infrared and far infrared M. A. Ordal, L. L. Long, R. J. Bell, S. E. Bell, R. R. Bell, R. W. Alexander, Jr., and C. A. Ward, 1 April 1983, Vol. 22, No. 7, APPLIED OPTICS

[18] Dragoman, D.; Dragoman, M. Progress in Quantum Electronics 2004, 28, 1-66.

[19] D. Mittleman, Ed., Sensing with Terahertz Radiation. Berlin: Springer, 2002.

[20] J. D. Wai Lam Chan and D. M. Mittleman, "Imaging with terahertz radiation," Rep. Prog. Phys., vol. 70, p. 1325, 2007.

[21] Y. S. Lee " Principles of Terahertz Science and Technology" Springer Science+Business Media, LLC, (2009)

[22] J. D. Wai Lam Chan and D. M. Mittleman, "Imaging with terahertz radiation," Rep. Prog. Phys., vol. 70, p. 1325, 2007.

[23] Y. Ung, B. M. Fischer, H. Ng and D. Abbott "Towards Quality Control of Food Using Terahertz" Proc. of SPIE 6799 (2007)

[24] M.R. Leahy-Hoppaa, M.J. Fitcha, X. Zhengb, L.M. Haydenb, R. Osiandera, Wideband terahertz spectroscopy of explosives, Chemical Physics Letters/Volume 434, Issues 4–6, 5 February 2007

[25] Al-Douseri, F., M., Applications of T-Ray spectroscopy in the petroleum field/1-80 (2005).

[26] Zhang, X. C. et al., Generation of femtosecond electromagnetic pulses from semiconductor surfaces, Appl. Phys. Lett., 56, 1011, 1990.

[27] Auston, D. H. and Cheung, K. P, Coherent time domain far-infrared spectroscopy, J.Opt. Soc. Am. B, 2, 606, 1985.

[28] Nahata, A., et al., Generation of terahertz radiation from a poled polymer, Appl. Phys. Lett., 67, 1358, 1995

[29] Marie S. C. Luo, Shun Lien Chuang, Paul C. M. Planken, Igal Brener, Hartmut G. Roskos, and Martin C. Nuss, Generation of Terahertz Electromagnetic Pulses from Quantum-Well Structures, IEEE Journal of Quantum Electronics, Vol. 30, No. 6, June 1994

[30] Weiss, C., Magnetic-field-enhanced generation of terahertz radiation in semiconductor surfaces, Applied Physics Letters, Volume:77 Issue:25/ 4160 - 4162 /2000

[31] Hartmut G. Roskos, Martin C. Nuss, Jagdeep Shah, Karl Leo, David A. B. Miller, Coherent Submillimeter-Wave emission from Charge Oscillations in a Double-Well Potential, Physical Review Letters/ volume 68, number 14, April 1992

[32] Anttı V. Flusane, Frequency Multipliers for Millimeter and Submillimeter Wavelengths, Proceedings of the IEEE/VOL. 80, No. 11, November 1992

[33] Tohru Takada, Masamichi Ohmori, Frequency Triplers and Quadruplers with GaAs Schottky-Barrier Diodes at 450 and 600 GHz, IEEE Transaction on Microwave Theory and techniques, VOL. MTT-27, NO. 5, MAY 1979, 519

[34] Colin Baker, I. Gregory, M. Evans, W. Tribe, E. Linfield, and M. Missous, All-optoelectronic terahertz system using low-temperature-grown InGaAs photomixers, Optics Express, Vol. 13, Issue 23, pp. 9639-9644 (2005)

[35] P. Canarelli, Z. Benko, R. Curl, and F. K. Tittel, Continuous-wave infrared laser spectrometer based on difference frequency generation in AgGaS2 for high-resolution spectroscopy, JOSA B, Vol. 9, Issue 2, pp. 197-202 (1992)

[36] Sergey Cherednichenko, Arvid Hammar, Stella Bevilacqua, Vladimir Drakinskiy, Jan Stake, Alexey Kalabukhov, A Room Temperature Bolometer for Terahertz Coherent and Incoherent Detection, IEEE Transactions on terahertz science and technology, Vol. 1, No. 2, 395, 2011

[37] E.R. Brown, A system-level analysis of Schottky diodes for incoherent THz imaging arrays, Solid-State Electronics 48 (2004) 2051–2053, March 2004

[38] P. Helisto, A. Luukanen, L. Gronberg, J. Penttila, H. Seppa, H. Sipola, C. Dietlein, and E. Grossman, "Antenna-coupled microbolometers for passive THz direct detection imaging arrays," European Microw. Conf. pp. 35–38, 10-13 Sept. 2006.

[39] Keiding, S. R. J. Phys. Chem. A 1997, 101, 5250-5254.

[40] Knoesel, E.; Bonn, M.; Shan, H.; Heinz, "Charge transport and carrier dynamics in liguids probed by THz-Time Domain Spectrscopy", T. F. Phys. Rev. Lett. 2001, 86, 340.

[41] Batop, http://www.batop.de/products/terahertz/photoconductive-antenna, last visited May 2012

[42] Dragoman D. , Dragoman M. Progress in Quantum Electronics 2004, 28, 1-66.

[43] Davies, A. G. Linfield, E. H.; Johnston, "The development of terahertz sources and their applications", M. B., Phys. Med. Biol. 47 (2002) 3679-3689.

[44] Justin T. Darrow, Xi-Cheng Zhang, David H. Auston, Jeffrey D. Morse/ Saturation Properties of Large-Aperture Photoconducting Antennas, IEEE Journal of quantum electronics, Vol. 28, No. 6, JUNE 1992

[45] Beard, M. C.; Turner, G. M.; Schmuttenmaer, "Transient Photoconductivity in Dye-Sensitized Nanocrystalline TiO2 Films as Measured by Time-Resolved THz Spectroscopy", C. A. J. Phys. Chem. A, 2002, 106, 878-883

[46] K. Sakai, and M. Tani, "Introduction to Terahertz Pulses" K. Sakai (Ed.): Terahertz Optoelectronics,Topics Appl. Phys., 97, 1-30 (2005)

[47] Ussama A. Elani, A New Method for the Determination of Carrier Lifetime in Silicon Wafers from Conductivity Modulation Measurements , Journal of semiconductor technology and science, Vol.8, No.4, December, 2008 311

[48] Yun-Shik Lee, Principles of Terahertz Science and Technology, Page 60, Springfield 2009

[49] R. Yano, H. Gotoh, Y. Hirayama, S. Miyashita, Y. Kadoya, Terahertz wave detection performance of photoconductive antennas: Role of antenna structure and gate pulse intensity, J. Appl. Phys. 97, 103103 (2005)

[50] Y. S. Lee " Principles of Terahertz Science and Technology" Springer Science and Business Media, LLC, (2009)

[51] M. V. Exter, Ch. Fattinger, and D. Grischkowsky, "High- brightness terahertz beams charecterized with an ultrafast detector" Appl. Phys. Lett. 55, 4, 337-339 (1989).

[52] Y. R. Shen, "Far-infrared generation by optical mixing," Prog. Quant. Electron., vol. 4, p. 207, 1976.

[53] D. Auston and K. Cheung, "Coherent time-domain far-infrared spectroscopy," J. Opt. Soc. Am. B, vol. 2, pp. 606–612, 1985.

[54] K. Kawase, K. Suizu, S. Hayashi, and T. Shibuya, Nonlinear Optical Terahertz Wave Sources, Optics and Spectroscopy, 2010, Vol. 108, No. 6, 2010

[55] Paul C. M. Planken, Han-Kwang Nienhuys, Huib J. Bakker, and Tom Wenckebach, Measurement and calculation of the orientation dependence of terahertz pulse detection in ZnTe, JOSA B, Vol. 18, Issue 3, pp. 313-317 (2001)

[56] R. A. Cheville, "Terahertz Time-Domain Spectroscopy with Photoconductive Antenna".

[57] S. Verghese, K. A. McIntosh, E. R. Brown: IEEE Trans. Microwave Th. Tech. 45, 1301 (1997).

[58] A. Nahata and H. Cao, "Broadband phase-matched generation and detection of terahertz radiation" Proceedings of SPIE 5411, 150-157 (2004)

[59] A. Nahata, D. H. Auston, T. F. Heinz and C. Wu, "Coherent detection of freely propagating terahertz radiation by electro-optic sampling" Appl. Phys. Lett. 68, 8, 150-152 (1996)

[60] Hakan Altan, Characteristics of nanocomposites and semiconductor heterostructure wafers using THz spectroscopy, Federated Physics Department of NJIT and Rutgers-Newark, January 2005

[61] Kindt, J.T. , Schmuttenmaer, C.A.: Far-Infrared dielectric properties of polar liquids probed by femtosecond THz pulse spectroscopy Journal of Physics Chemistry 100(1996) 10373-10379

[62] Lloyd R. Snyder,Joseph Jack Kirkland,John W. Dolan Introduction to modern liquid chromatography 2010 J&W

[63] G Ledoux, D Amans , C Dujardin and K Masenelli-Varlot / Facile and rapid synthesis of highly luminescent nanoparticles via Pulsed Laser Ablation in Liquid / Nanotechnology / 2009

[64] S.I. Dolgaeva, A.V. Simakina, V.V. Voronova, G.A. Shafeeva, F. Bozon-Verdurazb, Nanoparticles produced by laserablation of solids in liquid environment, Applied Surface Science Volume 186, Issues 1–4, 28 January 2002, Pages 546–551

[65] Jyrki Lappalainen, Johannes Frantti, Vilho Lantto, Applied Surface Science Effect of laser-ablation process parameters and post-annealing treatment on ferroelectric PZT thin films, Volume 142, Issues 1–4, April 1999, Pages 407–412

[66] Optical properties of Al, Fe, Ti, Ta, W, and Mo at submillimeter wavelengths/Mark A. Ordal, Robert J. Bell, Ralph W. Alexander, Jr., Lawrence A. Newquist, and Marvin R. Querry, 15 March 1988, Vol. 27, No. 6, APPLIED OPTICS

[67] M. A. Ordal, L. L. Long, R. J. Bell, S. E. Bell, R. R. Bell, R. W. Alexander, Jr., and C. A. Ward , Optical properties of the metals Al, Co, Cu, Au, Fe, Pb, Ni, Pd, Pt, Ag, Ti, and W in the infrared and far infrared, , APPLIED OPTICS ,Vol. 22, No. 7, 1983,

[68] H. E. Bennett and J. M. Bennett, Optical Properties and Electronics Structure of Metals and Alloys, ed. F. Abeles (North-Holland, 1966), p. 175.

[69] Dawid W. Lynch and W.R., Hunterhand book of optical constants of solids 2 edited by Edward D. Palik1991 Academic press.inc.

[70] Solids Ernest V. Loewenstein, Donald R. Smith, and Robert L. Morgan , Optical Constants of Far Infrared Materials. 2: Crystalline , APPLIED OPTICS, Vol. 12, No. 2 February 1973 [71] Robert H. Giles , Characterization of Material Properties at Terahertz Frequencies, Submillimeter Technology Laboratory University of Massachusetts, Lowell

[72] Brian J. Kirby, Ernest F. Hasselbrink Jr., review, Zeta potential of microfluidic substrates , Electrophoresis 2004, 25, 187–202

[73] David D. Smith, Lanee A. Snow, Laurent Sibille, Erica Ignont / Tunable optical properties of metal nanoparticle sol–gel composites , Journal of Non-Crystalline Solids Volume 285, Issues 1–3, June 2001, Pages 256–263

[74] S. ROBERTS AND D. D. COON , Far-Infrared Properties of Quartz and Sapphire/ JOURNAL OF THE OPTICAL SOCIETY OF AMERICA , VOLUME 52, NUMBER 9 SEPTEMBER 1962

[75] M. Born and E. Wolf , Principles of Optics, 7th ed., Cambridge U. Press, Cambridge, 1999

[76] Lionel Duvillaret, Fre´de´ric Garet, and Jean-Louis Coutaz , Highly precise determination of optical constants and sample thickness in terahertz time-domain spectroscopy , Optical Society of America , OCIS codes: 120.4530, 120.3940, 300.627/ 1999

[77] Y. Bouizem, A. Belfedal, J.D. Sib, L. Chahed , Determination of Absorption Coefficients From the Ratio Between Absorptance and Transmittance Measurements of Weakly Absorbing Films , Optics Communications 111–116, 2000

[78] Robert H. Giles , Characterization of Material Properties at Terahertz Frequencies , Submillimeter Technology Laboratory , University of Massachusetts , 1995

[79] R. Ruppin , Evaluation of extended Maxwell-Garnett theories , Optics Communications 182 _2000. 273–279

[80] Sample Spec Sheets of 10 nm Silver Nano particles , http://nanocomposix.com/sites/default/files/Ag10.pdf, last visited on MAY 2012

[81] Michael Schall and Peter Uhd Jepsen, Photoexcited GaAs surfaces studied by transient terahertz time-domain spectroscopy , Optics Letters , vol. 25, No.1 , 2000

[82] S. Sree Harsha, N. Laman and D. Grischkowsky, High-Q terahertz Bragg resonances within a metal parallel plate waveguide, APPLIED PHYSICS LETTERS 94, 091118, 2009